Geomorphometric studies of the seafloor topography of the Western Continental Margin of India

Thesis submitted for the Degree of

DOCTOR OF PHILOSOPHY

in

Earth Science

by

Andrew A A Menezes

Department of Earth Science
Goa University
Taleigao Plateau – 403206
Goa, India

2018

Dedicated To:

late Natalina Florintina Menezes
and
My Family

Statement

As required under the University ordinance OB-9.9 (v-vi), I state that this thesis entitled *Geomorphometric studies of the seafloor topography of the Western Continental Margin of India* is my original contribution and it has not been submitted on any previous occasion.

The literature related to the problem investigated has been cited. Due acknowledgements have been made wherever facilities and suggestions have been availed of.

CSIR-National Institute of Oceanography   Andrew A A Menezes
14th November, 2018

Certificate

This is to certify that the thesis entitled **Geomorphometric studies of the seafloor topography of the Western Continental Margin of India**, submitted by *Andrew A A Menezes* to the Goa University for the degree of Doctor of Philosophy, is based on his original studies carried out under our supervision. The thesis or any part thereof has not been previously submitted for any other degree or diploma in any university or institution.

Dr. Bishwajit Chakraborty
Chief Scientist
CSIR-National Institute of Oceanography, Goa.
14th November, 2018

Dr. Kotha Mahender
Professor
Goa University, Goa.
14th November, 2018

Acknowledgements

LIST OF FIGURE

CONTENTS

CHAPTER - 1

INTRODUCTION

1.1 Background

Technological advances in high-frequency based active sonars have extensively facilitated seafloor mapping and management of living and non-living resources of the seas. SONARs (SOund Navigation and Ranging) are now regularly used for seafloor exploration on account of its capabilities for large-scale data coverage and rapid acquisition. The evolution of Multi-Beam Echo-Sounder System (MBES) (Mayer, 2006) that has revolutionized seafloor mapping along with the advancement in computer processor technology is able to deliver voluminous data for analysis. Besides its bathymetric capability, the ability to provide spatially co-registered backscatter imagery using beam-forming technique has resulted in higher resolution of the MBES bathymetry and improved quality of backscatter data. With MBES as a mapping tool and application of Artificial Neural Networks (ANN) based architecture Self Organizing Maps (SOM) (Kohonen, 1990) together with geostatistical analyses of the data, the classification of seafloor types of the surveyed areas can be carried out and mapped.

The present work focuses on the classification of the seafloor using morphometric and soft computational techniques, concentrating on three distinct and discernible areas from the multibeam surveyed region along the central Western Continental Margins of India (WCMI), (Rao and Wagle, 1997), off Malvan to Malpe, in water depths ranging from 30 m to 2000 m. The multibeam data were acquired under the auspices of Exclusive Economic Zone (EEZ) mapping program of MoES and CSIR-National Institute of Oceanography. The three areas are a part of 24115.5 km² of the WCMI that has been mapped using 15003.5 line km of multibeam data. A sequestered area with a combination

of gullies, ridges and slumps along the slope stretching over 5,310 km^2 offshore Goa, (Chakraborty et al., 2014a) has been examined for seafloor characterization. The other categorical area dotted with pockmarks and fluid seepage lies in water depth varying from 145 m. in the northeast to 330 m covering the southwest region. It extends almost 72 km^2 (9.0 km x 8.0 km), revealing a large number of pockmarks that have been progenerated by the presence of gas and fluid seepages escaping from the subsurface along the faults, especially toward the western end of the area (Chakraborty et al., 2015). The third area is the discernible shallow water area with two coralline banks with an atypical environmental setting, away from the seepage area (Fig. 1.1).
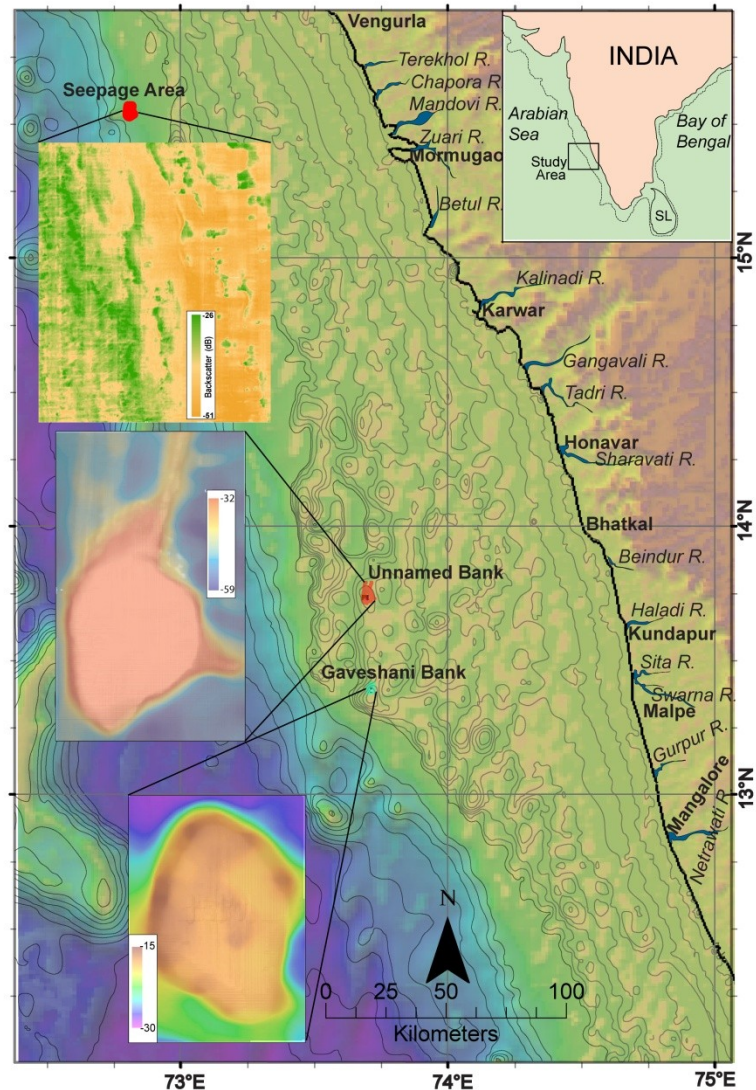
Fig. 1.1- Location of the study areas

The WCMI is a passive and divergent margin in the Indian Ocean, located in the eastern Arabian Sea, in the western part of the peninsula shield of India, which is a mosaic of various tectonic provinces dating in age from early Archaean to late Proterozoic (Kumar et al., 1996; Arora et al., 2012). The general orientation is NNW-SSE and parallel to the Dharwarian orogenic trend. The surveyed area is characterized by thick Neogene and Palaeogene carbonates with minor shale. The main drainage in the coastal area trends in general East-West direction and flows to the Arabian Sea in the west. Rivers such as the Gangavali, Sharavati and Netravati flow across the coastal plain and have an annual runoff of $1.5 \times 10^{13} \text{ m}^3 \text{ yr}^{-1}$ of water (Rao, 1972).

Studies carried out in the WCMI have revealed that the slope region has been subjected to extensive slumping during the late Pleistocene Epoch (Stackelberg 1972; Shetty 1972; Hussain and Guptha 1985; Rao et al., 1988; Guptha et al., 2002). The studies inferred that the slumping in the WCMI was set in motion during the Holocene. Although the late Pleistocene paleo-topography appears as a basic factor in controlling the areal distribution of Holocene deposits, modern processes have also had a significant effect in the area (Karisiddaiah et al., 2002). The Holocene sedimentary processes in the area were controlled primarily by bottom topography and dynamics of the current regime. Bottom currents play a major role in the continental margin sedimentation. The bottom currents in WCMI move northward carrying low-salinity water during the southwest monsoon (summer) and move southward carrying high-salinity water during the northeast monsoon (winter) (Shetye et al., 1990). This regional circulation characterized by seasonal reversal of monsoon-driven surface and bottom currents, summer upwelling and winter downwelling (Naqvi et al., 2010), create an unstable oceanographic condition over the area, modifying the seafloor morphology resulting in higher deposition or erosion. The ADCP deployed off Goa along the continental margin has confirmed that there is a

seasonal-based strong poleward and equatorward currents (~30 cm/s) off Goa slope (Stow et al., 2009). However, the main controlling factor of the slumps appears to be due to the dissociation of adjacent under-lying gas hydrates deposits as reported by Rao et al., (2001).

Seafloor characterization has a wide range of applications in strategic scientific research including defense, marine habitat mapping, and marine protected areas. Seafloor mapping is the first step in characterizing the seabed as it provides the foundation for scientific studies. More than 71% of the earth's surface (362 million km^2) is covered by oceans. Oceans contain natural resources both living and nonliving. Much of the nonliving resources lie on the seafloor and below it. Therefore understanding the ocean seafloor processes is vital (Fox and Hayes, 1985). For centuries producing maps of the seafloor has been a challenging task. Lead lines used to be the primitive method for measuring the depth. During the 1920s SONAR was being used for mapping that produced depth soundings along the ship track (Chakraborty and Fernandes, 2012).

The MBES can cost-effectively provide high-resolution bathymetry and backscatter data with an almost 100% coverage (de Moustier and Kleinrock, 1986). The application of co-registered bathymetry and backscatter datasets facilitates in exploring and researching seafloor classification, distribution of sediment types and seafloor features small-scale geo-morphological changes and marine habitat mapping studies (Haris et al., 2012).

The doctoral research envisaged is aimed at using high resolution MBES sonar data (bathymetry and acoustic backscatter image) along with other geological and geophysical inputs to quantitatively characterize the seafloor of the Western Continental Margin of India (WCMI) employing geomorphometric techniques. The spotlight here is on the

characterization of the seafloor of three distinct surveyed areas of the WCMI. The slope morphological characteristics and the related processes along the slope-confined gullies and ridges of the WCMI, off Goa, were investigated on a wider perspective on account of its role in assessing seabed stability. Both the bathymetry and single-channel seismic data has been made use of to explicate the presence of gas-charged sediments, gas-escape features in the form of fluid flow systems such as pockmarks, mud volcanoes, enhanced reflectors and pockmarked gullies in the area. Taking recourse to morphometry (Pike et al., 2009), i.e. characterizing or extracting discrete marine features, the slope parameters are used to characterize the profiles of the gullies, ridges and the slump zone, which has been well corroborated by the principle component analysis (PCA).

This thesis contains the original text, figures, and tables of papers that were submitted to international peer-reviewed journals that were the contribution of the author.

1.2 Seafloor classification and characterization

The seafloor consists of a range of individual landforms of different shapes and sizes that are structured by interacting processes operating on a variety of spatio-temporal scales (DeBoer, 1992). Seafloor mapping is the first step in characterizing the seabed as it provides the foundation for scientific studies. Quantitative characterization of the seafloor using geomorphometric techniques involves making use of mathematical and statistical processing methods. Quantifying features of the seabed improves the mapping, modeling and better understanding of the processes on the seafloor. Applications of geomorphometric methods have helped improve the geomorphological analyses in a wide range of environment settings (Irvin et al, 1997). The geomorphometric techniques enable the comparison between different seafloor surfaces and facilitate the extraction of quantitative morphological information objectively.

1.2.1 Soft computational approach

The seafloor characterization can be grouped into two categories, *viz.,* based on empirical methods and model-based techniques. The model-based approach optimizes the match between the measured data and the modeled signals to predict the seafloor characteristics for a given environmental condition (Jackson et al., 1986; Jackson et al., 1996; De and Chakraborty, 2011). However, the model-based approach cannot make use of the acquired data directly as most models support stationary input data (Chakraborty et al., 2015). Thus pre-processing or application of segmentation techniques to partition the dataset into stationary data segments becomes essential. Analysis of backscatter data using statistical or soft computational techniques like ANN and Fuzzy Logic (FL) can help reveal large-scale as well as fine-scale seafloor roughness (at textural level), and has been used to determine the number of data classes in the WCMI (De and Chakraborty, 2009).

This study espouses the seafloor characterization utilizing MBES data, segmenting it into stationary segments and consequent fine-scale roughness parameter estimation to provide quantitative information of the seepage-related seafloor along the WCMI (Dandapath et al., 2010, 2012). Using the ANN-based architecture SOM, the number of data classes are determined and subsequently validated by the multimodel PDF curve fitting to the histogram of backscatter data used. Fuzzy Logic based Fuzzy c-means (FCM) is then used to segment the data and thereafter the fine-scale roughness parameters are estimated using Power Spectral Density (PSD) function and making use of backscatter data. A gridded map is prepared based on the estimated roughness parameter that would provide an improved understanding of the seafloor.

The cogency of utilization of ANN-based SOM techniques experimented in a shallow water area sheltering the two coralline banks, with a varied environmental setting

well away from the seepage area is compelling. Coralline banks are home to a wide variety of marine species and are of importance to ecosystems, fisheries and shoreline protection. The ANN application was able to establish the distinct variation in the morphology of the two coral banks (Nair and Qasim, 1978), based on the data segmentation and roughness estimation technique. The summit of each bank could be distinctly identified for its relative higher roughness in relation to its surroundings. The distinct seafloor roughness patterns of the two structurally different coralline banks attest the capability of the method to detect variable seafloor morphology at finer scales.

1.3 Research Objectives

The general objective of this thesis is to achieve a degree of understanding to classify the seafloor by applying a quantitative, rather a soft computational approach. The doctoral study documented here makes use of the high-resolution MBES data acquired from the WCMI. The seafloor characterization technique provides a means to transform high-resolution multibeam bathymetry and acoustic backscatter data into meaningful information to understand the processes in the area (Lurton and Lamarche, 2015). The technique can be made use of in other seafloor areas with appropriate modifications in relations to the topography of the area. The roughness map prepared of the area can be used to study the spatial distribution of geologic material in the area. Roughness is the deviation of the depth values about the local linear trend of the data. The research work carried out focuses on seafloor characterization and addresses the following scientific and technical objectives:

- To provide detailed bathymetric seafloor models and charts of the multibeam surveyed areas that allow for classification of the seafloor, mapping of geological and seafloor data classes, and for utilization as background maps or baseline maps to monitor future changes in the area;

- Characterization of slope-confined gullies, ridges and the slump zone of the WCMI;

- Development of Artificial Neural Network based technique to generate map based on the estimated roughness parameter for an improved understanding of the seafloor;

- Characterization of seepage area of the WCMI, drawing on ANN based technique and multibeam data;

- Seafloor characterization of two coralline banks in the WCMI using MB data, to demonstrate the ability of the ANN approach to detect variable seafloor morphology at finer scales.

The study also demonstrates how the soft computational approach for seafloor characterization provides an improved understanding of a variety of characteristics of the seabed of WCMI.

1.4 Overview of the Thesis

The thesis elucidating the doctoral research carried out has been presented as follows: The first chapter provides a brief preface to Seafloor Mapping and the modus adopted to address the issues to map and characterize the multibeam surveyed part of the continental margins. Apart from providing an insight to the earlier studies carried out in mapping and classifying the seafloor, the new approach taken to map and classify the seafloor utilizing the acquired data is presented to exemplify the utility of the work that has been carried out. There is also a general introduction to the aims and the purpose of the study including the regional setting of the passive Western Continental Margins of India.

Chapter 2 provides the methodological procedures adopted in meeting the needs of the research work carried out. The methods used for seafloor classification are described therein with special emphasis on bathymetric depth measurement and multibeam angular backscatter data. This chapter also provides the background of the importance and necessity to classify the seafloor.

The study area and its regional setting have been elaborated in Chapter 3. Three distinct and discernible areas from the multibeam surveyed region along the central WCMI, off Malvan to Malpe, in water depths ranging from 30 m to 2000 m, were adopted for seafloor characterization. The three areas are a part of 24115.5 km² of the WCMI that has been mapped using 15003.5 line km of multibeam data. A sequestered area with a combination of gullies, ridges and slumps along the slope stretching over 5,310 km^2 offshore Goa, along the 300 m bathymetric contours with an average slope of 3.11º was examined for seafloor characterization. The other categorical area dotted with pockmarks and fluid seepage lies in water depth varying from 145 m. in the northeast to 330 m in the southwest region. It covers almost 72 km^2 (9.0 km x 8.0 km), revealing significant numbers of pockmarks that are produced by the presence of gas or fluid seepages escaping from the subsurface along the faults (Dandapath et al., 2010). The other discernible shallow water area with two coralline banks, Gaveshani bank and an unnamed bank, located off the coast of the Indian State of Karnataka has been examined.

Chapter 4 explicates the slope morphology characterization and discusses the related processes through the comprehensive usage of both the bathymetry and seismic data that are relevant for the continental margin investigations. Geomorphology has enhanced our understanding of the earth's physical changes, particularly the processes on the surface. The importance of geomorphology in managing and preventing environmental hazards, sustainable development of ecosystems cannot be overemphasized. With the advancements in remote sensing and GIS, geomorphometry has become expedient. Geomorphometry can be described as the quantitative assessment of terrain morphology using geosciences, mathematics and computer sciences. The analysis of slope configuration of the submarine gullies, ridges and the adjacent slump zone, off Goa, along the western continental margin of India utilizing multibeam bathymetric and

single-channel seismic data have been analyzed and presented. The fluid flow migration signature in the form of pockmark seepages, traces of mud volcanoes and enhanced reflectors have been observed in the area. Altogether thirty-three depth profiles from the gully, ridge and slump areas depict downslope progression in gully incision and varying gradients in the gullies and ridges, whereas the profiles of the slump zone are comparatively steady. The scatter plot of the three slope characteristics, *viz.*, gradient, mean depth and root mean square relief, characterizes the profiles of the gullies, ridges and slump zone into three distinct clusters. Principal Component Analysis as well as corroborates the characterization (Chakraborty et al., 2014a).

Chapter 5 adduces the utilization of soft computational techniques and artificial neural networks (ANN) for seafloor data classification. The basics of ANN relevant to the present study are presented. ANN based SOM, an unsupervised method, is explicated for the selection of an optimal subset of echo features to achieve a significant success in the classification of seafloor data. The algorithm for seafloor data classification, as well as the methodology utilized for segmenting the data, adapted from De and Chakraborty (2009) has been explained. Fuzzy c-means (FCM) method is employed for segmentation of the profile data using the number of the data classes determined by SOM.

In Chapter 6 seafloor characterization technique to determine the number of data classes in the pockmarked dotted seepage area, using multibeam echo-sounding backscatter data has been elucidated. The application of self-organizing maps (SOM) to backscatter profile data, developed to determine the likely number of classes is discussed. The fuzzy C-means (FCM) method is employed thereafter, using the number of the estimated class information, for backscatter profiles segmentation. The application of the soft-computational techniques to seafloor backscatter data for achieving stationary profile data sets, suitable for seafloor roughness model application is evaluated. The power

spectral density (PSD) function of the segmented profiles that provide the power law parameters (β and a') through curve fitting, using power-law expression is computed.

Chapter 7 presents the adaption of ANN-based SOM techniques with respect to the shallow seafloor with coralline banks. The application of ANN could establish a distinct difference in the coral bank morphology, employing the data segmentation and roughness estimation technique. The successful outcome of this technique in a distinct environment validating ANN-SOM capabilities to discrepate the sonar image profiles for classification and characterization in a shallow coralline environment is evaluated.

The last chapter provides a summary of the results from this work. The conclusions from the main findings are highlighted.

CHAPTER – 2

METHODOLGY

2.1 Multibeam Echo Sounding System (MBES)

For any contemporary seafloor studies, employment of multibeam data is indispensable, mainly for its high resolution and extensive coverage, and the potential use of derived data products that can be utilized for various marine applications including visualization and spatial modeling (Lucieer et al., 2018). Presently oceanographic surveys using Multibeam Echosounder System (MBES) are the main source of bathymetric data along with backscatter data. Bathymetry is the science of measuring and charting water depths to determine the topography of the seafloor or any water body (Weatherall et al., 2015). The depth soundings and the backscatter strength measurements are used in conjunction for mapping the seafloor. MBES used in marine surveys are designed for two purposes: bathymetric mapping of bottom topography (measuring water depth) and thematic imaging of the seafloor for bottom characterization (nature of the seafloor/ sediment type) (Chakraborty and Fernandes, 2012).

The MBES consist of two subsystems – sonar and navigation. The sonar subsystem typically mounted on the ship's hull implementing a cross fan beam geometry generated by two transducer arrays mounded at right angles to each other. It transmits a fan-shaped array-of-sound and records the distinctive echoes from returning beams reflected after hitting the seafloor (de Moustier, 1988). The time taken for the returning sound waves to reach the receiver after reflecting off the seafloor is used to compute the water depth. The navigational subsystem provides ship's attitude (roll, pitch, heading, and heave) and geographic position data. The reflected sonar returns are correlated with the navigational data. The horizontal and vertical positioning is precisely measured through the use of

Geographical Positioning System (GPS) and Inertial Measurement Unit (IMU). Measuring the movement and position of the vessel is imperative to preserve the accuracy of the data because the position of the sounding will change as the vessel moves in the water due to roll, heave, pitch and yaw. The IMU measures the angular offsets of the transducer resulting from vessel movement. It is usually mounted very close to the transducer to minimize any variation in the offset between them. These offset measurements are incorporated either at the time of collection or in a post-processing workflow to improve the accuracy of the sounding position. Usually the vessel attitude is integrated at the time of acquisition (Lurton, 2002).

The multi-beam echo-sounder systems are now the standard technology for marine surveys of the seafloor. It has become the mainstay of many marine surveys. MBES are active sonars that transmit a distinctive and controlled signal in direction of the seafloor. Unlike other sonars, multibeam systems use beamforming technology to obtain directional information from the returning acoustic waves, generating a narrow strip of depth soundings from a single ping. Spatial filtering or beamforming is a signal processing technique used in sensor arrays for separating signals coming from different propagation directions. Knowing the speed of sound in water and the two-way travel time - the time taken for acoustic waves to travel between the source and the seafloor and back to the source again, the range between the target and the sonar [range = (speed of sound in water) x (half the travel time)] can be estimated enabling the computation of depth. The speed of sound in water however, being greatly affected by temperature, salinity and pressure, necessitates undertaking of post-processing corrections (Peyton et al., 2009). Modern multibeam echosounding systems are also designed for thematic imaging of the seafloor for bottom characterization using the backscatter strength measurements, which is the energy retuning to the transducer. The intensity of this return (i.e. backscatter) can

be examined to provide information on the properties of the seafloor (e.g. surficial sediment texture or material type).

The accuracy of sounding data is dependent on the measurement of sound traveling through water at the time of acquisition. The speed of sound in water influenced by rising temperature, salinity and pressure (depth) (Ali et al., 2001), causes it to vary to some extent from less than 1,500 meters per second to more than 1,600 meters per second at depths greater than 2,500 meters. The MBES uses sound velocity information received from the velocity probe attached to the transducer. Additionally, sound velocity can also be integrated form external sound velocity profilers. During surveys, the sound velocity is measured as well by deploying an external sound probe that records the sound-velocity profile. Such measurements are routinely carried out at pre-defined positions or intervals, at least twice a day, or sometimes it may be necessary to have more measurements since variations in sound velocity through the water column affect depth calculations via ray tracing (Hovem, 2013). The measurement process entails stopping the survey, deploying and retrieving the probe, and corroborating the accuracy of the measured sound-velocity profiles.

With fast processing systems the MBES are now well equipped for online computing and processing of sonar data for display and recording. The multibeam sonars are being effectively used for acquisition of high-resolution bathymetric and acoustic data, in both shallow and deep water areas (de Moustier, 1988; Mills and Perry, 1992). Modern shallow-water MBESs are well equipped for measurements of shallow bathymetry with a spatial resolution of a few centimeters, and are routinely being used for detailed investigations of seabed geomorphology (Hughes Clarke et al., 1996; Dandapath et al., 2018).

2.1.1 MBES Description

MBES used for data acquisition are specialized equipment used for mapping the seafloor. Most of the MBES have to meet the performance standards defined by the International Hydrographic Organization. The instruments have capabilities of recording high resolution sounding data, with great accuracy and a dense pattern of soundings to determine the features on the seafloor. Besides acquiring depth data, the MBES also record backscatter data that can be used to produce image of the seabed. The backscatter data recorded by MBES is utilized for characterizing the sediments and features on the seabed.

In this study Kongsberg Simrad EM 1002 MBES operating at 95 kHz on board the CRV *Sagar Sukti*, was used during the coastal marine surveys (Cruise nos. SaSu-118 and SaSu-164) in November 2006 and February 2008 for mapping the study areas (the pockmarked seepage area and the coralline bank shallow area). EM 1002 (Anon., 2006) can operate in a variety of depths from shallow coastal waters to 1000 m. In shallow water the across-track coverage is up to 7.4 times the depth beneath the transducer. The survey lines are normally oriented parallel to the coast in N-S direction. A graphical representation of the components in the EM 1002 system used for the data collection on board (CRV *Sagar Sukti*) is given in Fig. 2.1.
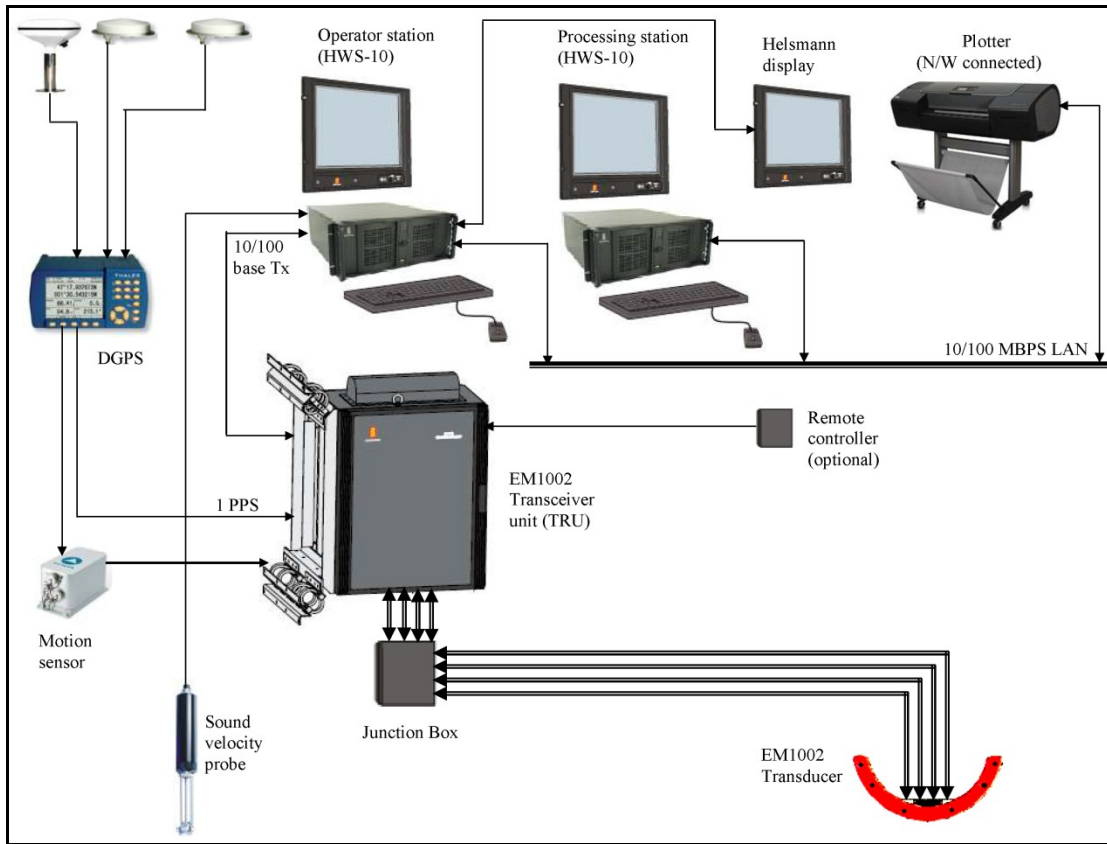
Fig. 2.1 - EM 1002 multibeam echo-sounder system (modified from Anon., 2006)

For the data acquisition in the WCMI, Kongsberg Simrad EM 302 MBES operating at 30 kHz on board the R/V *Sindhu Sankalp*, was used. Four surveys (Cruise nos. SSK-19, SSK-23, SSK-29 and SSK-54) were conducted in 2011, focusing on the shelf break, off Mormugao-Vengurla-Malwan. The survey lines were oriented in N-S direction parallel to the coast. The graphical representation of EM 302 components (Anon., 2012) on board R/V *Sindhu Sankalp* used for the data acquisition in the WCMI is also given in Fig. 2.2.
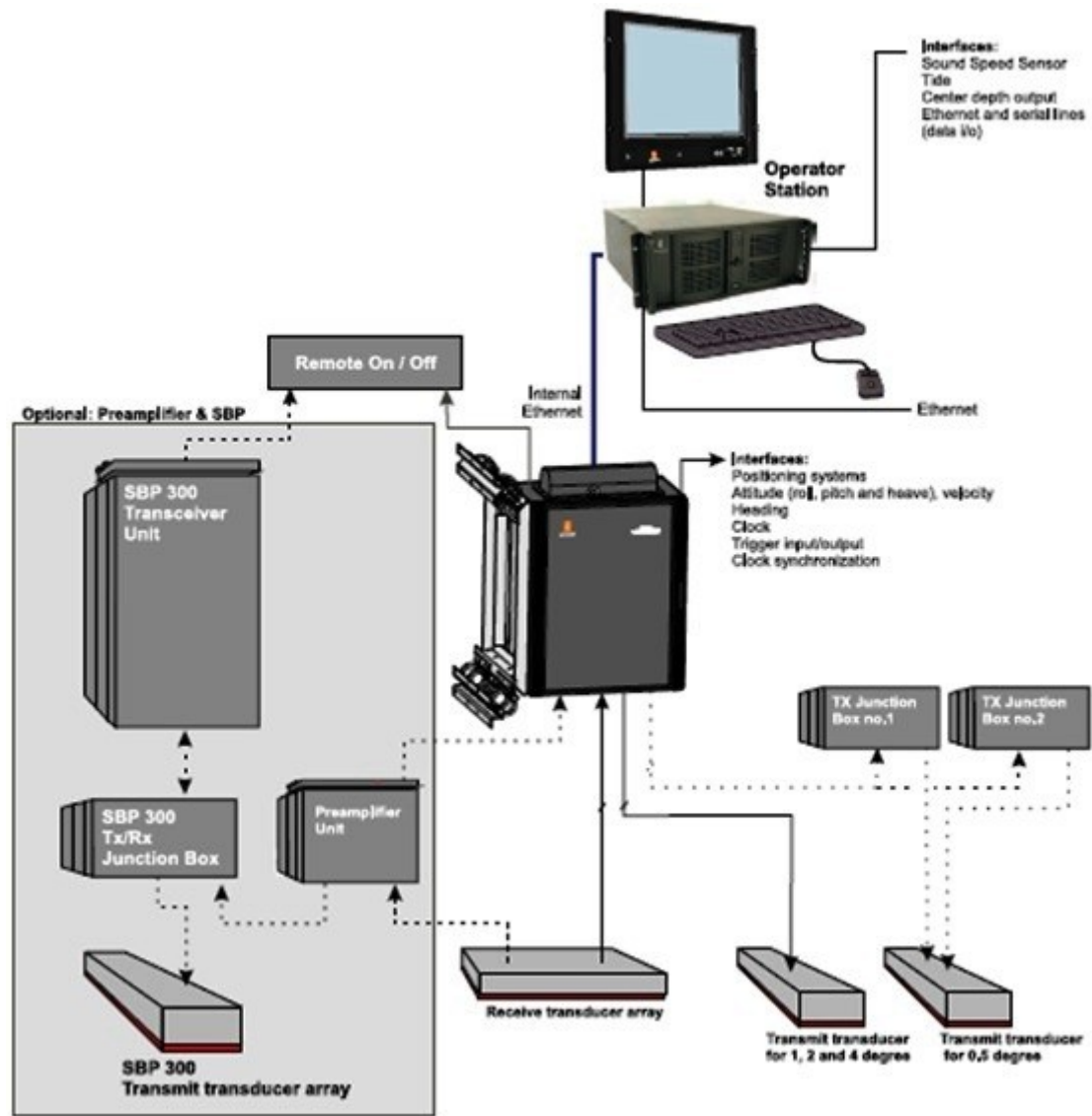
Fig. 2.2 - EM 302 multibeam echo-sounder system (modified from Anon., 2012)

2.1.2 MBES Components

The primary components of EM 1002 and EM 302 MBES (see Fig. 2.1 and Fig. 2.2) are the transducer array, transceiver unit, data logger, motion sensor, positioning sensor, and sound velocity sensor. They are listed as follows:

(i)   Transducer array: Fixed at the hull of the ship and is used to transmit and receive signal.

(ii)   Transceiver unit (TRU): Contains electronics and processor related to signal transmission, signal reception, beam forming, signal processing, bottom detection etc. and control all parameters with respect to gain, ping rate and transmit angles.

(iii) Operator station: High-end computing machine/ workstation, capable to handle large volume of data and heavy processing loads. 'HWS-10', a specifically designed workstation designed for real time gridding, filtering, storing and visualization (3D) of sounding data, is used for this purpose. Quality check of acquired data can be made at operator station.

(iv) Motion sensor: 'Octan', a gyrocompass and complete motion sensor, is used for this purpose to detect true heading (accuracy 0.1° secant latitude, resolution 0.01°), roll (accuracy 00.1° secant latitude, resolution 0.001°), pitch (accuracy 00.1° secant latitude, resolution 0.001°), surge, sway, heave (accuracy 5 cm or 5% whichever highest), speed, acceleration and rate of turn.

(v) Positioning sensor: 'Aquarius 22 DGPS system' (XY precision 1-2 m and Z precision 3 m) used to geo-referenced (including time stamps) the acquired sounding data.

(vi) Sound velocity sensor: Designed to measure sound velocity and temperature at the surface of the EM 1002 transducer.

The technical specification of EM 1002 (Anon., 2006) MBES are:

Operating frequency	: 95 kHz
Maximum ping rate	: >10 Hz
Number of beams per ping	: 111
Beam width	: 2*2°
Beam spacing angle	: equi-distance and equi-angle
Angular coverage	: up to 150°
Depth range from transducers	: 2 – 1000 m
Depth resolution	: 8 cm
Pulse length	: 0.2, 0.7 and 2 ms
Range sampling rate	: 9 kHz (8 cm)
Beam forming method	: phase interpolated
Economic survey speed	: 7 knots
Working sea state	: 03

The technical specification of EM 302 (Anon., 2012) MBES are:

Operating frequency	: 30 kHz
Soundings per ping	: up to 854
Beam width	: 0.5 to 24°
Depth range from transducers	: 10 – 7000 m
Swath width	: 5.5xdepth, to more than 8 km
Pulse forms	: CW and FM chirp
Swath profiles per ping	: 2
Motion compensation	
Yaw	: ± 10 degrees
Pitch	: ± 10 degrees
Roll	: ± 10 degrees
Sounding pattern	: Equidistant / equiangular
Range sampling rate	: 3.25 kHz (23 cm)
High resolution mode	: High density processing
Sidelobe suppression	: > 25 dB
Effective pulse length	: 0.4 ms CW to 200 ms FM
Suppression of sounding artefacts	: 8 frequency coded transmit sectors per swath
Beam focusing	: On transmit and receive
Beamforming method	: Time delay
Gain control	: Automatic
Swath width control	: Manual or automatic, all soundings intact when operated at reduced swath width
Seabed imagery/sidescan sonar image	: Standard
Water column display	: Standard
Mammal protection	: Standard
Sub-bottom profiling	: Yes, by integration with SBP 300 or Topas

2.1.3 MBES Calibration

Calibration of multi-beam echo-sounder is crucial before initiation of the data collection operation. It begins with the alignment and static offset of the sensors referenced to the centerline of the vessel/ship and the transducer to reduce the static corrections of each sensor. After that, a patch test is performed to ascertain the roll offset, pitch offset, azimuthal offset and positioning time delay. Testing is essential to verify

whether the data meets accuracy requirements for the survey. In addition to testing, a proper synchronization of all the components of multi-beam system is also carried out (Fernandes, 2007). The sequence of calibration is given below:

(i) Alignment and static offsets

(ii) Motion data (Octans) calibration

(a) Roll calibration

(b) Pitch calibration

(c) Heading calibration

(d) Outer beam calibration

(iii) Finding sources of errors (if any) and rectification of the same

2.1.4 MBES Data Acquisition

Marine Survey is a prerequisite for marine data acquisition. The technique involves the use of the acoustic return signal from a multibeam echosounder to estimate the depth and to make qualitative estimates of the seabed composition. The marine surveying methodology for bathymetric data has gone through sweeping changes, from measuring depth with lead lines to single-beam echo sounder, and presently to swath bathymetry (using multi-beam echo sounder). To efficiently utilize the information the acquired data is stored for sharing.

Bathymetric surveys provides information about the depths and shapes of the seafloor and has a range of uses that includes scientific marine research, nautical charting, harbor maintenance, particularly draft for shipping, monitoring dredging operations and for other strategic purposes. Each of these operations would have its own demands and requirements with regard to the quality of bathymetric data. The required quality for these different functions will be dependent on the design and spacing of the survey track lines to optimize the spacing of depth measurements. As the water depth affects the spatial resolution of the footprint of the soundings, the distance between transect lines

need to be prudently chosen to avoid data gaps between the survey lines. This is because the size of the beam footprint is dependent on its beam width and water depth. The geometric distance between the centers of the footprint in each beam approximates the spatial resolution of bathymetric data collected from multibeam echo sounders. A narrower beam width will result in a small sonar footprint and produce a finer spatial resolution. As such an overlap of 10 to 20 percent is usually considered to compensate for any degradation in the data acquired from the outer beams. The overlap factor ensures a comprehensive and continuous coverage of the seafloor without data gaps. The spacing between the survey lines is reduced in shallower waters while in deeper waters it is broadened to reduce the overlapping beams. With increasing water depth, the sonar pulse traveling away from the transducer array at each ping is subjected to spherical spreading; the intensity and amplitude decreasing with increasing distance from the transducer and the acoustic energy spreading out over a larger area. In shallower waters the pinging rate is faster as the signal returns much quicker. As a result the acquired data is dense with significantly higher spatial resolution. Consequently the bathymetric survey is planned according to the water depth, system type, vessel speed, and survey application.

2.1.5 Data Processing

Processing of multibeam data consists of cleaning and filtering navigation data, noise reduction, data editing and visualization. The multibeam data need to be corrected due to the vessel's attitude characteristics (movements as a result of sea conditions causing heave, pitch roll, etc.). After corrections for attitude are calculated, refraction corrections are applied based on the measured sound velocity profile and the depth to the seafloor for each beam is determined based on the two way time of the acoustic pulse, and the inclination angle of the beam (Farr, 1980). The data processing helps generate the

bathymetric map, which is the basis for characterization of the sea surface and further analysis and interpretations used in seafloor mapping.

An important aspect of the multibeam data is that the resolution and data density decrease with depth as a result of the beam geometry and lower multibeam frequencies used (Wilson et al., 2007). Most often positional data corrections are incorporated at the time of acquisition reducing post-processing time and improving the workflow. However a substantial amount of interactive post-processing, data cleaning, sound-velocity profile application, tidal adjustments and other systematic corrections are required to be carried out on the data.

Multibeam echo sounders along with depth data also record backscatter data, which can provide information about the nature of the seafloor. The backscatter is characterized by the intensity, or strength of the returned signal. The sound energy while propagating through the water column loses some energy through attenuation and absorption. More energy is lost in the sediment when it hits the seafloor; softer sediments such as mud and sand typically absorb more energy than hard or rocky surfaces. A sensor will record a stronger intensity from a rocky surface than from sand because more energy is returned from a harder surface. Backscatter maps are normally depicted in grey scale format, with darker pixels representing low backscatter i.e. weaker returns from softer sediments and lighter pixels representing high backscatter i.e. stronger returns from harder sediments. The quality of multibeam data is also often reviewed determined from the acquisition system perspective; it can vary greatly between different units that collect the data due to the corrections that may or may not have been applied at the time of acquisition. Besides the multibeam unit collecting the data may have inherent inaccuracies that engender artifacts. Post-processing of multibeam data constitutes rectification of these erroneous positional data and correction of erroneous depth measurements.

2.2 MBES Bathymetry

Contemporarily, multibeam bathymetry offers the most accurate, cost-effective system for obtaining high resolution data of the seafloor. A bathymetric map shows depth related information of the seafloor by representing the depth values in color scheme or in grey scales. It depicts the rise and fall of the seafloor at horizontal scale and also the water depth and shape of the seafloor, which is a fundamental parameter for understanding oceanic circulation, tides, tsunami fore-casting, fishing resources, wave action, sediment transport, environmental change, underwater geo-hazards, cable and pipeline routing, mineral extraction. Bathymetric data has a number of other uses, as in studies related to climate change effects, coastal erosion, sea-level rise and subsidence

2.2.1 Using 'Neptune'

'Neptune' is used as a post processing software package for the processing of raw multi-beam data of EM1002. Post processing of bathymetry here mainly includes removal of tide effects and depth outliers (Mitchell, 1991). After importing the collected data in 'Neptune' position processing is executed to correct positional errors caused by uneven geometry, shadow region etc. At the beginning, the collected raw data was converted to survey format by 'replay' sub-program, and then imported in main 'Neptune' and post processing was done by making rules including parameters like tide data and other distortions. The output was exported as ASCII file (*.xyz) for subsequent use in 'Arc GIS' and 'CFLOOR'. 'Neptune' is also useful for data cleaning, cross line matching, gridding of the raw or processed data etc.

2.2.2 Using 'CFLOOR'

Primarily 'CFLOOR 6.3.1' was used to visualize data by way of 3D image, plot, maps etc. (http://www.cfloor.no). 'CFLOOR' is also used to create a grid of 10 x 10 m resolution. Bathymetric contours and 3D display of seafloor in 'CFLOOR' help in

identifying the relief variations of seafloor vis-à-vis geomorphic features like pockmarks, mounds, faults, reefs etc.. Some of maps shown here are initially generated using 'CFLOOR' software package.

2.2.3 Using 'CARIS®'

CARIS is the acronym for Computer-Aided Resource Information System. Data acquired using EM 302 was processed using CARIS (HIPS and SIPS) (CARIS, 2007). CARIS (HIPS and SIPS) is a software suite offering capabilities and professional grade tools for hydrographic data processing. CARIS supports over 40 data formats; the software facilitates simultaneous processing of multibeam, backscatter, side scan sonar, single beam and lidar data,. It incorporates 3D visualization technology for the purpose of hydrography, oceanography and marine science. CARIS is used for post-processing of the acquired data that runs with Windows XP operating systems. CARIS HIPS (Hydrographic Information Processing System) is used for all initial processing of multibeam and vertical beam echosounder bathymetry data, including tide, sound velocity, and vessel offset correction and data cleaning. CARIS HIPS uses statistical modeling to create Bathymetry with Associated Statistical Error (BASE) surfaces in one of three ways: swath-angle weighted grids, uncertainty-weighted grids, and Combined Uncertainty and Bathymetry Estimator (CUBE) algorithm grids. CARIS SIPS (Side-scan Information Processing System) is used for all processing of side-scan sonar imagery, including cable layback correction, slant range correction, contact selection, tow point entry, and mosaic generation.

2.3 MBES Backscatter

Besides bathymetric data, the EM1002 as also EM 302 bring together backscatter data that provides supplementary quantitative data (extraction of classifying features); the backscatter is used for qualitative (image mosaics) assessment of seabed properties (Davis et al., 1996; Huvenne et al., 2002). The amount of acoustic energy reflected back

to the transducer is referred as the backscatter. This backscattered energy is a function of a variety of variables, including the grazing angle, the surface roughness of the seafloor and the nature of the material type. It is expressed in decibels (dB) and is the logarithmic ratio of the intensity of the acoustic energy scattered back by the seafloor and the incident intensity. It is sensitive to frequency and incidence/grazing angle, the geometry and roughness of the seafloor as well as the composition of the seabed; sediment grain size and type including biological coverage. The backscattering process is a cumulative effect of the acoustic frequency used, the variation in acoustic impedances between sediment and water, layering or sediment volume inhomogeneity and the interface roughness of the seafloor. The effect of volume scattering due to heterogeneities in the sediment play an important factor on account of acoustic penetration at the frequency used (Blondel, 2009). The consequence of scattering due to sediment volume inhomogeneity is relatively more significant at lower acoustic frequencies, and the scattering due to seafloor interface roughness it is relatively more important at higher acoustic frequencies. At lower frequencies, more acoustic energy penetrates the sediments (Urban, 2002). On account of the subterranean layers and the underlying inhomogeneities (shells, coarse sand particles, pebbles, gas bubbles etc.), the acoustic energy is most prone to get scattered.

Seafloor with sediment characteristics of rocks, gravels, coarse shells, steep slopes or hard surface, will exhibit high backscatter. Sandy areas or areas with soft sediments will exhibit low backscatter as fine sediments tend to absorb the signals and the reduced amount of energy reaching the transducer. Generally slopes facing in the direction of the sonar tend to produce more backscatter and rougher surfaces will invariably generate more backscatter. Conventionally maps with high backscatter are represented with dark shades, while low backscatter is shown as light shades. Gray-scale images from black to white are generated based on the strength of the signal within a range of 0-255 (Blondel

and Murton, 1997). Using backscatter data is an effective way in obtaining information of seafloor properties, however raw application of multibeam backscatter data is limited on account of inherent artifacts. Usually on a smooth seafloor, the angular backscatter intensity recorded at the normal incidence angles is higher than that of outer beam angles. Therefore, off-line corrections are incorporated to compensate for the outer-beam backscatter intensity in such a way that the effect of higher angular backscatter strength is nullified. The MBES assumes a plane seafloor during acquisition, but the seabed is not usually a plane surface. The effect of any online gain functions (Fernandes and Chakraborty, 2009) employed has to be neutralized as there may be large scale variations in seafloor slope, along and across track directions. Hence, post processing of backscatter data is necessitated even for moderately rough seafloor to produce a normalized acoustic image of the seabed suitable for carrying out classification studies.

Backscattering has several important applications. Backscatter data is useful in detecting features and the texture of the seafloor that are not discernible by bathymetry data. Imaging the seabed using sonar systems is widely used in the marine environment. The backscatter mosaic is a geo-referenced grayscale image representing the acoustic intensity scattered by the seabed, with different seabed types usually showing different levels of intensity. The acoustic image is utilized for obtaining complementary information about the reflected intensity of the acoustic signal on the seafloor and is useful for classifying the seafloor (Beyer, et al., 2007).

2.3.1 Using 'PROBASI II'

The beam pattern effects are present in collected backscatter data caused by fluctuations in acoustic intensity among groups of elements of the transducer array. The data gets recorded in a packet format called datagram stored for every ping (Hammerstad, 2000; Fernandes and Chakraborty, 2009). The background of using PROBASI II is

explicated in de Moustier and Alexandrou (1991) and Chakraborty et al. (2000). The backscatter data is eventually corrected for propagation and other effects (Mitchell and Somers, 1989) mainly by PROcessing of BAckscatter Signal II (PROBASI II) algorithm. 'PROBASI II' developed indigenously by the researchers from National Institute of Oceanography, Goa.

In EM 1002 multi-beam system, online amplifier gain correction is employed through use of mean backscattering coefficients such as: BS_N and BS_O applied at 0° and at crossover incidence angles (normally 25°) respectively (Hammerstad, 2000; Fernandes and Chakraborty, 2009). Thereafter, the raw backscatter intensities recorded in the raw (*.all) files are corrected during data acquisition employing Lambert's law (Simrad Model). However, for lower incidence angles (within the $0-25^o$) the gain settings require a reasonably smooth gain with incidence angle i.e., the gain between BS_N and BSo changes linearly. The sample amplitudes are also corrected suitably incorporating transmitted source level and transducer receiver sensitivity. Further, sonar image amplitudes though corrected online needs further improvement to generate normalized images for the seafloor area. This is especially needed for incidence beam angles within the $+/- 10^o$ angles (to remove routine artifacts in the raw backscatter data near normal incidence angles). Hence, post processing is essential to be carried out even for moderately rough seafloor. In addition to the artifacts close to normal incidence beams, the EM1002 multi-beam data show some residual amplitude due to beam pattern effect, and thus real-time system algorithm is unable to compensate such routine situation. As discussed, the EM1002 multi-beam echo-sounder system automatically carries out considerable amount of processing on raw backscatter intensities. Even then, the data show some residuals, which are required to be corrected before further studies.

2.4 Geographical Information System (GIS) for Seafloor Mapping

With the enormous increase in the availability of multibeam data and the increased perceptibility by which classification can be carried out using GIS there is enough impetus for researchers to use geomorphometric techniques for exploration of the marine environment (Pike et al, 2008). GIS is now being used in all areas of ocean mapping. Scientists and engineers use the software for processing, quality control, and analysis of multibeam sonar along with related data. The software has significantly improved the efficiency in preparing nautical charts, geological interpretation, assessment of seabed habitats, and identification and assessment of geohazards.

In this study, preparation of bathymetry/ backscatter maps is carried out using GIS platform. GIS has expanded the utility of digital maps by providing visualization of depth information for any location on the surveyed seafloor at the click of the mouse. It can provide exact location of any seabed feature in terms of latitude, longitude, and depth values altogether. Multibeam generates two types of data: discrete points representing depth and geo-graphical position, and backscatter images. All geospatial data can be organized into either vector or raster format. Points are a form of vector data, as are lines and polygons, the three basic geospatial data types. Raster data also referred to as image data, are a matrix of rectangular cells arranged as rows and columns (Burrough, 1998).

GIS is now being employed to leverage bathymetric data by using it with other databases for a wide range of purposes that require seafloor information. It is now much easy to handle bathymetric charts based on new and updated nautical information. Preparation of bathymetry map making use of GIS platform has enlarged the scope for further utilization of bathymetric data. Taking advantage of faster processors/data loggers has further increased the rate with which data can be collected, thus providing greater detail to seafloor mapping. The processed multibeam data along with other geophysical

data can be used to create a composite surface model. This composite surface model can be used as a source to create 3D point data for spatially analysis with the ArcGIS Spatial Analyst.

2.4.1 Geostatistical Analysis

The geo-referenced data points, containing backscatter strength (dB) and depth values (m) are imported to 'ArcGIS' (m/s ESRI Inc., USA). In 'ArcGIS' the best possible raster resolution as per the processed data was set and the generated shape (*.shp) file preserved all positional and attribute aspects (longitude, latitude and water depth or backscatter) in a defined geographic co-ordinate system (WGS 84). The data were then interpolated to raster using cubic convolution methods and subsequently high resolution image with distinct color scheme was generated. Cubic convolution tends to sharpen the data as compared to other methods such as bilinear interpolation etc. Cubic convolution technique employs weighted average values of the sixteen nearest input cell centers, whereas bilinear interpolation method uses only four nearest input cell centers to determine the value of the output raster. For the first time from the western continental margin of India, detailed seafloor morphology was studied with the help of 'ArcGIS'. Spatial analyst extension (a separate module added with ArcGIS) was also used for raster based spatial analyses of data. All the measurements were done using 'ArcGIS' tools (Johnston et al., 2004).

2.4.2 Contouring

Bathymetric data is often presented as a contour isobaths representation. Contour isobaths are vector data represented as lines connecting depths of equal value. The interval between lines is dependent on scale, application, and other factors, but contours

that are closer together represent a high variability or steep seafloor; whereas contours that are farther apart indicate a very gentle slope or a smooth seafloor.

Studying the bathymetric contours shape and alignment, morphological features such as depression/pockmarks, fault, small mounds, terrace etc. can be identified. Bathymetric contours at different intervals generated to superimpose over bathymetry and backscatter map helps achieve this. Contouring at very small interval (up to 10 cm) helps measure the dimensional characteristics (i.e., length, width, relief, perimeter etc.) of such features.

Bathymetric profiles provide a cross-sectional perspective of the seafloor. They are generated from high-density bathymetric data and provide a 'skyline view' of the sea floor where the sea mounts are seen as rises and troughs/basins as depressions. They are particularly useful for cable and pipeline route analysis and infrastructure installation, and are an example complementary representation of the seafloor.

2.4.3 Digital Elevation Model

A Digital Elevation Model (DEM) is the simplest form of digital representation of topography. It is a digital model or 3D representation of a terrain's surface. A DEM is also referred as a gridded array of elevations. In its raw form it is a high-density data in ASCII or text file, transformed into new points, contour lines, triangulated irregular networks (TINs), raster products, polygons such as depth areas, or a combination of these. DEM has numerous applications in research and practice. Most GIS applications use DEMs. The quality of a DEM is a measure of how accurate depth is at each point and how accurate the morphology is represented. Several factors play an important role for quality of a DEM, including terrain roughness, sampling density (how many beams), the depth of water (deeper water provides yields lower resolution), the interpolation algorithm and the terrain analysis algorithm (smoothing and extrapolation).

Using spatial functionality of GIS can add more value to DEM for modeling purposes. A digital elevation model (DEM) is an important part of many geoinformatic/ geomorphometric applications. By definition a DEM is a collection of elevation points, the points are not related to each other in ways that defines objects. DEM vector files are commonly referred to as XYZ files; these store position and elevation information for each data point. It is possible to convert a shape file into a point file but processing is required for the reverse operation. A shape file generally contains less information that the DEM from which it was processed because any data points between the contour lines are discarded. The raster format assumes that the elevation data is stored in a regular grid layout. A common raster file format stores only one position as a reference point and then it stores the x and y size of a raster cell (e.g. pixel) and the total number of x cells and y cells. With this information an application can calculate the position of each and every raster cell in a raster grid. The raster file then stores a list of elevation values corresponding to the position calculated for each raster cell. There are variations on this theme that store slightly different information but the general principal of the raster file format is the same.

2.4.4 Terrain Analyses

A variety of methods are available combining inverse distance weighting, spline functions, kriging and triangulated irregular networks to calculate terrain models of the seafloor that can be used for further analysis, presentation, contouring and charting. Computers enable users to render seabed terrain using both realistic and highly abstract, symbolized methods. While DEMs provide the benefit of computer based analysis, they also present an opportunity to those who perform manual (visual) analyses of the seabed surface an intuitively comprehensible visual display of the terrain characteristics for viewing the surface models and the data derived from them. The human visual system is also capable of identifying patterns and relationships between features and their

41

attributes. Symbolized representations make it easy for targeting a particular aspect of the seabed terrain to detect hidden patterns that are being obscured by unrelated noise. In addition to the analysis, visualization of seabed terrain data assists in the presentation and communication of decisive information particularly for those that are not trained to read maps. For example, this can be accomplished by composing a hill- shaded image of the surface with relevant thematic information for display on a map. Alternatively, a 3-D perspective with data overlain on top of a terrain model can improve one's understanding of the problem. Hillshades and other terrain visualization tools can also be used for quality control purposes.

Digital elevation models have proved to be increasingly more important in geological and geo-morphological studies. DEMs and their software can be used as a tool in a complex analysis of the Earth's topography and legible data visualization. Quick construction of color contour maps or shaded relief maps represents only basic application of digital elevation data. Digital models are also helpful in fast construction of a number of derivative maps, like those of slope, gradient, aspect, extent of ice-sheet or marine transgressions, as well as former extent of dammed lakes. Application of DEMs can enhance drawing of geological cross-sections of any orientation. Apart from present-day topography, it is also possible to digitally analyze buried surfaces basing on welllogs and geophysical data. Such models need, however, specially prepared well-log and geophysical data bases, and the density of subsurface data points is usually lower than that of surface models.

2.4.5 Geomorphometry

Geomorphometry or quantitative terrain characterization, has raised interest in its employment to investigate the marine environment. Owing to the increasing availability

of digital bathymetric data and the ease by which geomorphometry can be investigated using geographic information systems (GISs) and spatial analysis software.

Over the last decade or so, a multitude of geomorphometric techniques (e.g. terrain attributes, feature extraction, automated classification) have been applied to characterize seabed terrain from the coastal zone to the deep sea. Nevertheless, applications of geomorphometric techniques are limited in the marine environment as compared to the terrestrial environments. This is at least partly due to difficulties associated with capturing, classifying, and validating terrain characteristics underwater. With common ground between terrestrial and marine applications in development for marine geomorphometry, we learn from experiences in terrestrial studies. As stated before, not all terrestrial solutions can be adopted by marine geomorphometric studies, since the dynamic four-dimensional (4-D) nature of the marine environment causes its own issues throughout the geomorphometry workflow. For instance, issues with underwater positioning, variations in sound velocity in the water column affecting acoustic-based mapping, and our inability to directly observe and measure depth and morphological features on the seafloor are all issues specific to the application of geomorphometry in the marine environment.

2.4.6 Data Formats

Most measuring systems use different hardware designs, different processing schema and different storage formats. These differences affect accuracy of measured information as well as the type and quantity of relevant meta-data. In some cases the elevation and/or position information is not measured directly but is instead calculated or modeled based on some other measured attribute. Two distinct format categories have emerged, one based on representing each elevation data point as a vector and another based on raster representation.

Elevation information is often visualized as contour lines, a common version of the vector category format is to represent such terrain as data lines rather than data points. The contours are defined by sets of points with connecting relationships indicating how the contour lines connect the points. Such vector information is stored in shape files where each contour is an object, or shape, defined in the file. Data can be represented at its original resolution and form without generalization. In vector form no data conversion is required. Accuracy of geographic location of data is maintained.

For raster data the geographic location of each cell is implied by its position in the cell matrix. Accordingly, other than an origin point, no geographic coordinates are stored. Due to the nature of the data storage technique data analysis is usually easy to program and quick to perform. The inherent nature of raster maps is ideally suited for mathematical modeling and quantitative analysis. Discrete data, is accommodated equally well as continuous data like elevation data, and facilitates the integration of the two data types. Grid-cell systems are very compatible with raster-based output devices, e.g. electrostatic plotters, graphic terminals. Raster data however has downsides; the cell size determines the resolution at which the data is represented. It is especially difficult to adequately represent linear features depending on the cell resolution. Accordingly, network linkages are difficult to establish. Processing of associated attribute data may be cumbersome if large amounts of data exist. Raster maps inherently reflect only one attribute or characteristic for an area. Since most input data is in vector form, data must undergo vector-to-raster conversion. Besides increased processing requirements this may introduce data integrity concerns due to generalization and choice of inappropriate cell size. Most output maps from grid-cell systems do not conform to high-quality cartographic needs. Raster files also have the drawback of needing to store 'no-data' values for each raster cell without an elevation value. Raster files are generally significantly smaller than a corresponding vector file because it does not store detailed position information of point to point relations. Both vector and raster categories have many different implementations of their respective

styles. Specialized applications have been developed just to handle the translation between the many formats.

The Navigation Surface data object represents bathymetry, uncertainty, and methods for the manipulation, combination and utilization of such objects. The Bathymetric Attributed Grid (BAG) file format stores elevation, uncertainty, and metadata in the same raster file. The importance of the format is that it is designed as a universal standard that can contain raw survey data to certified navigation DEM in the same file format. The uniform file format is designed to allow data to be passed seamlessly between different software applications and organizations. Many existing applications that handle DEM are incorporating this standard as an optional format.

2.5 Principal Component Analysis

PCA is a multivariate technique that can be used for analysis of inter-correlated quantitative dependent variables. PCA is a tool for exploratory data analysis and for making predictive models. The goal of the analysis is to determine a set of orthogonal variables called principal components, (vectors along which the data have the most variance), and depict a pattern of similarity of the observations and of the variables as points in maps. In the process the dimensionality of the data set, in which there may be a large number of interrelated variables, is reduced (Jolliffe, 1986) and the variation present in the data can be viewed. The principal components, which are uncorrelated, and are, ordered in such a way that the first principal component retains as much of the variability in the data as possible, and the succeeding components account for the remaining variability. The analysis provides eigenvalue/eigenvector pairs equal to the number of components. The eigenvectors provide the direction for each principal component while the corresponding eigenvalue provides a number indicating the variance in that

dimension. A comprehensive discussion on PCA can be found in textbooks (Hotelling, 1933; Duda, 2001)

The principal components loading can be visualized by a two dimensional biplot. Such a biplot can depict the first two components to visualize the principal component coefficients and the principal component scores for each observation in a single plot for the first two components.

2.6 Multimodal Probability Density Function

Curve fitting of the backscatter PDF data was carried out to validate the results with ANN-SOM analysis. Fitting distributions consist of finding a mathematical function which represents suitable statistical variable. There are three steps in curve fitting of the PDF: i) model/function choice, ii) estimate parameters, and iii) evaluate quality of fit i.e., goodness of fit tests. Accordingly, individual distribution as a Gaussian function (Le Gonidec et al., 2003) was selected. After selecting a function or model, that can mathematically represent given data by mixing of more than one model (i.e., Gaussian mixtures model), estimation of such model parameters becomes important. There are several estimation methods, out of which Maximum Likelihood Estimation (MLE) was employed. MLE is used in statistical inference to estimate parameters. MLE begins with the mathematical expression known as a likelihood function of the sample data. Generally, the likelihood of a set of data is the probability of obtaining that particular set of data given the chosen probability model. For MLE, the expression contains unknown parameters, and these parameters maximize the sample likelihood. Estimated proportions, means and standard deviation without constraints (i.e., floating) are provided after a few iterations, and a good fit of overall and component populations are obtained along with

their mean and standard deviations. Kolomogorov-Smirnov goodness of fit was used for testing the same.

2.7 Power Spectral Density

Seafloor bathymetric data of the submerged objects have an extremely wide range of spatiotemporal scales, necessitating the application of the power law (Fox and Hayes 1985). Power Spectral Density shows the strength of the variations/energy as a function of frequency. PSD shows at which frequencies variations are strong and at which frequencies variations are weak. In the context of seafloor morphology it provides a quantitative characterization of feature amplitude or morphological roughness as a function of scale, which is important for constraining physical models that attempt to predict the relationship between sedimentary processes and seafloor morphology. PSD can be computed using FFT or by computing autocorrelation function and then transforming it.

2.8 Single Channel Seismic Reflector Data

High resolution single channel seismic reflection data was acquired during marine geophysical surveys in connection with hydrocarbon related studies. The single channel sparker profile generally shows long and complex seismic signatures as black and white graphics representing sub-bottom imagery. Sparkers are high-frequency (100–2500 Hz) sound source commonly used during marine geophysical seismic surveys to provide high-resolution imagery of the shallow sub-bottom (i.e., < 1000 m) (Kluesner et al., 2018).

Likewise sub-bottom profiler data use the techniques of reflection seismology to create a 2D image of shallow (<100m) sub-surface geology i.e., a record of acoustic energy reflected by the layers beneath the seafloor (Caress et al., 2008) hence, are capable to give an indication about the sediment volume information. The penetration

capacity below the seafloor differs based on the operating frequency of the profiler. Sparker data along with 3.5 kHz seismic profile provides the best means for interpreting neo-tectonic and sedimentary processes hence widely used in geophysical surveys.

High resolution (4.5 kJ) single channel sparker seismic reflection profile and 3.5 kHz sub-bottom seismic profiler data in the study area was collected earlier and utilized to detect the seismic reflection in the sediments and bedrock over the area. The seismic data sets were used as complementary data for to understand the sub-seafloor structures of the study area in an earlier study.

CHAPTER – 3

THE STUDY AREA

3.1 Introduction

The continental margins of India cover an area of more than 2 million km^2, which is roughly equivalent to two-thirds of the terrain of the country. The margins have their genesis at the time when India broke and drifted away from East Antarctica, Madagascar and Seychelles at various geological times. The Western Continental Margin of India (WCMI) seems to have developed in an oblique rift setting with elements of strike-slip while the Eastern Continental Margin of India (ECMI) appears to have evolved in a complex rift in its northern area and with shear tectonic settings in the southern part (Subrahmanyam and Chand, 2006). Tectonically the WCMI is the divergent and passive type of margin (Thompson, 1976; Pratsch, 1978) with several islands and seamounts characterizing the seafloor. The margin depicts a likeness of extensional tectonics that occurred during continental rifting in the early stages of passive margin formation (Chaubey and Ajay, 2008).

The initial phase of rifting resulted in a system of NNW-SSE trending horsts and grabens parallel to the margin. The geomorphology of the marginal part of western India is mostly controlled by the three principal structural trends of NNW-SSE Dharwar, NE-SW Aravalli orogenies and west-east Narmada graben, displaying a straight coastline. The boundaries of these basins are broadly denned by transverse ridge-type structural features. The offshore region along the WCMI correspond to Kutch, Saurashtra, Bombay and Konkan-Kerala sedimentary basins which have evolved through the rift and drift phases in a passive divergent margin set up. The northern part of WCMI is a geologically a complex region and has significant potential for hydrocarbon exploitation (Rastogi et al., 1999).

The WCMI extends approximately from 07ºN to 23ºN latitudes and 68ºE to 76ºE longitudes. The WCMI has an area of about 310 000 km^2 and can be divided into two parts, an inner shelf with modern clayey silt and silty clay sediments with high organic matter and low carbonate content, and an outer shelf having relict carbonate sediments, coarse sands with low organic matter and high carbonates (Siddique et al., 1987; Rao and Murthy, 1990). The mid-shelf has somewhat an uneven topography, and the outer shelf is intermittently obtruded by shore-parallel ridges and reefs having a relief of 2 to18 m (Faruque and Ramachandran, 2014). The shape of the continental margin having a shelf with varying width (345 km off Daman to 120 km off Goa) and a reduced slope length in the north compared to a narrow shelf (60 km off Kochi) and a longer slope length in the south is markedly evident (Mukhopadhyay et al., 2008). A number of deep-seated faults, reefs and basement highs and ridge systems abound the western continental margin of India.

The study areas are an integral part of the eastern Arabian Sea and the western part of the peninsular shield of India. It fits into the mosaic of various tectonic provinces dating in age from early Archaean (between 550 to 2400 m.y.) to late Proterozoic (2400 to 3000 m.y.) (Kumar et al., 1996; Arora et al., 2012). The general orientation of these structural features is NNW-SSE and parallel to the Dharwarian orogenic trend with several flat-topped bathymetric highs of considerable areal extent, 256 to 1165 km^2 area each at the base. They are interspersed by bathymetric lows, thereby, forming a chain of horst and graben structures covered by thick sediments (Rao et al., 2010). The structures are a consequence of crustal deformation of the South Indian shield (Katz, 1978).

The inner section of the continental shelf is represented by recent clayey sediments while the outer shelf is covered by relict sands (Rao and Wagle, 1997). The surficial sediments of the upper continental slope are clayey sand (50% sand, 31% clay, and 19%

silt) (Rao and Veerayya, 2000) and the lower and mid-slope is covered by silty clay with an admixture of dominant terrigenous and biogenic components (Rao and Rao 1995) .The general slope is in the direction of west-southwest and increases rapidly towards the deep. The latitudinal and longitudinal extents of the study area is 15°29'50"N to 15°37'30"N and 72°47'13"E to 72°52'27"E respectively. The characteristic of the WCMI, wherein the study area is located, is regulated by episodic changes and dynamics related to its tectonic evolution, eustatic sea-level fluctuations, prevailing geology and sedimentation, the pattern of oceanographic circulation and the biological environment.

The geomorphology of the seafloor along the WCMI is driven by many global and local events that occurred in the past. Tectonically, the WCMI is a part of the Indo-Australian plate. It can be inferred that the origin and evolution of the margin are the resultant of the tectonic and sedimentary processes as evolved before and after the collision of the Indo-Australian plate with the Eurasian plate. The WCMI has been formed as a consequence of the break-up of India from Madagascar during mid-cretaceous and from Seychelles during early-tertiary (Bhattacharya and Chaubey, 2001). It has been adduced that a larger area along the western offshore region of India has been submerged in the Arabian Sea thereby impacting the shape and dynamics of the margin. The present-day crustal structures along the western continental margin reflect the pre-existing geology of the region. The WCMI has also been markedly impacted by the eustatic sea level changes over glacial and inter-glacial periods (Rao, 2003) as encountered across the globe. This is evident in form of various submerged geomorphic features (e.g., submerged reefs, terraces, buried channels etc.) formed during the respective tectonic, hydrodynamic and sedimentological regimes (Dandapath et al., 2018)

3.2 Geological set-up

The WCMI is a typical passive (Atlantic type) and dissected margin. A number of deep-seated faults, fractures, reefs, basement highs, and ridge systems have dissected the area (Bhattacharya and Chaubey, 2001; Chakraborty et al., 2006; Mukhopadhyay et al., 2008). The general orientation of these structural features is NNW-SSE and parallel to the coast. The faults in this region are also parallel to the Dharwar Precambrian orogenic trend (Biswas, 1987) that has influenced the depositional pattern. On a regional scale, a series of parallel sets of longitudinal extension faults and NW–SE trending structural features (Laccadive ridge, Laxmi ridge, Prathap ridge complex, Panikkar ridge) abound the western offshore. Ramification and network of all these faults have virtually configured and molded the geomorphology of the study area. Some of these faults act as channel ways for the migration of hydrocarbon gas and fluids (Dandapath et al., 2010; 2012). Reineck and Singh (1980) and the recent studies carried out by Chakraborty et al., (2014a) construed that the upper slope region located in the proximity of the shelf break/edge is influenced by a complex hydrodynamic environment, which also affects the sedimentological regime. Acoustic blanking and Bottom Simulating Reflectors (BSRs) were observed during the recent geological and geophysical surveys in the region (Karisiddaiah and Veerayya, 1994; Satyavani et al., 2005; Dewangan and Ramprasad, 2007).

3.2.1 Oceanographic Condition

The regional oceanic circulations, characterized by seasonal reversal of monsoon-driven surface and bottom currents, summer upwelling and winter downwelling, create unstable oceanographic conditions in the WCMI at ~ 250 m water depth (Amol et al., 2012). Bottom currents are strong and wide (~40 km) and run opposite to the direction of surface currents (Shetye et al., 1990). During southwest monsoon the bottom currents

moving parallely to the coast advance northwards (SSE-NNW), carrying low salinity water and move southwards (NNW-SSE) carrying high salinity water during northeast monsoon. The average current speed and direction in the deeper part of the study area measured using mooring systems at the commencement of the south-west monsoon (June-September), is 12.6 cm/s and 94.5°N respectively. Similarly, during the north-east monsoon (November-February), the mean current speed and directions measured is 12.5 cm/s and 296.6°N respectively (Shenoi and Antony, 1991). The water depth at which the bottom currents is active ranges between 100 m and 250 m (Rao and Rao, 1995).

3.3 Regional setting of the study areas

The study sites entailed in this doctoral work are crucial locations for researchers from other scientific disciplines, as this region offers the possibility of uncovering groundbreaking economic prospects. The seafloor of three distinct areas in the central WCMI, off Malvan to Malpe, in water depths ranging from 30 m to 2000 m, have been examined for seafloor characterization. One of the locations involved represent an area related to gas discharge and occurrence of gas hydrates. The other locale consist of a combination of gullies, ridges and slumps, stretching over 5,310 km^2 offshore Goa, along the slope. The southern part of the study area is distinguished by a shallow seafloor with two coralline banks. The methods employed for the characterization of the seafloor are based on soft computational techniques. The data analyzed represent acoustic measurements of the ship-borne hull-mounted multibeam echo sounding system.

3.3.1 The slope area

The slope area investigated stretches N-S with a combination of gullies, ridges and slumps along the slope in the WCMI. EM302 multibeam system was operated in the outer shelf and upper slope region at the water depths ranging from 150 to 280 m. The

slope morphology of this area can broadly be divided into two subdivisions viz., a) gently (~0.63º) sloping north-eastern part of the study area within the 150-220 m water depth having disoriented fault pattern, and b) the adjoining steep slope (~0.90°) between the water depth 220-280 m along the south-western part featuring NE-SW trending fault system with occasional slumping (beyond the 230 m depth) (Fig. 3.1). The area covers over 5,310 km^2 offshore Goa, with an average slope of 3.11º. The study area is dissected by NNW–SSE trending faults, fractures and a ridge system (Chakraborty et al., 2006; Mukhopadhyay et al., 2008, Bhattacharya and Chaubey, 2001). The area can be described as a formation of gullies and ridges in the north and slump toward the south within a quadrangle that extends from 15º10'N - 16º20'N and 72º10'E - 73ºE. The main controlling factor of the slump appears to be due to the dissociation of adjacent underlying gas hydrates deposits (Fig. 3.1) as reported by Rao et al. (2001). The combination of the gullies, ridges, and slumps has the shelf break and modified the upper slope of this study area. From the earlier studies/surveys in the WCMI, the existence of bottom-simulating reflector (BSR) zone almost 50 km from the present study area has been documented (Dandapath et al., 2010). Current-controlled pockmarks have also been identified in the adjoining area that are indicative of the strength of the bottom currents in modifying the seafloor. Multibeam bathymetric data of the study area reveal gullies of varying length. The gullies are steep-sided confined channels incised by surface and subsurface flow that are common features on the continental slopes (Spinelli and Field, 2001), submarine canyon walls (Lastras et al., 2007) and delta slopes (Maillet et al., 2006). Submarine gullies play important role in the general evolution of continental margins over relatively long periods of time (Field et al., 1999). Gullies are important agents of submarine erosion and down-slope sediment transfer from the upper slope to the continental rise (Dowdeswell et al., 2008). They contribute to the facies of slope deposits (Syvitski et al.,

1996) and also occasionally considered as an important architecture of the petroleum reservoirs (Hewlett and Jordan, 1993).

The upper slope region adjacent to the shelf break experiences complex hydrodynamic environment, which also affects the sedimentological regime of the area (Chakraborty et al., 2014a). In this area bottom simulating reflectors (BSRs) and acoustic blanking were detected during recent geological and geophysical surveys (Karisiddaiah and Veerayya, 1994; Satyavani et al., 2005; Dewangan and Ramprasad, 2007).
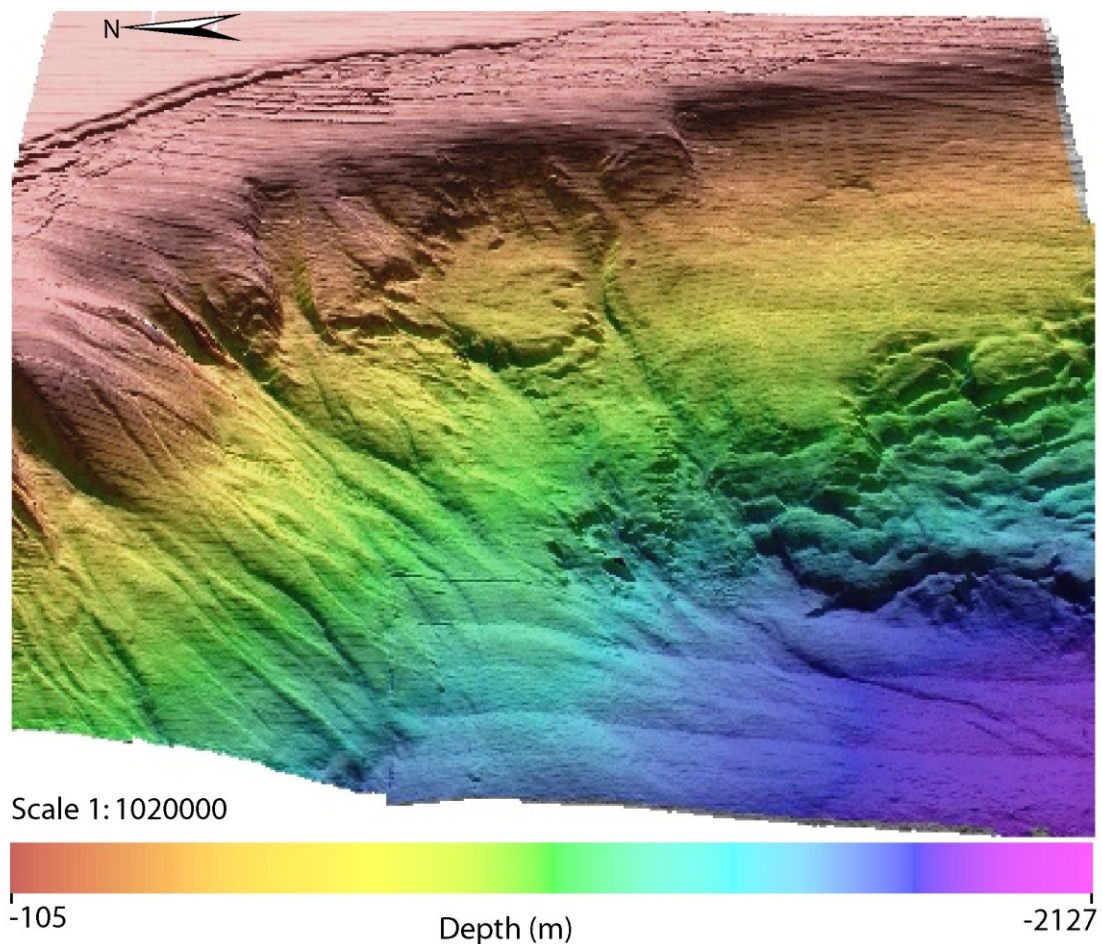
Fig. 3.1 - Multibeam surveyed slope in the WCMI

Earlier studies of the WCMI have reported that the slope region has been subjected to extensive slumping during the late Pleistocene Epoch (Stackelberg, 1972; Shetty, 1972; Hussain and Guptha, 1985; Rao et al., 1988; Guptha et al., 2002). The studies have construed that the slumping in the WCMI was triggered during the Holocene period.

Congruously the Holocene sedimentary processes in the area are found to be greatly influenced by the local dynamics of the current regime and bottom topography. Modern processes are also active, although the late Pleistocene paleotopography appears to be the controlling factor in the spatial distribution of Holocene deposits (Karisiddaiah et al., 2002).

3.3.2 The pockmarked area

The location of study area represents an area characterized by active sediment and transport processes and occurrence of gas hydrate in the WCMI. The multibeam suevey of this area is carried out using EM1002 – a shallow water multibeam system. The area is dotted with pockmarks and fluid seepages and lie in water depths varying from 145 m. in the northeast to 330 m in the southwest, covering nearly 72 km^2 (9.0 km x 8.0 km), with a large number of pockmarks, progenerated by the presence of gas and fluid seepages fronting the outer slope of the margin. The pockmarks might have been produced by the presence of gas or fluid seepages escaping from the subsurface along the faults, mainly in the western end of the area. This study area stretches over 105 km² area and lies at 102 km west off Marmagao (offshore Goa). The general slope is in the direction of west-southwest that increases rapidly towards the deep. The latitudinal and longitudinal extents of the study area is 15°29'50"N to 15°37'30"N and 72°47'13"E to 72°52'27"E respectively. In the recent past due to the discovery of the existence of subsurface hydrocarbon, mainly methane, this area was the focus of much research for its gas hydrates potential (Fig. 3.2).
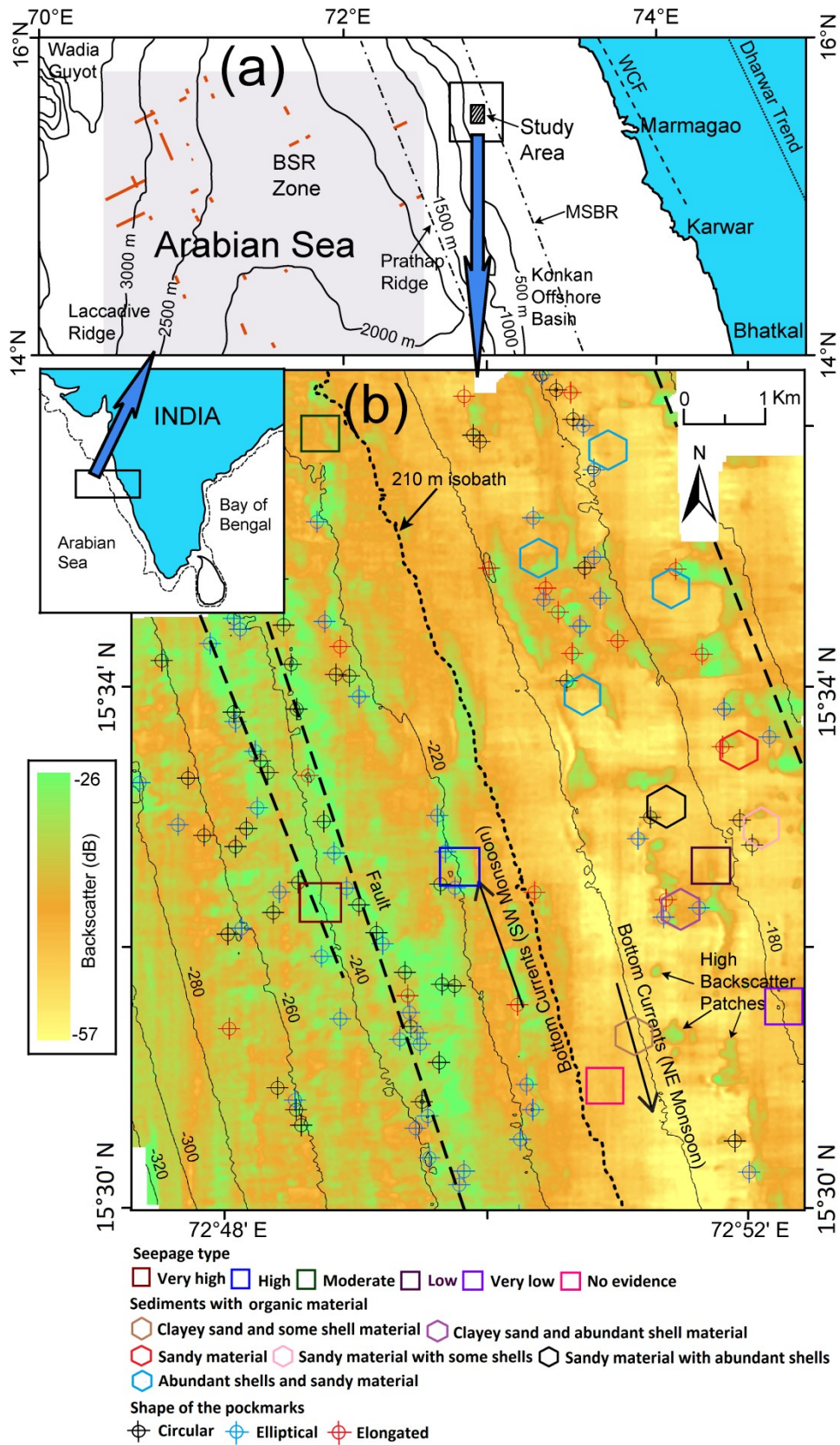
Fig. 3.2 - Pockmark dotted seepage area in the WCMI

3.3.3 The coralline banks

Farther south, another discernible shallow water area with two coralline banks with an atypical environmental setting, away from the seepage area has also been examined. This study area lies off coastal Karnataka in the Konkan basin, the NNW- SSE trending shoreline is aligned with the predominant Precambrian tectonic trend of the crystalline rocks often exposed along the shoreline. Rivers such as the Gangavali, Sharavati and Netravati flow across the coastal plain and have an annual runoff of 1.5×10^{13} m^3 yr^{-1} of water. A series of sand dunes, oriented parallel to the general direction of the coastline, hinders at places the flow of the rivers, thereby trapping sediments and enlarging the alluvial plains. The drainage of the coastal area trending in the East-West direction flows into the Arabian Sea in the west. The western margin of India receives a large sediment supply during the SW monsoon (June-September) (Chakraborty et al., 2016). An underwater current of about 40 km wide at the depth interval between 100 and 250 m, with the characteristic of the Bay of Bengal waters, subsists during the SW monsoon. A southerly surface current, ~150 km wide, develops along the margin during this season in water depths of 50 m on the shelf. During the NE monsoon (November-February), the southerly surface current is replaced by a northerly surface current with signatures of the Bay of Bengal waters intruding onto the SW coast of India.

The Gaveshani bank is approximately 100 km west off Malpe along the Karnataka coast. The bank is about 1500 m wide and 2000 m long and rises 42 m from the seafloor. The area surrounding the Gaveshani bank encompasses a gentle gradient, the main topographic feature being the abruptly rising fringe. The seafloor sediment around the bank is silty sand, predominantly carbonate, consisting of foraminifera shells, mollusks fragments, and corals. The other unnamed bank lies 37 km north of the Gaveshani Bank

with its peak soaring at 55 m water depth. This coralline bank is about 4300 m wide with a maximum length of 5900 m and elevation of 24 m from the seafloor. Both the banks have evolved with distinct geomorphic features such that the Gaveshani bank is unaffected by any attrition, while the unnamed bank is impinged by active seafloor processes (Fig. 3.3). The multibeam survey of this area is carried out using EM1002 – a shallow water multibeam system.
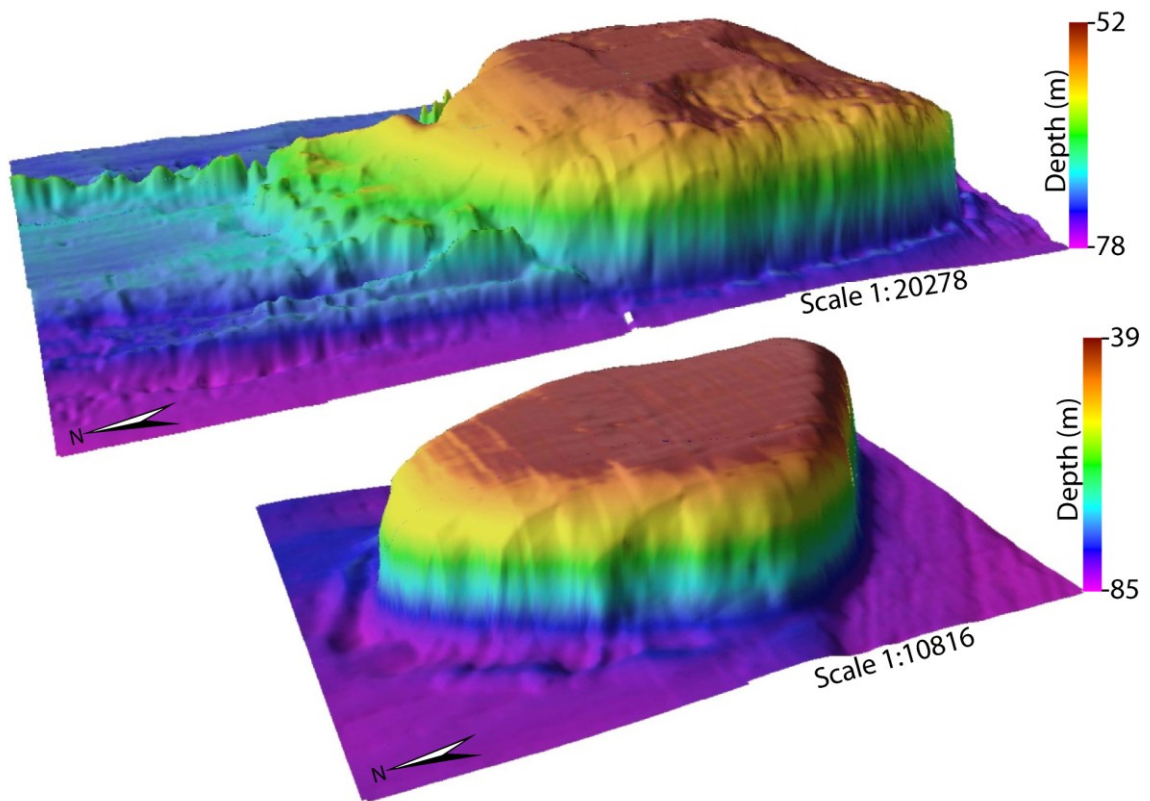
Fig. 3.3 - Perspective view of Gaveshani Bank (bottom) and the unnamed bank (top)

CHAPTER – 4

SLOPE MORPHOLOGY OF WCMI

4.1 Introduction

The high-resolution multibeam data acquired along the slope, off the coast of Malwan-Vegurla-Goa, covering an area of 6,500 km^2, reveal significant facets of the WCMI slope morphology. The fluid flow migration signature in the form of pockmark seepages, traces of mud volcanoes and enhanced reflectors is observed in the area. The area represents a slope configuration of submarine gullies, ridges and an adjacent slump zone. Geomorphic processes such as slumping and mass movements play a vital role in altering the shape and configuration of physiographic provinces along continental margins. Mass movements and sediment mobilization can alter the slope topography and generate turbidite sedimentation on the deep ocean floor along continental margins.

Along the WCMI, several bottom simulating reflectors have been identified on single-channel seismic records, some of them located in areas where slumping and mass wasting are observed (Karisiddaiah et al., 2002). The causes, consequences and degree of geographic variation of these geomorphic processes has been assessed in terms of possible gas-hydrate dissociation during Pleistocene sea-level changes, high sedimentation resulting in under-consolidation, and seismotectonic activity prevailing along the WCMI margin (Rao et al., 2002). One consequence of possible gas-hydrate dissociation along the continental slope could be sediment failure and mass transport down the slope. Contrastingly, in the flat deep-sea areas, gas-hydrate dissociation may have led to gas seepage and the development of pockmarks on the seafloor (Dandapath et al., 2010). Generally, slope failures are explained as being caused by earthquake activity or rapid sedimentation resulting in under-consolidation of sediments. Such causes of slope failure have been hypothesized in other parts of the continental margins across the

world oceans (Dillon et al., 1993, 1998). It could be caused by dissociation of gas hydrates during sea-level low-stands (Kvenvolden, 1993). Many studies have indicated that gas hydrates lying beneath submarine slopes can trigger submarine slides (Shanmugam, 2012). Investigation of morphological processes along the slope and characterization of slope morphology, utilizing both the bathymetry and seismic data are germane to the exploration of the continental margins (Mitchell 2005). Any such investigation can reveal significant facets of the WCMI slope morphology.

High-resolution seismic reflection profiler data were collected normal to the coast, along the central western margin of India with a spacing of 20 km during the 30th and 71st cruises of R.V. Gaveshani. The data were obtained using a Huntec Hydrosonde (main pulse: 5 kHz), and an ORE sub-bottom profiler (3.5kHz) together with side-scan sonar (EG&G Mark IB, dual channel recorder: 259-3 and tow fish 272), and Kelvin and Hughes MS-45 (30kHz) echosounder (Karisiddaiah et al., 2002).

The extent of the area covering the slope morphological studies stretches over 5,310 km^2 offshore Goa, and has an average slope of 3.11º. The area covers the gullies, ridges in the north and slump toward the south within the quadrangle of 15º10'N to16º20'N and 72º10'E to 73º00'E. From the earlier studies/surveys based on the analyses of multibeam bathymetric data coupled with the single-channel seismic data in this region, it was observed that there exist bottom-simulating reflector (BSR) zone almost 50 km from the present study area (Dandapath et al., 2010) [Fig. 4.1(a)].

4.2 Processing of multibeam data

The present work is based on the analyses of multibeam bathymetric data coupled with the single-channel seismic data. The bathymetry data were collected in accordance with hydrographic standards using high-quality (DGPS) positioning, standard sound

velocity profiles, and calibration offsets from a thorough patch-test. The data files for this study area, stored as binary SIMRAD (raw data format), were reprocessed by the author using CARIS HIPS 7.1 and ultimately used to produce a bathymetry grid with a cell size of 15 m.

Further calculations were performed on ASCII gridded data and the gridded data were converted to GIS raster grids for terrain/slope analysis. The geo-referenced data points containing depth values were imported to ArcGIS (Geographical Information System developed by ESRI Inc.). During data processing, the data was checked for good quality, with sounding densities and depth. Spurious data was weeded out particularly on account of the outer beams. Overall the multibeam swath accuracy was well maintained within hydrographic standards of IHO. The data were then interpolated to raster using cubic convolution methods, and subsequently, high-resolution images were generated. Cubic convolution tends to sharpen the data and is more accurate as compared to other methods such as bilinear interpolation. The processed bathymetric grid of the slope terrain resulted with good detail with a few artifacts common while processing multibeam data (Hughes Clarke 2003).

4.3 Slope characteristics vis-à-vis bottom currents and regional circulation

Following the processing the multibeam bathymetric data of the study area, it was evident that the length of the gully is of variable dimension. Generally, gullies are steep-sided confined channels incised by surface or subsurface flow, and are seen as common features on the continental slopes (Spinelli and Field, 2001), submarine canyon walls (Lastras et al., 2007) and delta slopes (Maillet et al., 2006). Submarine gullies play a pivotal role in the general evolution of continental margins over relatively long periods of time (Field et al., 1999). Gullies are important agents of submarine erosion and downslope sediment transfer from the upper slope to the continental rise (Dowdeswell et

al., 2008). They contribute to the facies of slope deposits (Syvitski et al., 1996) and also occasionally considered as an important architecture of the petroleum reservoirs (Hewlett and Jordan, 1993). Studies on the WCMI have demonstrated that the slope region has been subjected to extensive slumping during the late Pleistocene Epoch (Stackelberg, 1972; Shetty, 1972; Hussain and Guptha, 1985; Rao et al., 1988; Guptha et al., 2002). These studies inferred that the slumping in the WCMI was set in motion during the Holocene. Holocene sedimentary processes in the area are controlled primarily by bottom topography and dynamics of the current regime. Although the late Pleistocene paleotopography appears as a basic factor in controlling the areal distribution of Holocene deposits, modern processes also have been influential (Karisiddaiah et al., 2002). Main controlling factor of slump appears to be due to the dissociation of adjacent underlying gas hydrates deposits [Fig. 4.1(a)] as reported by Rao et al., (2001).

The bottom currents generally play a major role in the continental margin sedimentation. They are able to erode, mold, transport and redistribute the sediments supplied to the slope by downslope flows and vertical settings (Weaver et al., 2000). Hovland et al., (2002) demonstrated the strength of bottom currents in modifying the seafloor shape including pockmarks. Similar observation was noticed in the adjacent study area (Dandapath et al., 2010). Bøe et al., (1998) have also reported current-controlled pockmarks elsewhere. The bottom currents in WCMI move northward carrying low-salinity water during the southwest monsoon (summer) and move southward carrying high-salinity water during the northeast monsoon (winter). These currents are parallel to the bathymetric contours (~250 m). This suggests that the bottom currents actively participating in modifying the seafloor morphology indicate higher sediment deposition or erosion. The regional circulation along the WCMI is particularly affected by seasonal reversal of monsoon driven surface and bottom currents reversal of
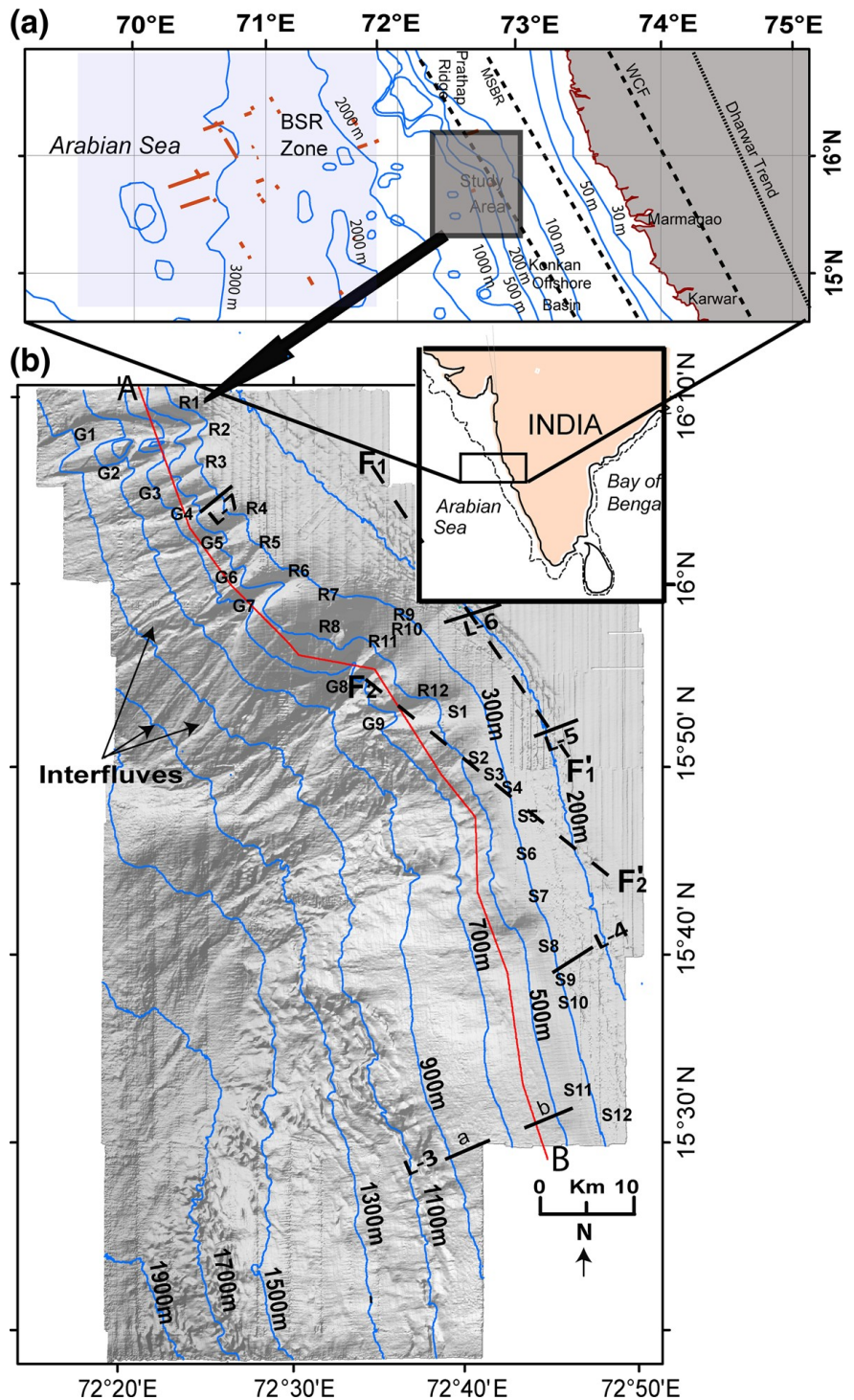
Fig. 4.1 - (a) Location of the study area including some of the main structural features (adapted from Dandapath et al., 2012) of the region. On land, the Dharwarian trend indicated by *dotted lines* is the NNW–SSE trending Precambrian orogenic structure. The west coast fault shown with *thick dotted lines* is different from the Dharwar trend. *Red highlighted lines* and *gray shade* indicate the reported BSRs zone (Dandapath et al., 2010). Traces of two faults are marked as F1–F1', and F2–F2'; (b) Perspective view of the study area in 3D [Fig. 4.2(b)], and the representative seismic sections (6 *black lines*) explained in detail in Fig. 4.3. The locations of thirty-three profiles (Fig. 4.4) of gullies (G1–G9), ridges (R1–R12) and slump zones (S1–S12) are indicated. The northern area visibly indicates characteristic gullies and intervening ridges, whereas the southern area contains hardly any visible gullies; however, interfluves of second generation gullies are observed here. The NW–SE trending line A–B (*red in color*) is the line of view taken of the gullies, ridges and slope zone being studied and depicted in Fig. 4.5.
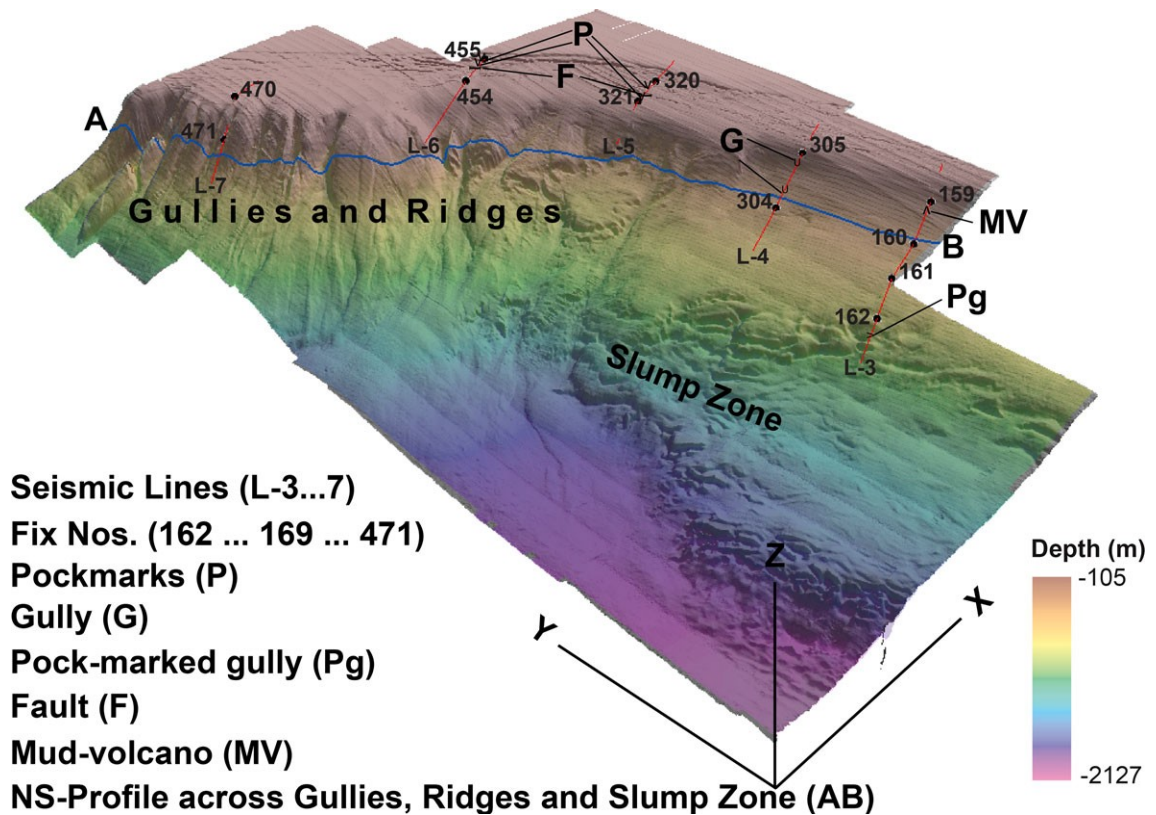
Fig. 4.2 - Perspective view of the study area showing characteristics of gullies, ridges and slump zones. Location of studied pockmarks (P, Pg), mud volcano (MV), two faults (F), gullies (G) are shown along with ridges and slump collectively. AB represents a northwest-southeast trending profile cutting gullies, ridges and slump zone. Fix nos. are given as numerals (162 …169… 471). Thin red lines L-3…7 are the seismic lines that have been evaluated. (Map not to scale).

currents actively participating in modifying the seafloor morphology indicate higher sediment deposition or erosion. The regional circulation along the WCMI is particularly affected by seasonal reversal of monsoon driven surface and bottom currents, summer upwelling and winter downwelling (Naqvi et al., 2010) that create an unstable oceano-graphic condition over the area. A strong coast parallel (NNW–SSE trending) bottom current covering 40 km wide runs through the present study area (Shetye et al., 1990). In view of the observations of Hernandez-Molina et al., (2011) and applying it to our work, it can be postulated that such circulation of water masses might lead to the development of the along-slope currents and generate an erosion and depositional environment within the gullies, ridges and slump zone. Bottom currents investigation using ADCP deployed along the continental margin, off Goa has revealed that there exist a seasonal-based

strong poleward and equatorward currents (~30 cm/s) along the slope off Goa (Stow et al. 2009). The magnitude of the currents is higher towards the slope region (off Bhatkal) in the south than in the north (off Jaigarh) (Amol et al., 2012). This diverse current pattern especially off Goa slope region appears to be one of the influencing factors in controlling and molding the configuration of the slope morphology. The combination of gullies, ridges and slumps has carved the shelf break and upper slope of the study area (Fig. 4.2).

4.4 Seismic interpretation of the line tracks

Single-channel seismic data (4.5–8 kJ) (Fig. 4.3) can provide a wide range of information of the subsurface and help explain the linkage between the pockmarked gullies and the adjacent BSR zone. The seismic reflection profiles [Figs. 4.3 (a-f); L-(3–7)] reveal the presence of pockmarks (P), stratified reflectors (S), acoustically transparent zone (A), unconformity (U), pockmarked gully (Pg) that depicts gas seepage activity, enhanced reflector (E) and trace of mud volcano (MV). Mud volcano is a dome shaped formation caused by eruption of mud or slurries, water and gases. Along the slope, three pockmarks (P) [Fig. 4.3(b); L-6, fixes 454–455] with varying dimension, 159, 79 and 53 m width and 54, 24 and 15 m depth (measured along east to west) respectively, are observed. Also identified are two pockmarks (P) of rounded type and a BG [Fig. 4.3(c); L-5, fixes 320–321]; two slope gullies [Fig. 4.3(d); L-4, fixes 304–305] of width 71 and 60 m and depth of 3 m and 2 m, respectively; shallow dipping reflectors (DR); traces of faults (F1–F10) [Figs. 4.3(b), 4.3(c)], and MV. The entire study area data with a maximum penetration up to 220 m below the seafloor was processed for characterizing the reflectors with variable thickness. An unconformable reflector (U) is seen in the [Fig. 4.3(a); L-7, fixes 470–471], [Fig. 4.3(d); L-4, fixes 304–305], and [Fig. 4.3(f); L-3]. This reflector signifies a surface devoid of deposition, weathering or erosion, depicting a separated grouping of strata with continuity in deposition connecting them. Based on the
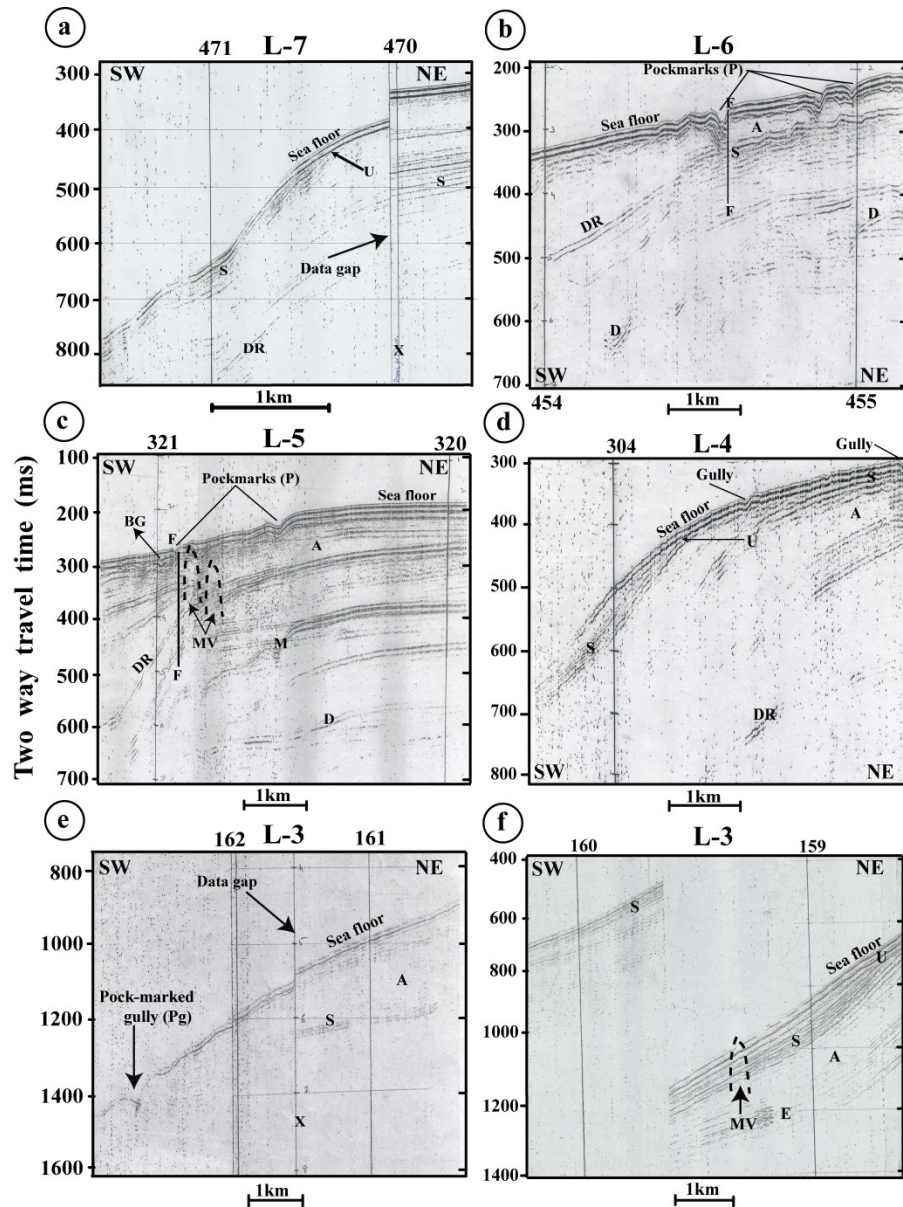
Fig. 4.3 - Single-channel (4.5 - 8 kJ) seismic reflection profiles in the study area off Goa.

(a) A cross-section of line 7 (L-7) (between fixes 470–471) showing typical slope region with stratified reflectors (S), DR and an unconformity (U) at a depth of ~25 m bsf (below seafloor) conspicuously demarcating the sequence boundary of top reflector with the underlying stratified layers.

(b) A transect of line 6 (L-6) showing typical cross-section of three pockmarks (P) with variable dimensions (see text), note the dipping (DR) as well as deep reflectors (D). Max. penetration: up to 350 bsf.

(c) A small portion of line 5 (L-5) showing two pockmarks (P) of rounded type, a BG, shallow DR, traces of faulting (F1–F10), MV, an acoustically transparent zone (A) and deep reflectors (D); M indicates multiple reflector.

(d) This section of line 4 (L-4) depicts a cross-view of two slope gullies that appear as faulted, together with DR, an unconformity (U) and deep stratified reflectors (S).

(e) A small portion of line 3a (L-3a) from the southernmost slump zone shows stratified reflectors (S), acoustically transparent zone (A), an unconformity (U), trace of mud volcano (MV) and an adjacent enhanced reflector (E).

(f) Another small stretch of line 3b (L-3b) from deeper portion shows a pockmarked gulley, depicting gas seepage activity along with stratified reflectors (S). X denotes the gap in seismic data recording for 15 min, depicting changes in topography, resulting in artifact (and not a fault).

classification of Vail et al., (1984), the unconformity recorded here belongs to the second type, wherein the sub-areal surface does not reach the shelf break. Relying on the findings of Gay et al. (2007), it can be implied that in this study area the unconformities and pockmark link appears to be a conduit for fluid migration. The fault traces on to the map trending NW-SE have been demarcated in [Fig. 4.1(b); F1–F1')] while the fault trace (F2–F2') has been extrapolated from the recent reports (Dandapath et al., 2010, 2012).

4.5 Slope Analysis

The processed multibeam data has revealed a slope configuration of submarine gullies, ridges and an adjacent slump zone off Goa, along the WCMI. The quantitative analyses of average slope angle and root mean square (rms) relief relating to slope morphology were carried out following the techniques of Goff (2001) and Green et al. (2007), respectively. The determination of slope curvature was carried out by curve fitting (Adams and Schlager, 2000). The slope analysis (Chakraborty, 2014a) of the thirty three depth profiles from the gully, ridge and slump areas indicate downslope progression in gully incision and varying gradients in the gullies (1.19 - 4.07º) and ridges (2.13 - 3.70º), whereas the profiles of the slump zone are comparatively steady (2.25 - 2.51º). The slope angle is computed by taking the arctangent of the difference in mean depth over adjacent profile divided by the down-slope spacing of the profile. The gradient values and rms relief were estimated at every 100 m water depth along the profile, and the average gradient, depth and rms relief were calculated for the entire profile length. The rms relief represents square root of morphological variance as a function of depth. It measures the average variability about the mean value along each profile. Three slope parameters, gradient, mean depth and rms relief of the depth profiles were made use of, to characterize the slope-confined gullies and ridges of the area on a wider perspective.
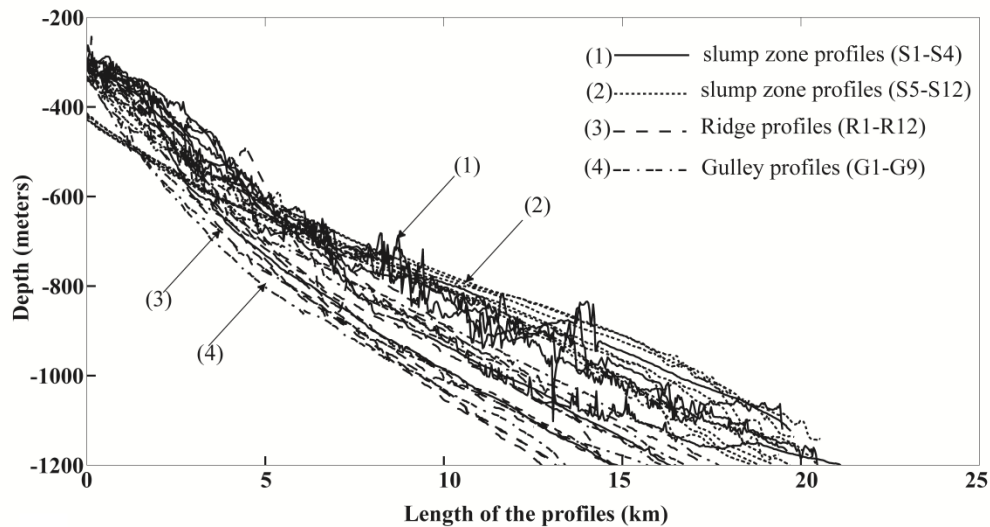
Fig. 4.4 - A composite diagram showing thirty-three depth profiles from the study area comprising of gullies (G1–G9), ridges (R1–R12) and slump zone (S1–S12). Representative undulating slump zone profiles (S1–S4) are indicated as (1), and remaining slump zone profiles (S5–S12) is represented by (2), whereas (3) and (4) represent ridge and gully profiles, respectively.

The focus of this study was to characterize the slope morphology and map its spatial heterogeneity. The gullies can be characteristically described as having higher depth at the central part and lower indention in its lower and higher reaches, as they were formed by the removal of soft sediment due to bottom currents.

4.5.1 Evaluation of slope morphology based on the multi-beam bathymetry

Following the demarcation of the isobaths at 200 m. interval, thirty three profiles were identified considering the configuration of gully, ridge and slump zones [(Figs. 4.1(a) and 4.1(b)]. The profiles include nine from the gullies, twelve associated with the ridges and twelve from the slump zone [Fig. 4.1(b)]. The processed multibeam bathymetric data proffer varying dimensions of the gullies ranging from 3.72 to 18.6 km in length, and their widths ranging from 0.18 to 1.86 km. The mid-width of the gullies typically ranges from 1.5 to 5.7 km and the maximum relief determined is 550 m. The sloping walls of the gullies are steep on the southern side (2.60º) and (2.43º) on the northern side. The initial expression of the gullies is by and large smooth, negative relief

with relatively smooth sloping walls. The relief increases as the inter-gully areas aggrades more than the gully axis. The gullies are relatively linear features that are perpendicular to the contours and act as migration pathways for fluid flow. The transverse section [A–B in Fig. 4.1(b)] of the slope morphology is depicted in Fig. 4.4, and the corresponding profiles are portrayed in Fig. 4.5. The ridges [Fig. 4.1(b)] are contiguous with the gullies and coalesce with each other; their length varies from 5.58 to 16.74 km, while their width is in the range of 0.18 - 0.93 km.
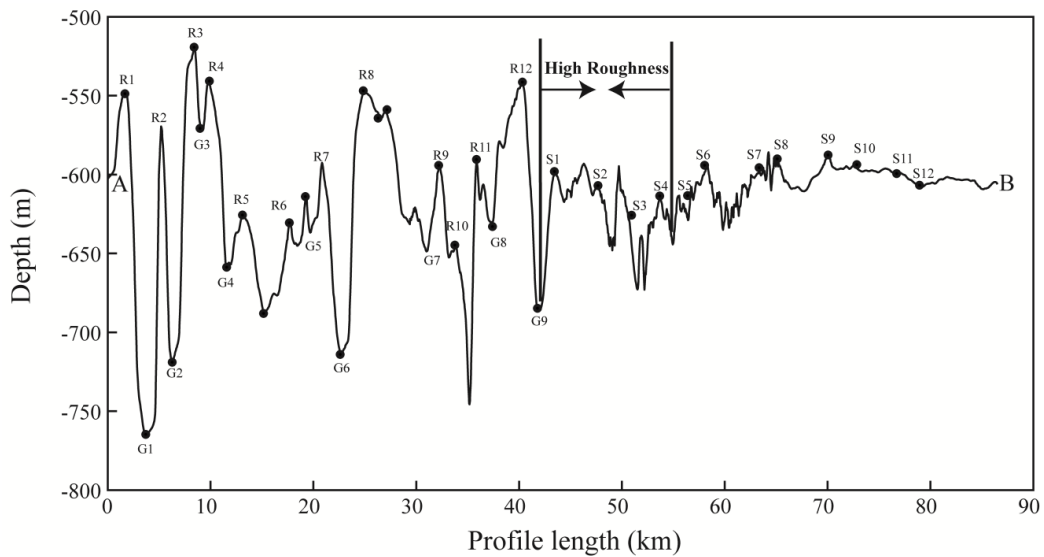
Fig. 4.5 - A schematic line diagram A–B describing in detail all the ridges, gullies and slumps across the chosen profiles. For profile locations, please see Fig. 4.2.

4.6 Principal Component Analysis

Principal component analysis (PCA) can be used for exploratory multivariate data analysis to determine the relationship among the seafloor parameters (Davis 2002). PCA was formulated in statistics and uses an orthogonal transformation to convert a set of observations of possibly correlated variables into a set of values of uncorrelated variables called principal components. Many of the functions of PCA are connected with finding relationships between objects or ascertaining the number of classes of similar objects. In this study, PCA has been utilized to examine the data variability in order to comprehend

the interrelationship between three singular slope morphological characteristics. Thirty-three depth profiles of the gullies in the WCMI were examined using the slope parameters *viz.*, gradient, root mean square (rms) relief and depth. The number of profiles considered is critical and if inappropriate, may influence the accuracy of results. There being no agreed mode for relating the number of observations versus the number of variables, the method conjectured by Good and Hardin (2009) has been resorted to. The gullies for the most part are particularly characterized by higher depth midway along the course compared to both its ends, as they appear to have been formed by the removal of soft sediment due to the bottom currents. A positive correlation could be established between the mean water depth and the rms relief in the gully region. The gullies are also characterized by its gradients with higher roughness in the low-gradient section. Hence, it can be concluded that the gradient of the gullies is reduced with increased rms relief caused by high sedimentation activity. The gully area with characteristic higher depth values is negatively correlated to rms relief and positively associated with the gradient. In the case of ridges located in the northern part of the slope area, distribution of gradient, rms relief and depth is wide as seen in the scatter plot [Fig. 4.6(a)]. It is also evident that there is a considerable variation in rms relief. Hence, it can be attributed that reciprocity between the rms relief and the gradient as well as mean depth is significantly congruous. There is positive association between mean depth values and gradient, while the variation in roughness increases with mean depth. The PCA was used to assess the varying trends of rms relief, gradients and mean depths. The PCA and the scatter plot suggest that the three parameters are influencing factors that control the profile characteristics of the ridge, gully and the slump region respectively. The PCA could establish a fundamental link between the parameters and the thirty three profiles generated along the three different morphological features (gradient, rms relief and depth).
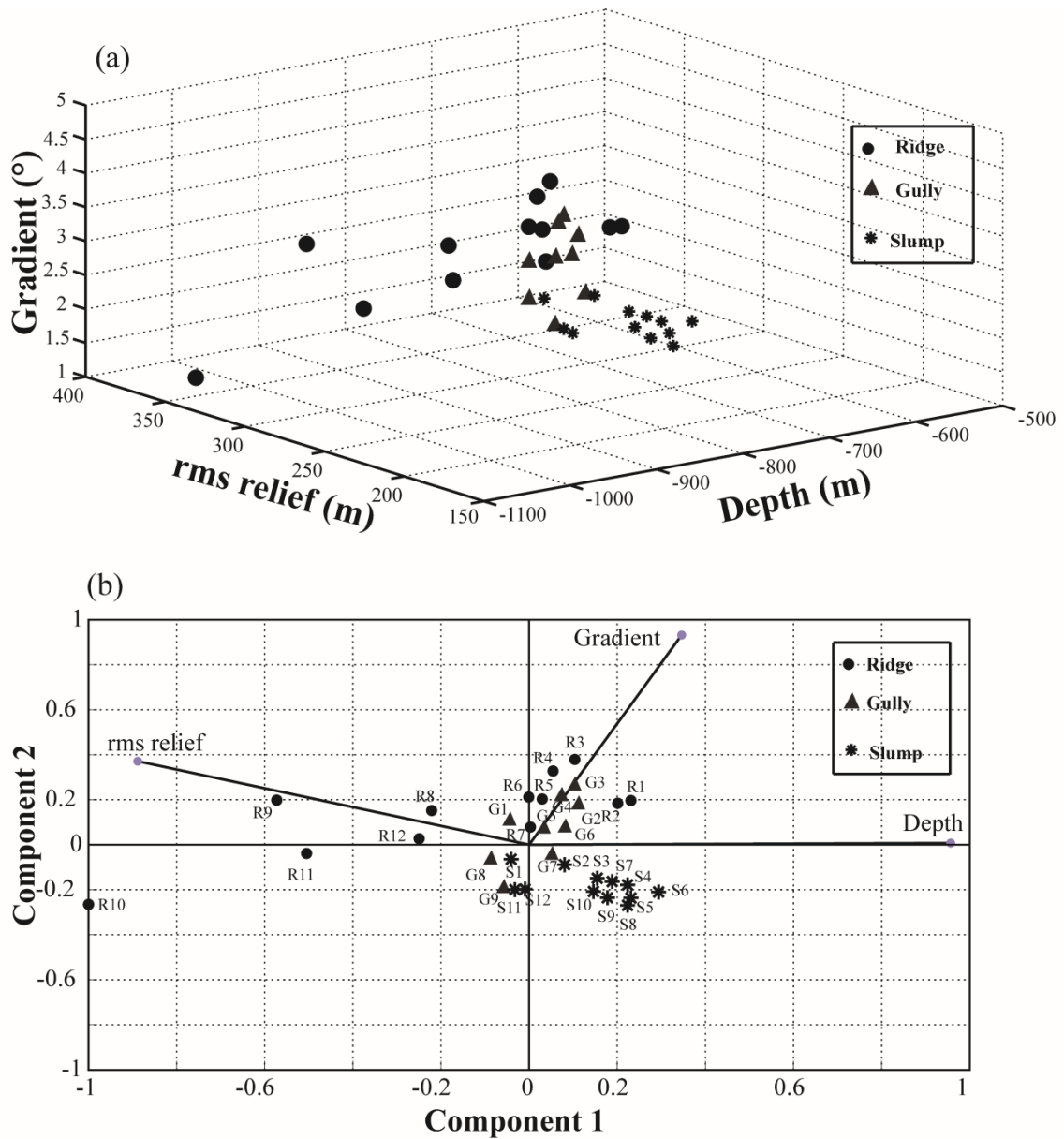
Fig. 4.6 - (a) Scatter plot drawn considering mean water depth, gradients and rms relief of all the thirty-three profiles; (b) Figure represents the biplot that reveals that the profiles in the slump zones are characterized by higher depths and those of the ridges (R8–R12) from the southern area are distinctly associated with higher roughness, while most of the remaining profiles of the gullies (G1–G7) and ridges (R1–R7) from the northern area are influenced by their gradients.

It was observed that the first two principal components (PC1 and PC2) together explain 94.33% of the total variance in the data. The PC1 variance has comparable magnitude (60.81 %) and the variance of the next two PC2 and PC3 is comparatively less (33.52 and 5.67%, respectively). The PCA as indicated in [Fig. 4.6(b)], demonstrate that the profiles (S1to S12) (Fig. 4.5) from the slump zones show similarities and can be grouped together, which may represent processes at greater depth. Similar outcome from

the scatter plot [Fig. 4.6(a)] supports this observation. The biplot [Fig. 4.6(b)] reveals that the profiles in slump zones are associated with greater depths, and those of the ridges (R8 to R12) from the southern area are distinctively correlated with higher rms relief. However, most of the profiles of the gullies (G1 to G7) and ridges (R1 to R7) from the northern area are characterized by steeper gradients.

4.6.1 Correlation and principal component analysis (PCA)

The scatter plot [Fig. 4.6(a)] of three parameters, gradient, rms relief and depth of the thirty three profiles shows prominent clustering for gullies and slumps. In particular, for slumps, there is a positive correlation between the rms relief and gradients. Since rms relief is a measure of the large-scale roughness, it indicates that the roughness is increasing with the slope gradient. However, this reciprocity is noticed often between rms reliefs and depth. The association between the mean depth and the slope gradient is negligible for the slump zone. The gullies are characterized by greater depth midway along the profiles and low depth at its two ends, as they are formed by the removal of soft sediment due to the bottom currents. The correlation between the mean depth and the rms relief in gully area is high. Gullies are characterized by gradients, i.e., the roughness is high for low-gradient region. Hence, it can be concluded that due to the higher sedimentation rate, the gradient is reduced and rms relief is high. The gully region having characteristically greater depth is negatively correlated to the rms relief and positively correlated to the gradients.

In the case of ridges in the northern block, the spreading among the three parameters in the scatter plot is wide [Fig. 4.6(a)], and it is also clear that there is a considerable variation in rms relief. Hence, it is attributed that reciprocity between the rms relief and the gradient as well as mean depth is of significance. A positive correlation is observed between mean depth and gradient. Further, the variation in the roughness

with increasing mean depth is of significance. To compare the performance of the three features, the PCA technique is employed. PCA is an exploratory multivariate statistics that can be used to examine data variability. Here, the PCA and scatter plot suggests that the three parameters, viz., rms relief, gradients and mean depths are influencing factors that control the profile characteristics in the ridge, gully and the slump region, respectively. The gradient values and rms relief were estimated at every 100 m. water depth along the profile, and the average gradient, depth and rms relief were calculated for the entire profile length.

The first two principal components (PC1 and PC2) of the PCA can jointly explicate 94.33 % of the total variance in the data. The PC1 has comparable magnitude (60.81 %), with PC2 and PC3 showing lesser (33.52 and 5.67 %, respectively) values. The PCA analyses also indicate [Fig. 4.6(b)] that profiles (S1–S12) (Fig. 4.5) from the slump zones are consistently groped and may represent the processes at higher depth. The same is also corroborated by the scatter plot [Fig. 4.6(a)]. The biplot [Fig. 4.6(b)] reveals that the profiles in slump zones are characterized with higher depths and those of the ridges (R8–R12) from the southern area are distinctively associated with higher rms relief. However, most of the profiles of the gullies (G1–G7) and ridges (R1–R7) from the northern area are characterized by their steeper gradients.

4.7 Discussion

The scatter plot [Fig. 4.6(a)] bears out that the gullies and slump zones are clustered, whereas the profile parameters of ridges show wide spreading. These observations are well corroborating with the correlation results (please see section 4.6.1) that has been validated using PCA studies [Fig. 4.6(b)]. This signifies that the combination of rms relief, gradients and depths is well suited to discern the profiles of the ridge, gully and the

slump regions. The two principal components (PC1 and PC2) together explicate 94.33 % of the total variance. The PC1 has significant magnitude (60.81 %), whereas the PC2 depicts less (33.52 %). The PCA analyses also indicate that the slump zone profiles (S1–S12) are consistently grouped [Fig. 4.6(b)] as an entity. The biplot [Fig. 4.6(b)] reveals that the profiles in the slump zones are characterized by higher depths and those of the ridges (R8–R12) from the southern area [Fig. 4.1(b)] are distinctly associated with greater roughness, while the rest of gully profiles (G1–G7) and ridges (R1–R7) from the northern area are characterized by their respective gradients.

It is assumed that there is slumping or material flow associated with the four profiles (S1–S4) and the single-ridge profile (R12) [Fig. 4.1(b)]. Interestingly, this postulation could be clarified neither from the scatter plot nor from the PCA. However further study resolved the matter through utilization of a stochastic multifractal technique (Chakraborty, 2014a), which has advantages to address the intermittency in the framework of higher-order nonlinear dynamical system. Nonetheless the three distinct parameters were used to understand the system with multifractal approach (i.e., high dimensionality), that established that the gullies, ridges and slump zones form a separate cluster pattern, signifying a more suitable way for defining fine-scale seafloor aspects (Chakraborty et. al. 2014b). Use of multifractal stochastic processes is not included in the scope of this study.

As stated earlier that the slumping in the WCMI was engendered till the 11ky B.P. (Hussain and Guptha 1985) and the magnitude of the slumping was minimal thereafter. Regardless, it is has been put forward that the formation of methane gas during the Holocene might have also triggered the small-scale process of slumping. This has caused to believe that after the sea level attaining the present state, there are no signs of large-scale slumping taking place. However, the characteristic slump zone in the study area

[Fig. 4.1(b)] with the presence of gas-escape features is an added factor to consider the relevance of this slumping. In that case, Guptha et al., (2002) had shown that the methane-bearing gas charged sediments (Karisiddaiah et al., 1993) might be the main cause of the slumping. Thus, with the pockmarks existing in the region and the investigation of Dandapath et al. (2010; 2012) in their morphological characteristics (e.g., shape, sidewall slope etc.) strengthen the possibilities of slumping.

Further, it is postulated that the vertical rising of gas bubbles and gravitational pulls along the sidewall of the pockmarks might have initiated slumping. Similar events due to upward migration of gas have been also recorded (Ergün et al., 2002). By and large the slope area with the dominant pockmark seepages coupled with the fault traces clearly reflects a structurally weak zone [Fig. 4.1(b) and Fig. 4.2]. The main controlling factor of the slump appears to be due to the dissociation of adjacent deep-seated gas hydrate zones [Fig. 4.1(a)] as reported by Rao et al., (2001). The presence of gully and ridges in the slope region may be related to the Holocene turbidite events. However, these gullies appear to survive more in the northern part of the study area, but the southern slump zone is either masked or has very few such features due to erosional factors. Hence, it can be presumed that the source for such erosional processes may possibly be related to the dominant poleward bottom currents off Goa slope region (during the winter monsoon) than the weaker equator-ward bottom currents (during the summer monsoon) (Amol et al., 2012).

Around the slope region of WCMI under study, the magnitude of bottom currents is higher toward the south (Bhatkal in Karnataka) than in the north (Jaigarh in Maharashtra). Interestingly the cross-section of the profiles along 600 m contour depicts strong erosional effect in the southern part of the slump zone (Fig. 4.4), whereas the effect of erosion is minimal toward the north such that the gully and ridge features are

found to be intact. Therefore, it is postulated that the convoluted nature of the slope containing the four profiles (S1–S4) that tend to change gradually to the extent that they may diminish at a later stage due to the interaction between the diverse pole/equator-ward current patterns in association with the inherent geodynamic fabric of the slope.

There are very few pockmarked gullies [Pg; Fig. 4.3 (e), L-3] in the study area. These are slightly different from the other gullies as the former ones are the fluid flow conduits. These gullies could have formed through the interaction of slope failure and fluid-escape processes (Pilcher and Argent 2007). Their presence in the southern area strengthens the view that probably this area is partly devoid of gullies, even though Fig. 4.5 depicts their presence. It is observed that there is an affinity between pockmark (P) and gullies in the form of fluid flow systems such as few traces of MV [Fig. 4.3 (c, f)] and enhanced reflectors (E), [Fig. 4.3(f)]. Similar observation has been reported elsewhere (Field et al., 1999; Moss et al., 2012). The pockmarks (as reported by Dandapath et al., 2010, close to the study area) are in proximity to gullies and thus might act as preferred escape routes for the migration of gas. The contribution of offshore currents and the negative and positive geomorphic features are not to be viewed as exceptional. It may be relevant to refer to the work of Leon et al. (2006) on the occurrence of offshore currents and their effect on the formation of MV and pockmarks on the Moroccan (Gulf of Cadiz) continental margin.

4.8 Conclusion

The morphological characteristics of the WCMI, off Goa, display varying slope angles for gullies and ridges, while it is comparable in the slump zone from north to south. The seismic construal explains the presence of gas-charged sediments, gas-escape features in the form of fluid flow systems such as pockmarks, MV, enhanced reflectors and pockmarked gullies in the study area. The scatter plot involving average slope

gradient, rms relief and mean depth of the thirty-three profiles depict unsettled huddling of the ridge profiles, whereas the gullies and the slump zones show good clustering. These observations were validated using PCA. However, the presence of slump or material flow along the four profiles (S1–S4) in the slump zone and the single ridge profile (R12) that has been depicted within the mapped area [Fig. 4.1(b)] could not be explicated by means of the scatter plots and PCA. The matter was resolved through utilization of a stochastic multifractal technique that established that the gullies, ridges and slump zones form a separate cluster pattern. Interestingly, the study area holds fault traces [Fig. 4.1(b)] along with the dominant pockmark seepages indicating a structurally weak zone.

Sun et al., (2012) reports that structures that are indicative of focused fluid flow, such as seismic chimneys, mud diapirs, MV, pipes, faults, sand injections and pockmarks, are wide spread in passive and active continental margins, and they have received increasing attention over the last decade due to the wider appreciation of their importance for understanding fluid flow in sedimentary basins. They are also being investigated because of their role in assessing seabed stability. The presence of gullies and ridges in the slope region seems to be connected with the Holocene turbidite events. These gullies appear to be confined within the northern part of the study area. Interestingly the southern slump zone has rendered itself to erosional processes. Hence, we can deduce that the source for such erosional activities may possibly be connected with the dominant poleward bottom currents in the slope region off Goa (during the winter) and the weakened equatorward bottom currents (during the summer monsoon). The slender narrowing of the shelf (15º50"N - 16ºN) changes the aspect of the slope containing the four profiles (S1–S4). The diverse current patterns and the unique seafloor topography portend gradual changes in dislocating the inherent slope morphology.

CHAPTER – 5

SOFT COMPUTATION FOR SEAFLOOR CLASSIFICATION

5.1 Introduction

Soft computing encompasses a collection of computational techniques and algorithms that are used to deal with complex systems (Pal and Pal, 2003). Soft-computing techniques can be an alternative for conventional methods that are time consuming and resource intensive. In comparison to conventional or hard computing, soft computing include methods (fuzzy logic, genetic algorithms, artificial neural networks, machine learning and expert systems) for dealing with ambiguous situations like inexactness, uncertainty to obtain hardy solutions at reasonable costs (Sivanandam and Deepa, 2011). The following are some of the primary methods that fall under soft computing: Fuzzy C-Means (FCM) of Fuzzy Systems and Artificial Neural Networks (ANN) architectures like Self-Organizing Map (SOM) and Multi-Layer Perceptron (MLP).

5.2 Artificial Neural Network (ANN)

An ANN is a biologically inspired mathematical model designed to simulate the functionality of biological neural networks. It can also be viewed as a nonlinear information processing system particularly useful for mapping input vectors to specific outputs (Beale and Jackson, 1990). The basic building block of the ANN is the artificial neuron that can be considered as a mathematical algorithm that learns the relationships and the patterns in a given dataset. ANN have been used in several areas such as process control, chemistry, gaming, radar systems, automotive industry, space industry, astronomy, genetics, banking, etc. and solving of problems like function approximation, regression analysis, time series prediction, classification, pattern recognition, decision making, data processing, filtering, clustering, etc. ANN is an analogy of a biological

neuron (Hertz et al., 1991). The schematic diagram of a biological neuron is shown in Fig. 5.1.
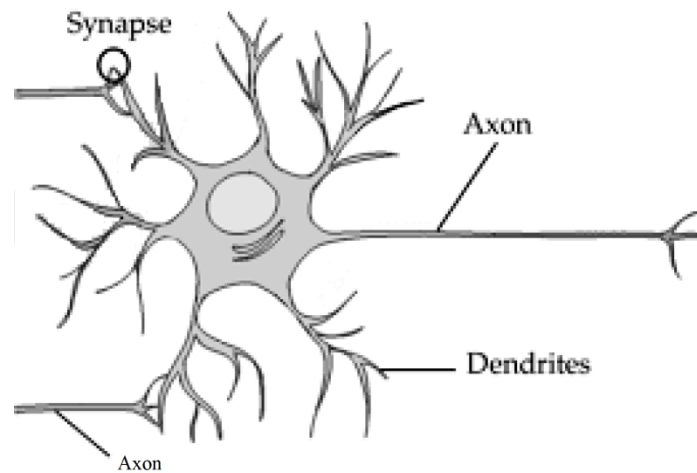
Fig. 5.1 - Schematic diagram of a typical biological neuron

The human brain is composed of about 10^{11} neurons (nerve cells). A typical neuron is divided into three parts: the soma or cell body which contains the nucleus, dendrites - a tree like network, and an axon which is a single long fiber extending from the cell body, the axon eventually branches into strands and sub-strands. The ends of these branches are called synaptic junction or synapses, which transmit signals to the other neurons. The receiving ends of these junctions on other cells may be located on the dendrites as well as on the cell bodies. A few thousand synapses exist on the axon of a typical neuron. Transmission of a signal from one cell to the other through synapses is a complex chemical process. Specific chemicals are released from the sending side of the junction in order to raise or lower the electrical potential inside the body of a receiving cell. When this potential reaches a threshold value, a pulse, called action potential, with certain strength and duration is fired through the axon. The pulse moves from one cell to the other through these synapses. After firing, there is a refractory period during which a cell waits for a specific time, before the next firing.

The aim of an ANN is to replicate the functional behavior of neurons in a brain; its ability to adapt to the current information and changing circumstances. The performance of a neural network is critically dependant on the ability to learn from previous instances and apply this information to future iterations. The fundamental processing element of a neural network is also called a neuron. It receives external inputs that it performs non-linear operations on, and then outputs the final results.

In ANN, several neurons (also referred to as nodes) are interconnected in accordance with some topology to perform a specific task. The output of each neuron may be given to several neurons. The amount of output from one neuron received by another neuron depends on the strength of the connection between the neurons establishing a weight (also called synaptic weight) of the connection links. At any instant of time, each neuron has a unique activation value and a unique output value. In a typical operation, a neuron may receive inputs from any interconnected neurons or from an external source. A weighted sum of the inputs and a specific activation value determine the actual output of an ANN. Therefore, an artificial network consists of architecture (i.e., the topology) of a network, training or learning algorithm (of the weights between neurons), and activation function (Beale and Jackson, 1990)

There are several books (Beale and Jackson, 1990; Hertz et al., 1991; Yegnanarayana, 2001; Sivanandam et al., 2006) that are good resources for ANN. The basics of neural networks and in particular Self-Organising Maps (SOM) architecture/networks are elucidated in this chapter. Later on the approach followed to utilize ANN for seafloor classification using SOM based networks is presented in chapter 6 and chapter 7.

5.2.1 ANN terminologies

A few ANN terminologies are explained here.

5.2.1.1 Weight

The strength associated with the interconnection between two neurons determines a weight for that connection. Weight in neural networks is in reference to the information used by the network to solve a specific problem and the destination it needs to achieve it. The inputs to a neuron may come from the outputs of other neurons or from external sources. Therein the amount of output from one neuron received by another neuron depends on the strength of the interconnection (or weights) between the neurons.

5.2.1.2 Activation Function

The activation function or the transfer function determines an actual output from a neuron. The activation function can be linear or non-linear. Each input signal (say x,) is multiplied by a weight (say w,) and the product is summed. The net input is given by the sum of the weighted input signal.

$$NET = \sum_i x_i w_i$$

In order to produce an output signal, the activation function can be applied to modify the net input (i.e., *NET*). A non-linear activation function is generally used to map a non-linear process. It is also used to ensure that a neuron's response is bounded – that is, the actual response of the neuron is conditioned or dampened as a result of large or small activating stimuli and is thus controllable.

Certain nonlinear functions are used to achieve the benefits of multilayer networks from a single-layer network. When a signal is fed through a multilayer network with linear activation functions, the output obtained remains the same as that which could be obtained using a single-layer network. In that regard, nonlinear functions are widely used in multilayer networks as compared to linear functions. Sigmoidal functions as activation functions are used because of the relationship between value of a function at a point and

value of the derivative at that point that reduces computing difficulty in training. A logistic function also termed as logistic sigmoid function or unipolar sigmoid function (S-shaped curve), is used for its self-limiting nature or a squashing function (Sivanandam and Deepa, 2011; Beale and Jackson, 1990; Hertz et al., 1991).

5.2.1.3 Bias

The *bias* is included by adding the product of a bias weight (say *b*) with input signal (x_0 = 1) to the net input; if introduced the *NET* is calculated as $(NET = b + \sum_i x_i w_i)$. It is often advantageous to have a bias weight for rapid convergence of a training process. Bias weight allows the neuron to have an output even if the input is zero. The main purpose of the bias is to shift the origin of an activation function. These weights are trainable just as well as the other weights. (Sivanandam et al., 2006),

5.2.1.4 Threshold

The threshold is a limiting value of a neuron to produce an output. The weighted sum of inputs (NET) must reach or exceed the threshold value (Hertz et al., 1991) for a neuron to fire (i.e., to get an output). Its behavior can be represented as $f(NET) = \begin{cases} 1, & NET \geq \theta \\ 0, & NET < \theta \end{cases}$ where θ is fixed threshold value.

5.2.1.5 Training

Training can be referred to as learning process with an objective to achieve an expected output by modifying the weights of the interconnection between different layers of the network (Sivanandam et al., 2006). There are three types of learning such as supervised learning, unsupervised learning, and reinforcement learning. Supervised learning of a network makes use of target vectors. The input and the target vector together are known as a training pair. If expected target vectors are not available, the training method adopted is unsupervised learning. In the unsupervised learning, the weights of the network are adjusted in such a

way that similar input vectors are grouped or clustered for assignment to the same output unit. Reinforced learning is similar to supervised learning, but the network receives some feedback from its environment called a *reinforcement signal.* While in supervised learning the target output values are known for each input pattern, in some cases less information might be available. For example, the network might be told its actual output *is* only "50% correct" or so. Thus, here only critic information is available and not the exact information. Feedback obtained however, is only evaluative and not instructive. External reinforcement signals are processed in the critic signal generator, and the obtained critic signals are sent to the ANN for adjustment of weights properly so as to get better critic feedback in future. (Sivanandam and Deepa, 2011)

5.2.2 Fundamental Model of ANN

McCulloch and Pitts (1943) formulated a synthetic neuron model, based on the concept of a simplified biological model. The input values are connected to neurons either by excitatory (positive) or inhibitory (negative) weights. A neuron fires if the net input to the neuron is greater than a threshold value. Any number of inputs can be added to a neuron.

5.2.3 Perceptrons

The simplest form of a neural network is a single layer perceptron. This type of network model is generally used for the classification of patterns that are linearly separable. A layered feed-forward neural network is a multi layered perceptron. Rosenblatt (1962) and Minsky and Papert (1969) developed this perceptron. Originally it had three layers e.g., sensory unit (input), association unit (hidden), and response unit (output). The sensory units are connected to association units with fixed weights having values 1, 0 or -l, which are assigned at random. The binary activation function is used in sensory unit and associator unit. The response unit has an activation of l, 0 or -1. The binary step with fixed threshold θ *is* used

as activation for associator. The output signals that are sent from the associator unit to the response unit are only binary. All the units have their own weights. The association unit performs the predetermined mathematical operations on its inputs. The perceptron model differs from the McCulloch-Pitts model by the learning function (adjustment of weights) introduced in the perceptron (Sivanandam et al., 2006). The desired or target output (T) is compared with the actual output (y), and the error (δ) is calculated to adjust the weights. The output signal is given by $y = F(NET)$, where $(NET = \sum_i x_i w_i + b - \theta_{th})$. The error term is calculated as, $\delta = (T - y)$. If the error associated with the input vector x_i is δx_i, then the change in weight (Δw_i) is expressed as, $\Delta w_i = \eta \delta x_i$, where η is called the learning rate parameter (Yegnanarayana, 2001).

5.2.4 Network Architectures

Neural network architecture is the arrangement of neurons into layers and the pattern of connections among the neurons in various layers (Beale and Jackson, 1990). The number of layers or the number of neurons in a layer has no maximum limit. However, computational requirement increases with the increase in the number of neurons (and weights). Various types of network architectures exist such as feed forward net, feedback net, competitive net, and recurrent net.

5.2.5 Kohonen's Self Organizing Map (SOM)

Two basic methods of learning namely supervised and unsupervised are means that networks learn to execute a specific task. An unsupervised learning method called competitive learning has only one neuron in the output unit. Only one neuron in a group is a winner and therefore this neuron is often called the winner-take-all neuron (Hertz et al., 1991). Based on its inherent characteristics, the objective of such networks is to cluster or categorize input data. Unsupervised learning method operates with unlabeled

input data. Calculation of error (between desired target and achieved output) is not required to train such networks. The network itself discovers patterns, similar features, and regularities in an input data. Kohonen's Self Organizing Map (SOM) is such a network (Kohonen, 1989, 1990). On the other hand, for networks learning from labeled sets of input data or supervised learning; the classes are predefined and each training data is tagged with a correct class in a supervised architecture.

Professor Kohonen (1990) proposed an unsupervised neural network called Self Organizing Map. Its architecture consists of two layers, an input layer and an output layer. There exist feed-forward connections to every neuron in the output layer for each in the input layer. Fig. 5.2 illustrates a Kohenon network in two-dimensional grid. Here the neurons are not arranged in layers as in a multilayer perceptron (input, hidden, and output) but rather on a flat grid. The goal of the network is the mapping of n-dimensional input vectors into one- or two-dimensional lattice (of the output layer). For a given input vector, one and only one neuron with the maximum value in the output layer is set to a logical one (winner) and all other neurons are set to zero.
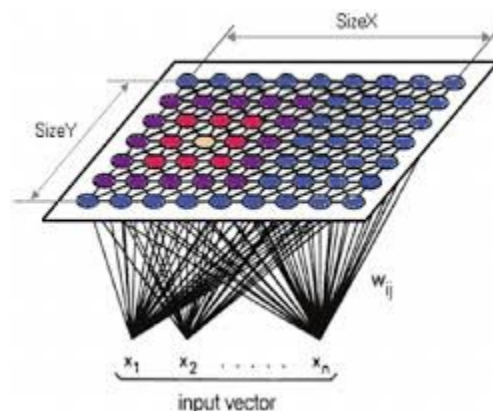
Fig. 5.2 - A two-dimensional SOM network

In general, input data (or input vectors or patterns) are normalized before applying to a Kohonen Network. Normalized input vector is obtained from each component of the input vector by dividing the length of the vector. Randomly initialized weight vectors are

also normalized in these networks. Various steps in the training of a SOM network are as follows (Beale and Jackson, 1990).

5.3 ANN-SOM architecture for seafloor study

Artificial neural networks (ANN) are generally employed in classification systems on account of its relatively fast, computationally cost-effective and reliable delivery compared to other applications. In this study, the potentiality of ANN has been made use of for seafloor data classification. In this regard, the SOM based ANN developed for classification of seafloor data, and its successful application to data from the pock mark dotted seepage area of the WCMI, was subsequently adopted for other marked locales in the WCMI.

For classification of the seafloor using multibeam sonar data, the choice of a practical and effective classifier is required. Hence preprocessing of the multibeam backscatter and bathymetry is a prerequisite. The processed multibeam sonar data is used to produce bathymetric maps, and image mosaic from the backscatter data. Several methods in connection with classification and characterization of the seafloor exist (Chakraborty et al., 2000, and references therein). Neural network methods (Chakraborty et al., 2000; Chakraborty et al., 2001; Chakraborty et al., 2003a) using echo features derived from multibeam data, have been found effective for efficient classification of the seabed. Besides echo features, other input variables like seabed roughness derived from bathymetry data can be utilized for classification of the seafloor. Neural network classifiers being non-parametric have an advantage over statistical methods.

It can learn from association by going through different examples of classes and ascertaining the similarities and differences between them, which is similar to the process of the brain establishing a pattern with repeated association of a pattern, thus building a

dynamic association over a period. ANNs can also learn based on principles of self-organization, unsupervised learning where learning is solely based on training inputs. This classical method of making use of unsupervised architecture called Self Organizing Map (SOM) has been well documented for single-beam (Chakraborty et al., 2001, Chakraborty et al., 2003a, Chakraborty et al., 2004) and multi-beam backscatter data (Alexandrou and Pantzartzis, 1993; Michalopoulou et al., 1995; Chakraborty et al., 2003b; Zhou and Chen, 2005). ANNs are now commonly used for classification in data science. It can categorize a group of feature vectors into classes besides allowing new data (input) to be accordingly categorized. The SOM algorithm, also known as Kohonen's SOM neural network based on unsupervised competitive learning, can automatically learn the classification of input vectors according to the nearest-neighbor method by calculating the Euclidean distance (Kohonen, 1989, 1990). SOM has wide ranging uses in data exploration.

5.4 ANN-SOM for seafloor classification

Multibeam echo-sounding (MBES) systems allow coincident acquisition of high-resolution seafloor backscatter and bathymetric data (Mayer, 2006; Simons and Snellen, 2009), which enormously sustains the marine exploration applications. The remotely acquired bathymetric and backscatter data respectively reveal large-scale as well as fine-scale seafloor roughness (at the textural level) (Fox and Hayes, 1985; Goff et al., 1999). In general, the quantitative or inversion models are not directly applicable to the acquired data, and hence, the bathymetric and backscatter data preprocessing is imperative before modeling is employed (Haris et al., 2011). Quantitative model application using non-stationary data is a major obstacle as most of the models presume that the input data are stationary, and therefore the application of segmentation techniques to divide the data set into stationary segments become necessary (Malinverno, 1989).

ANN is a powerful tool for solving classification problems. In the past, ANN techniques have been proposed for hydro-acoustic data classification (Chakraborty et al., 2001). An ANN can learn the classification task from a set of examples known as training set. The Kohonen's Self-Organizing Map (SOM) is a competitive-learning neural network that can be trained to classify the input vectors according to the nearest-neighbour method by calculating the Euclidean distance. SOM can efficiently carry out the classification without any *a priori* knowledge of the data classes of the surveyed area. SOM is a neural network architecture that has the determinant ability to uncover the underlying patterns in the input data to cluster or categorize the input data based on its inherent characteristics. The unsupervised learning is solely based on the unlabeled input data and not dependent on any target output vector. The SOM network can recognize patterns, compare features and ascertain similarities in the input data.

ANN based self-organizing map (SOM) architecture exercises unsupervised competitive learning on the unknown data set (input) onto coarser clusters, i.e., primary classifications (Chakraborty et al., 2003b). The employed SOM architecture is comprised of a flat 1-D neuron grid. The feature vectors are connected to the SOM network. The study carried out involves the employment of SOM for the characterization and classification of pockmark dotted seepage seafloor (Chapter-6) and coralline banks (Chapter-7). The backscatter and roughness data are utilized as the input feature vectors to the SOM architecture. On presenting the input vectors to the SOM architecture, the neurons in the grid compete among themselves to get activated. The weights of those neurons in its neighborhood are updated iteratively to form a representative cluster (refer to Chakraborty et al., 2001) for more details about the neighborhood reduction technique used in the SOM). This is known as tuning of the weights in response to a given class of input vectors. The SOM algorithm organizes the nodes in the grid into local

neighborhoods that act as an input feature. An initial weight matrix having a small random value is used. Initially, two input feature vectors are presented as a training sample, and then the Euclidean distance (d_j) between the input vector and the weight of the neurons in the 1-D grid is computed

$$d_j = \sum_{i=1}^{j} [x_i(t) - w_{ij}(t)]^2$$

where $x_i(t)$ is the input vector to node i at time t, and $w_{ij}(t)$, $0 \le i \le n\text{-}1$, is the random weight vector from input nodes i to j for initialization of the weights from n inputs to the nodes having small random values. Only one neuron having the least distance is designated as the "winner" neuron and as a result this neuron is often designated the winner-take-all neuron (Hertz et al., 1991). The weights of this neuron are updated, and the distance matrix is computed iteratively for the same input vectors to minimize the error through the use of the expression

$$w_{ij}(t+1) = w_{ij}(t) + h(t) \times [x_i(t) - w_{ij}(t)]$$

This procedure is invariably repeated a number of times until the value of d_{min} (the minimum distance) is reduced below that of a pre-specified error value. The term h(t) is a learning function $(0 < h(t) < 1)$, gradually reducing the magnitude of the weight update as the error is successful. The neighborhood size also decreases as the number of iterations increases, thus localizing the area of maximum activity in response to input vectors in the SOM architecture (Chakraborty and Haris, 2012). To determine the number of classes using the SOM architecture, two input feature vectors of each data point are presented to the random weight matrix (1 x 50) and the nearest neuron is selected to be the firing neuron for the input data.

The closest neurons on either side of the firing neuron are updated using the learning function $[h(t) \sim X/t^{0.2}]$ (Chakraborty et al., 2001). As t increases, the neighborhood is reduced to one, i.e., at the end, only the firing neurons are updated. The value of $h(t)$ gets altered from its initial value of X. The training stops when the error is less than the pre-assigned value or reaches the pre-set 't' value. Each time a new input class is presented to the network, the winning node must first be identified. This marks the region of the map that will have its weights updated. In this study, the number of iterations to reach the pre-specified error value is optimized based on the purposed testing of the data. The testing of the input features commences once the training is completed, and the excited neurons during the testing processes are plotted. If testing results show that the winning neuron exists within the cluster (a group of five neurons around the central neuron) of the trained neuron, then it is assumed to be belonging to the same class as the data where it was trained earlier. Otherwise, further training is initiated in the search of a firing neuron, and the training/testing process is resumed. At the end of the training/testing process, the percentage of the number of times the different neurons have been excited is plotted as a bar diagram with respect to the neuron numbers. The maximum numbers of classes are equal or larger than the number of occurrences, i.e., 20% of the highest neuron firing. Though the soft-computational technique (SOM) is useful for real-time data classification purposes, there is a necessity to validate the extent of success employing other relevant discrete techniques.

5.5 Fuzzy logic

Soft computing is a combination of several methods, such as fuzzy logic, neural networks, and genetic algorithms that can complement each other and can be used jointly to solve a given problem (Buckley and Hayashi, 1994). Fuzzy logic is tolerant of imprecise data and is based on natural language that often cannot express an event as 'true' or

'false' (but rather as 'partially true'). Fuzzy logic deals with in terms of logical variables that take continuous values between 0 and 1. Normal digital logic operates based on discrete values of either 1 or 0 (true or false). The inputs to fuzzy systems are general mapped by sets of membership functions, known as 'fuzzy sets'. The fuzzy logic system can be considered as a nonlinear mapping of input data set to a scalar output data. The process includes 'fuzzification' that converts a crisp input value to a fuzzy value, and conversely defuzzification. Thereupon, an inference is made based on a set of rules, and the resulting fuzzy output is mapped to a crisp output using the membership functions, in the defuzzifiation process. The combination of fuzzy logic and neuro-computing leading to neuro-fuzzy systems has been an important development having varied applications.

5.5.1 Fuzzy c-means

Fuzzy c-means (FCM) is one of the most frequently used fuzzy clustering algorithms. Clustering of numerical data forms the basis of many classifications. The purpose of clustering is to categorize the natural groupings of data from a larger data set. It involves the task of dividing the data points in the set into homogeneous classes or clusters so that items in the same class are as similar as possible and different from items in other classes. The classes themselves would be as dissimilar as possible. In other words it is a means for grouping the data in such a way that observations are more alike within a group and differing from the observations in other groups.

Clustering by FCM is more flexible (say) as compared to Fuzzy K-means, because it depicts the objects as having some interface with more than one cluster in the partition. In hard clustering, the data is divided into neat clusters, where each data point belongs to exactly one cluster. In FCM, the data points can belong to more than one cluster with a varying measure of association. Each data point would be associated with what could be

called membership grades which indicate the degree to which the data points belong to the different clusters. In our work we have utilized the Fuzzy c-means - **fcm** function implemented in MATLAB, for clustering the input data to SOM network for identifying the segments.

In MATLAB[©], the Fuzzy Logic Toolbox[™] the function **fcm** performs the FCM data clustering, in which the dataset is grouped into *n* clusters with every data point in the dataset belonging to every cluster to a certain degree, i.e. a certain data point found close to the center of a cluster will have a high degree of association or membership to that cluster, as compared to another data point that lies away from the cluster center would have a less degree of belonging or membership to that cluster. The function **fcm** starts with an initial guess for the cluster centers, which are projected to signify a normal location of each cluster. The initial presumption for these clusters may not be the correct one. The function **fcm** then assigns every data point a membership grade for each cluster. By iteratively updating the cluster centers and the membership grades for each data point, the **fcm** function iteratively moves the cluster centers to the 'correct location' within a data set. This iteration is based on minimizing an objective function *J* that represents the distance from any given data point to a cluster center weighted by the membership grade of that data point which can be expressed as (Mingoti and Lima, 2006):

$$J = \sum_{i=l}^{n} \sum_{l=1}^{c} (w_{il})^{\lambda} \, d_{il}^{2}$$

restricted to the condition $\sum_{l=1}^{c} w_{il}=1$; $i = 1, 2,\dots n$, where w_{il} is the degree of membership of object *i* to the cluster *l*, $\lambda >1$ is fuzzy exponent that determines the degree the degree of fuzziness of the final partition, or in other words the degree of overlap between groups, d_{il}^{2} is the squared distance between the vector of observations of object *i* to the vector representing the centroid (prototype) of cluster *l* and *n* is the number of sample

observations. The solution with highest degree of fuzziness is related to λ approaching to infinity. Fuzzy c-means is generally stable even in the presence of outliers and overlapping data. However in fuzzy clustering the desired number of clusters *n* has to be predefined which in our case has been adopted in synchroneity with the SOM network output. Clustering data along the profiles help identify the data segments using FCM algorithm.

5.6 Conclusion

In this chapter SOM-ANN and FCM has been briefly presented. The SOM based unsupervised method essentially reduces the requirement for collecting a voluminous data in an unknown area. This method can be efficiently used in combination with other data classifiers. Moreover, the FCM based data-driven features selection process can also be used as a preprocessor with other existing classification methods for improving the success in the classification of the seafloor.

CHAPTER – 6

POCKMARK DOTTED SEEPAGE AREA

6.1 Introduction

A number of studies have been conducted along the WCMI (shelf and slope region) mainly because of its proximity to coast and high resource potential. The coral reefs wherever it exist, present biological diversity. Generally the seafloor topography can be broadly divided into comprehensive geomorphological units with distinct characteristics. The continental margins consist of shelf, slope and the rise, often incised by submarine canyons, trenches that make it to the abyssal plains. The seafloor has its fair share of seamounts, reefs, guyots and the characteristic mid-oceanic ridge systems (Garrison, 2010). The present study engages a combination of soft-computational (SOM and FCM) and numerical techniques (power spectral density at short and fine scales) to effectively characterize the seafloor, along with the processes and the associated sedimentological dynamics in a complex geographical environment (including the pockmarks and faulted structures) that are subjected to strong bottom currents and seasonal upwelling.

The multibeam data used for classifying the pockmarked seepage area was acquired from the WCMI, off Goa. Kongsberg Simrad EM 1002 MBES operating at 95 kHz on board the CRV *Sagar Sukti*, was used during the coastal marine surveys (Cruise no. SaSu-118), in November 2006, for mapping the study area (the pockmarked seepage area). The survey lines were oriented parallel to the coast in N-S direction. The water depth of the surveyed area varied from 145 m in the northeast to 330 m in the southwest region [Fig. 6.1(a)] (Dandapath et al., 2010). The survey covered nearly 72 km^2 (9.0 km x 8.0 km), revealing significant numbers of the pockmarks that are produced by the presence of gas or fluid seepages escaping from the subsurface along the faults, largely in

the western part of the area. The presence of such seepages has economic significance as an indicator for hydrocarbon occurrence (King and MacLean, 1970; Hovland and Judd, 1988). This study area is also characterized by active sediment transport processes.

A general discussion of the data processing schemes are covered in Chapter 2. Here, a brief coverage of the multibeam data processing is provided. The MBES data recorded was corrected for propagation and other effects including tide corrections using Neptune software for bathymetry data. PROBASI II, software developed (in house) for processing backscatter data (Fernandes and Chakraborty, 2009) and data normalization. The CFLOOR (Cfloor AS) software was utilized for improved visualization and gridding (grid resolution: 10 x10 m). The geo-referenced backscatter strength (dB) and depth values (m) were imported to ArcGIS. The data were then interpolated to raster using cubic convolution methods and subsequently high resolution image with distinct color scheme was generated. Cubic convolution tends to sharpen the data as compared to other methods such as bilinear interpolation etc. Cubic convolution technique employs weighted average values of the sixteen nearest input cell centers, whereas bilinear interpolation method uses only four nearest input cell centers to determine the value of the output raster.

The backscattering strength of this area ranged from 25 to 57 dB (Fig. 6.1b). The angular back-scatter data strength usually show higher values at normal incidence angles compared to the outer beam angles, thereby engendering artifacts that have to be eliminated. Further enhancement of the image data quality was carried out employing a four-stage image processing technique. The remotely acquired bathymetric and backscatter data, revealed large-scale as well as fine-scale seafloor roughness respectively, albeit at textural level (Hughes Clarke, 2012; Blondel, 2009).

6.2 Study Objectives in the Pockmark dotted Seepage Seafloor

This study aims to advance the understanding of the fine-scale roughness associated with the seepage-related seafloor. Generally, the quantitative or inversion models are not directly applicable to the acquired data, hence the bathymetric and backscatter data preprocessing is imperative before modeling is employed (Haris et al., 2011). However, quantitative model application using non-stationary data is a major impediment as most of the models presume that the input data are stationary, therefore the application of segmentation techniques to divide the data set into stationary segments becomes indispensible (Malinverno, 1989). Therefore, the success of the remote acoustic model parameter estimations engages data segmentation techniques. This leads toward the development of soft computing techniques that can be used for dimensional reduction applications, representing input vectors to a specific output (Kohonen, 1990; Alexandrou and Pantzartzis, 1993; Michalopoulou et al., 1995). The soft-computing technique including artificial neural networks (ANNs) employs inexact solutions for computationally difficult tasks. In the past, ANN techniques were proposed for hydro-acoustic data classification (Chakraborty et al., 2001). ANN based self-organizing map (SOM) architecture exercises unsupervised competitive learning on the unknown data set (input) onto coarser clusters, i.e., primary classifications (Chakraborty et al., 2003a). For realtime survey applications, the SOM can be utilized to formulate a decision regarding the number of data classes during the online data acquisition that are then used as an input to the fuzzy C-means (FCM) algorithms for data segmentation (De and Chakraborty, 2009). FCM will require the initial information about the number of available data classes obtained using the SOM architecture. Once the profiles are segmented, the spectral techniques, e.g., the power spectral density (PSD) function of the spatial data as a function of frequency (Fox and Hayes, 1985; Berkson and Matthews,

1984; Chakraborty et al., 2006), are required to calculate the seafloor roughness parameters. Accordingly, the seafloor spectral parameters such as power law exponent (β) and intercept (a') of the segmented geomorphic regions are estimated. The curve fitting of the power law function in the log_{10} - log_{10} plot of the PSD versus the wave-number (k) curves of the backscatter traces are used. This study endeavors to improve the understanding of the fine-scale roughness associated with the seepage-related seafloor (Dandapath et al., 2010). The seafloor characterization using the backscatter profile involves segmentation and subsequent fine-scale roughness parameter estimations.

In this study these techniques are used for seafloor characterization to unravel the maximum possible number of data classes using multi-beam echo-sounding backscatter data. The Kohonen's self-organizing map (SOM) is well suited for ascertaining the number of classes in a given data set, where no *a priori* knowledge of the data classes is available. The ANN based SOM has been applied to backscatter profile data from pockmarked seepage area to determine the number of classes and accordingly the fuzzy C-means (FCM) method is employed thereafter, incorporating the number of data classes determined by SOM.

Seventeen profiles were selected for this work. Each of the selected 17 profiles from the backscatter map of the survey area holds 447 data points, and the distance between the two consecutive data points (along the profile) is nearly 20 m. The uniform separation between the 17 parallel profiles is 0.46 km. In all, 7599 data points of the processed MBES backscatter data were used from the 17 selected profiles.
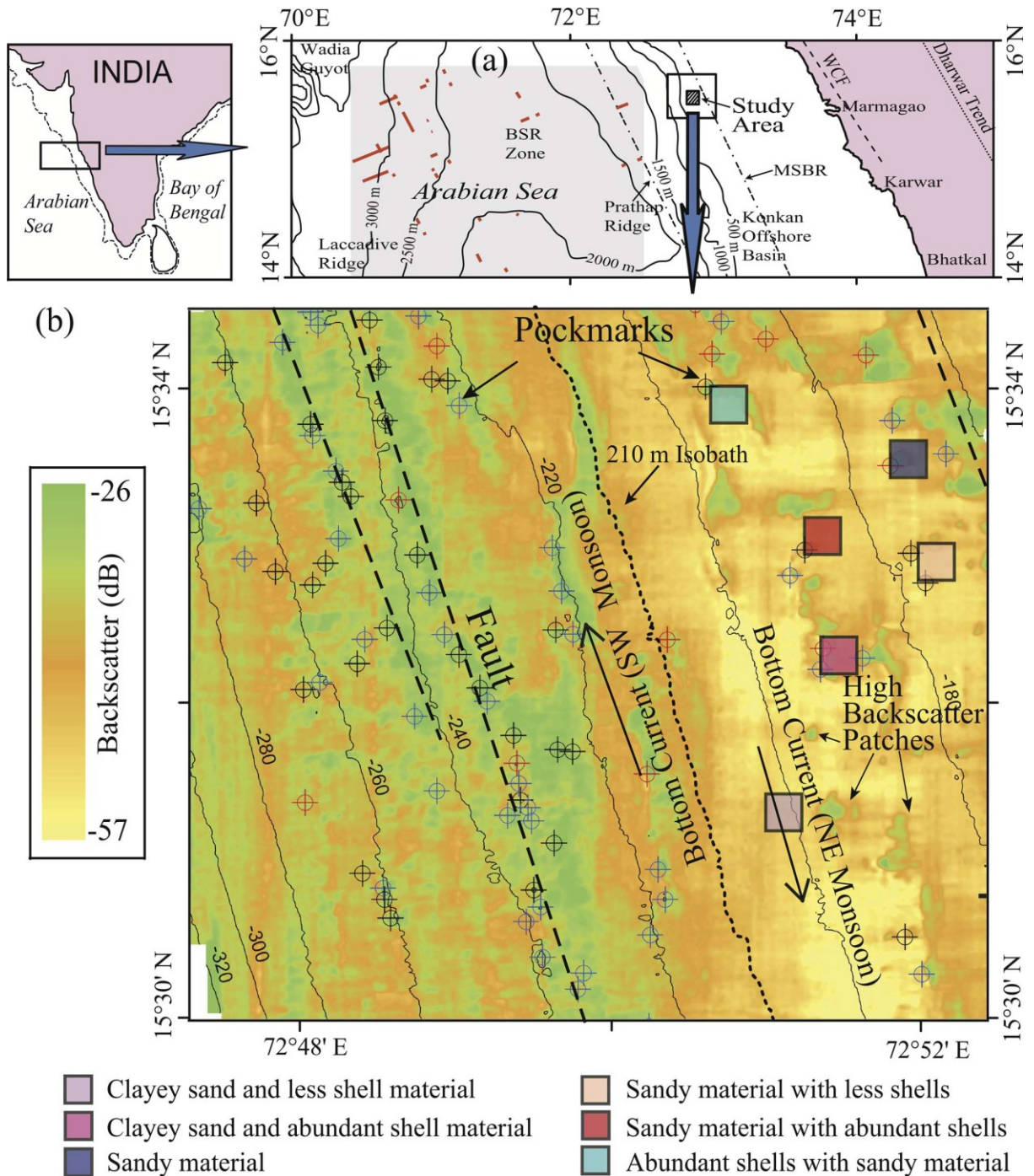
Fig. 6.1 - (a) Location of the study area, including some of the main structural features of the region. On-land Dharwarian trend, commonly used for Archaean rocks that have a NNW–SSE trending, Precambrian orogenic structure shown as dotted lines. Red highlighted lines and gray shade indicate the identified bottom simulating reflectors (BSRs). MSBR refers to mid-shelf basement ridge, and WCF indicates West Coast fault; (b) Backscatter map of the study area showing 160–320 m isobaths with an interval of 20-m depth. Pockmarks are indicated by crossed circles. Black, blue and red circles with cross markings represent circular, elliptical and elongated pockmarks respectively. Dashed lines indicate the location of identified faults. Black arrows show bottom current directions. Solid colored squares represent sediment types (see the legend). The inset shows the outline map of theWCMI with the location of the part of the Arabian Sea. Reproduced from Dandapath et al. (2010).

6.3 ANN-SOM Approach to Seafloor Classification

The work developed here shows that the employed technique can efficiently classify the survey area using linear data traces (backscatter/bathymetric) varying along the geographical south to the north (Fig. 6.2). These traces are mentioned as 'profiles'. If a statistical technique is applied to the profile data having unpredictable mixtures of the statistical parameters (mean, variance, probability density function) of the smooth and rough seafloor, the estimated model parameter accuracy would be reduced (Bansal and Dimri, 1999). Therefore, it would be imperative to divide the profile data into stationary segments before any quantitative analyses of the data segment are carried out. Here, we have applied the backscatter profile data segmentation through a combined use of SOMs and FCMs (De and Chakraborty, 2009). The SOM uses an unsupervised learning, where the network is unaware of the number of classes in which a particular backscatter data set would be segregated.

The extracted 17 backscatter profiles from the calibrated image data are subjected to a 20-point moving average. A moving average is a type of filter generally used with temporal or spatial series data to smooth out short-term fluctuations. For a time or space series, the first element of the moving average can be obtained by taking the average of the initial fixed subset of the series. This subset is then modified by 'shifting forward,' i.e., by excluding the first number of the series and including the next number following the original subset in the series, i.e., average of the data within the sliding window of 400 m along the backscatter profile [Fig. 6.3(a)]. Thereafter, the normalization of the data is employed using the given technique (Chakraborty et al., 2001). The corresponding depth values are also used to calculate the seafloor local roughness, i.e., large-scale roughness. In the case of profile segmentation application proposed here, the backscatter and depth data are employed to cover fine-scale as well as large-scale roughness aspects of the sea-
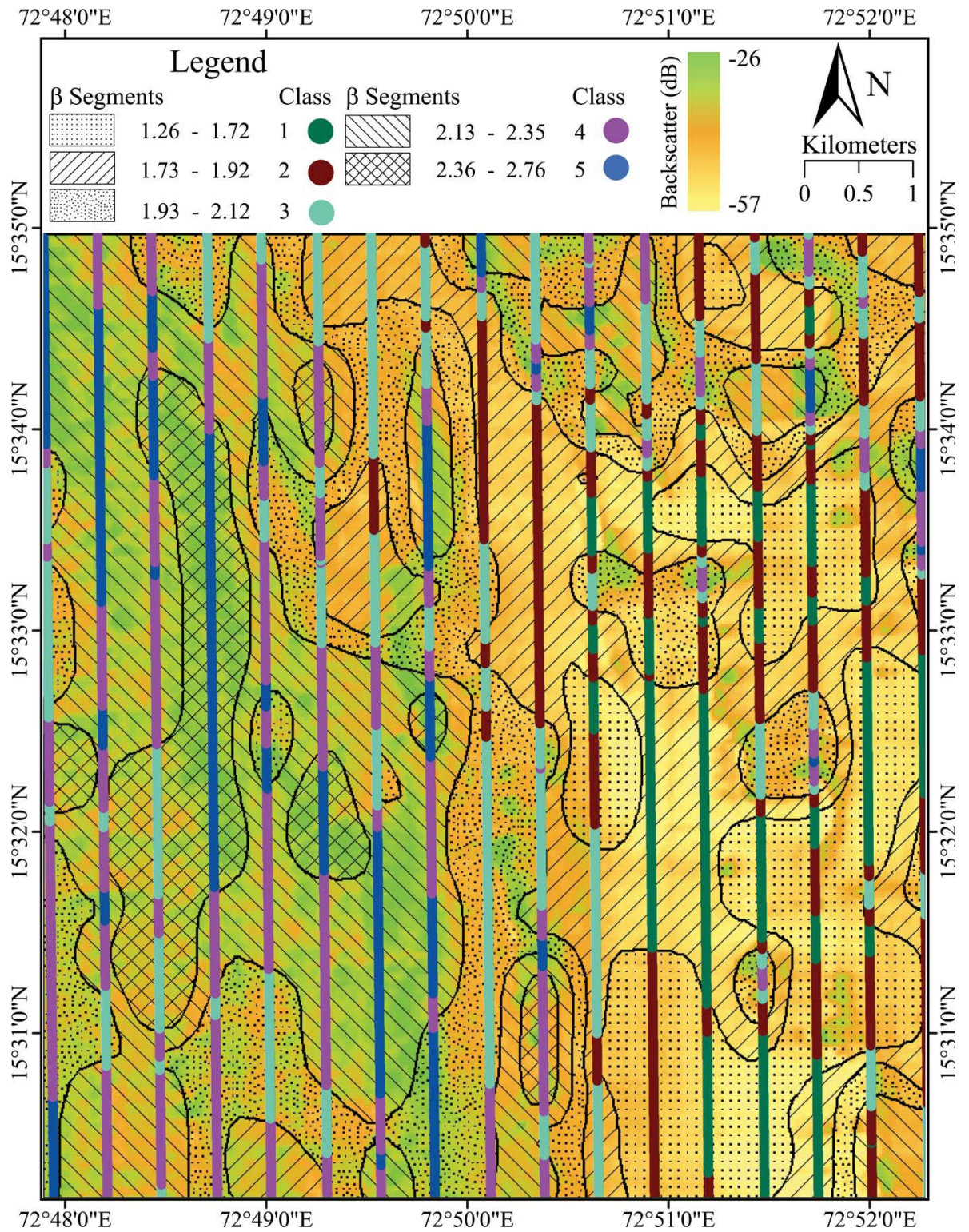
Fig. 6.2 - Seventeen backscatter profiles classified into five different classes (depicted in color) overlaid on a rasterized map of (β) values that have been estimated using the segmented profiles of the five classes.

floor respectively and these two characteristics are then used as feature vectors. The 'roughness' parameter, i.e., the absolute value of 'y', is the deviation of the depth value about the local linear trend of the data. The large-scale roughness parameter was estimated for each of the nine data points (180 m) for the depth data profiles. If the deviations with respect to the local linear trends are large, then the seafloor surface is considered as rough, otherwise the surface is smooth. Furthermore, the sliding window (400 m), i.e., the 20-point moving average and normalization technique, is also applied to the computed roughness values of the depth data as an additional feature [Fig. 6.3(a)].
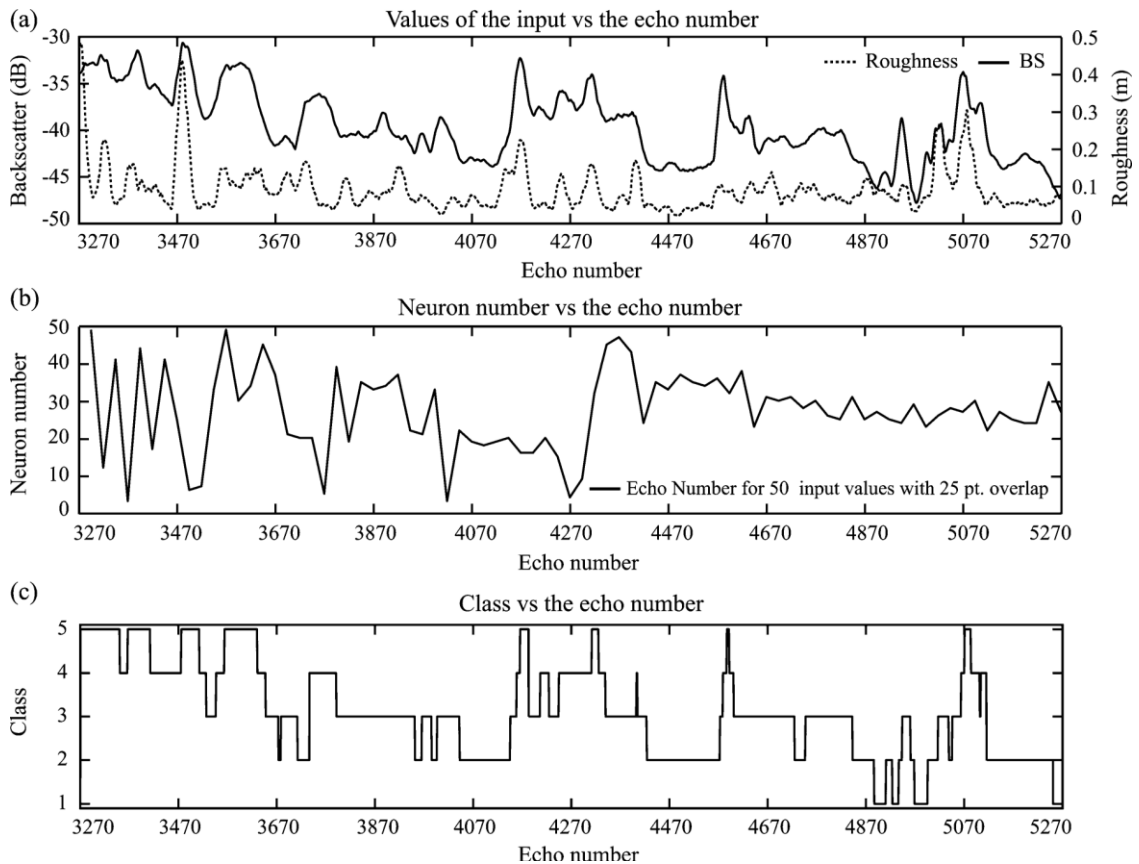
Fig. 6.3 - (a) Representative plot of the input values (backscatter and roughness) from a section of the data profile. (b) Firing neurons correspond to the SOM output of the two input feature vectors for the above data. (c) Classification of the data points using FCM.

The flowchart depicted in Fig. 6.4 explicates the operation of the entire technique for data segmentation as well as employment of another methodology (PSD) used for the segmented data. The employed SOM architecture comprised of a flat 1-D neuron grid. As
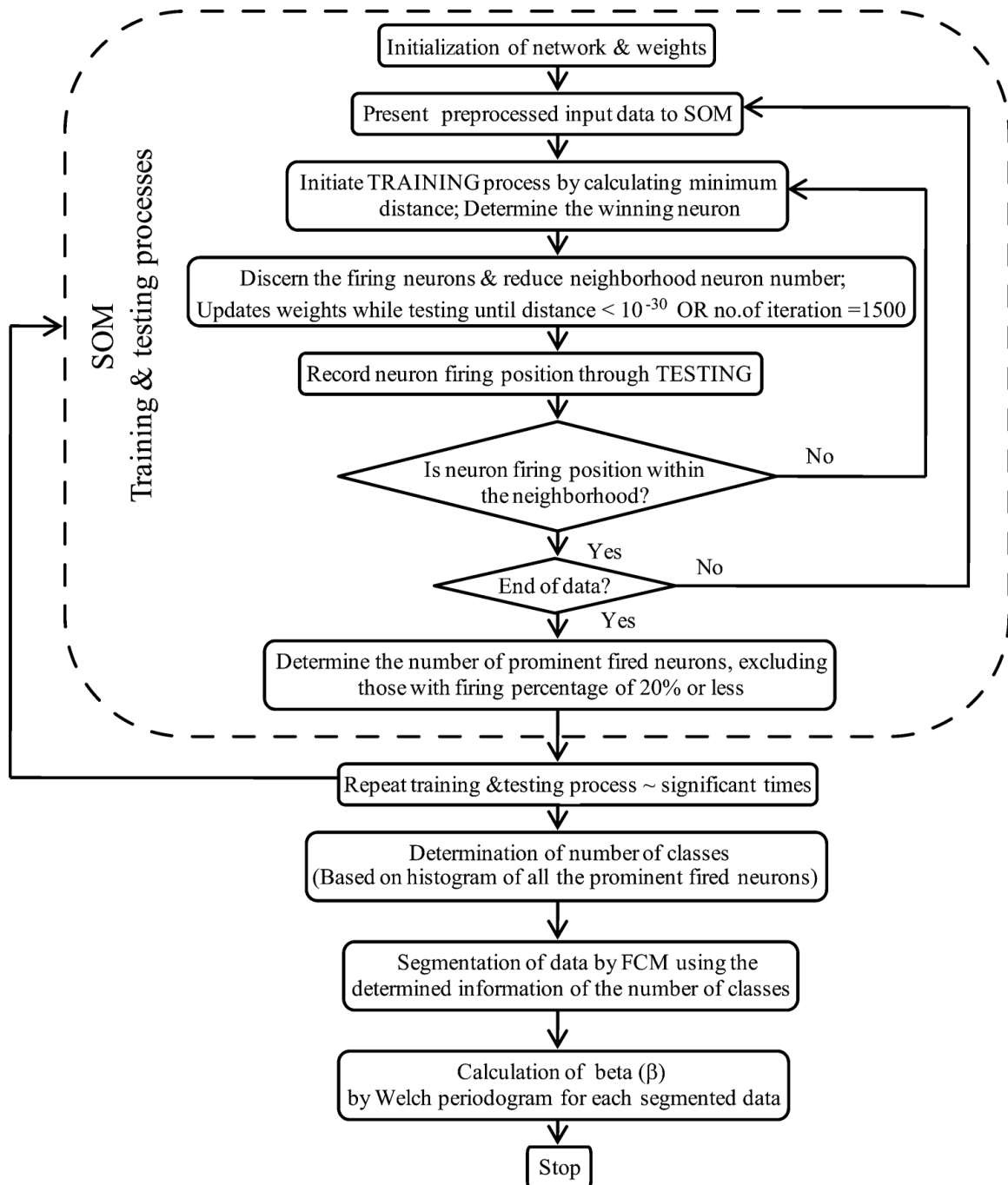
Fig. 6.4 - Flowchart of the methodology followed including SOM and FCM for determining the number of seafloor classes, and parameters using 17 selected profiles from the backscatter map.

already mentioned, the backscatter strength along with the seafloor roughness calculated

using the depth data from the profiles are used as the two input features. The feature

vectors are connected to the SOM network that consists of 50 output neurons in the grid.

When the backscatter and roughness data are employed as input vectors to the SOM

architecture, the neurons in the grid compete among themselves to get activated. Weights

of those neurons in its neighborhood are updated iteratively to form a representative cluster (refer to Chakraborty et al., 2001) for more details about the neighborhood reduction technique used in the SOM). This is known as tuning of the weights in response to a given class of input vectors. The algorithm organizes the nodes in the grid into local neighborhoods that act as an input feature.

An initial weight matrix having a small random value is used. Initially, two input feature vectors are presented as a training sample, and then the Euclidean distance between the input vector and the weight of the neurons in the 1-D grid is computed. The neuron having the smallest distance is designated as the "winner" neuron. The weights of this neuron are updated, and the distance matrix is computed iteratively for the same input vectors to minimize the error. This procedure is consistently repeated a number of times until the value (of the minimum distance) is reduced below that of a pre-specified error value. The learning function aids in gradually reduction of the magnitude of the weight update as the error is successful. The neighborhood size also decreases as the number of iterations increases, thus localizing the area of maximum activity in response to input vectors in the SOM architecture (De and Chakraborty, 2009). To ascertain the number of classes using the SOM architecture, two input feature vectors of each data point were presented to the random weight matrix (1 x 50) and the nearest neuron was selected to be the firing neurons for the input data. The closest neighborhood neurons on either side of the firing neuron are updated using the learning function (Chakraborty et al, 2001). The updation is iteratively carried on till the neighborhood is reduced to one, i.e., at the end, only the firing neurons are updated. The initial value of the learning function reduces during the iteration and the training stops when the error is less than 10^{-30} or till the number of iterations arrive at the pre-specified value. Each time a new input class is
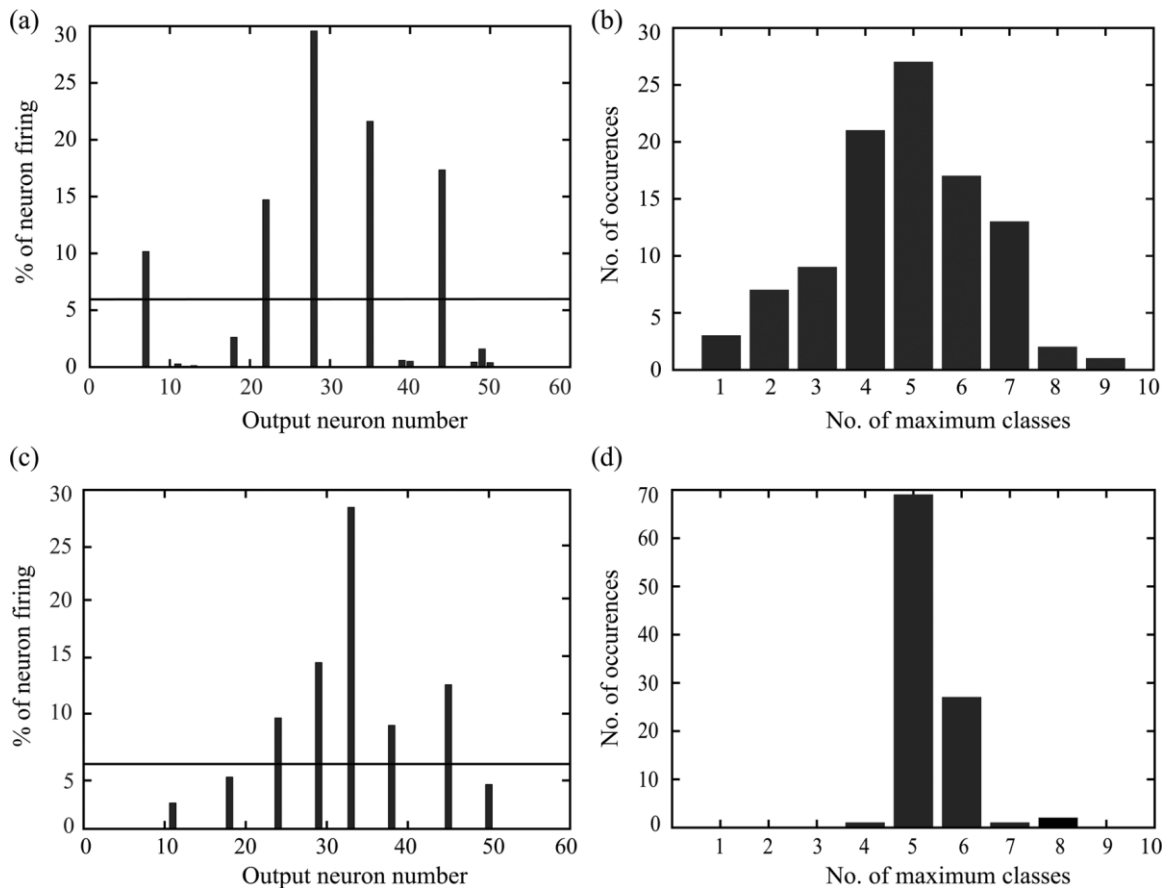
Fig. 6.5 - (a) and (c) Horizontal line represents the line of 20% of the maximum number of neuron firings. Here, there are five bars above the line indicating five classes obtained from one training/testing process for different moving averaging schemes of input data; (b) and (d) Histograms of the number of occurrences of the maximum number of classes obtained from the 100 training/testing processes employing the SOM analysis, i.e., indicating the number of classes available in data sets.

applied to the network, the winning node must first be located. This identifies the region of the map that will have its weights updated. In this study, the number of iterations to reach the pre-specified error value is optimized based on the employed trial runs of the data. The testing of the input features is initiated once the training is completed and the excited neurons during the testing processes are plotted [Fig. 6.5(b)]. If testing results show that the winning neuron exists within the cluster (a group of five neurons around the central neuron) of the trained neuron, then it is assumed to be belonging to the same class as the data where it was trained earlier. Otherwise, further training is initiated in the search of a firing neuron, and the training/testing process is resumed. At the end of the training/testing process, the percentage of the number of times the different neurons have

been excited is plotted as a bar diagram with respect to the neuron numbers. The maximum numbers of classes are equal to the number of occurrences that are equal to or larger than 20% of the highest neuron firing (Fig. 6.5). Even though the soft-computational technique (SOM) establishes the number of data classes, there is a necessity to validate the extent of success by employing other different techniques.

6.4 Validation of the Classification Technique using Multimodal Histogram

To corroborate the number of classes obtained using SOM and FCM, multimodal statistical techniques were employed here. The histogram of the backscatter data points of the 17 backscatter profile data is fitted using multimodal curves considering each curve as Gaussian distribution. The probability density functions (**pdf**) of the backscatter strengths are computed as in Pearson et al., (1992), where the estimated scaling
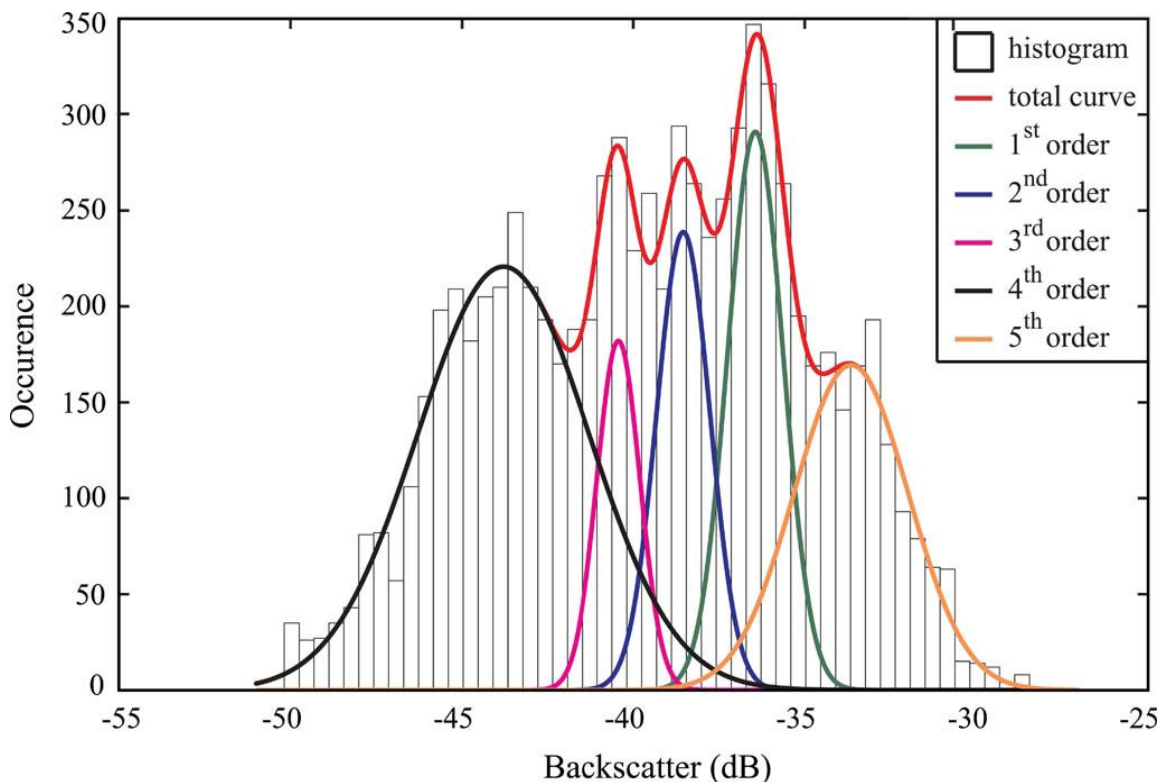
Fig. 6.6 - Occurrences of backscatter strength (in decibels) with respect to the rasterized backscatter pixels (in decibels) of the study area and fitted multimodal curves of the total and five **pdf** components.

amplitude (to scale the height of the curve), mean deviation, and standard deviation of the **pdf** components are estimated using curve fitting between the experimental and predictive **pdf**s, which involve a comparison between the estimated correlation coefficients and the sum squared of the residuals (SSR criteria) (Seuront, 2010). Mixtures of the normal distributions of the five components are presented (Fig. 6.6). The highest correlation coefficients and the lowest errors (SSR) have been considered to determine the five predictive components and the resultant (mixture) **pdf**s through the use of the experimental data. The study carried out here supports the fact that the backscatter data exhibit the number of available classes in the data set as a means to support the SOM-based study.

6.5 Fuzzy c-means for segmentation

The aim of this work is to develop a system for a segmented seafloor classification (based on SOM and FCM) and subsequent characterization (PSD) of the mapped backscatter data using the selected profiles. This helps in achieving an operational advantage for seafloor data acquisition and interpretation. The use of diverse unsupervised algorithms such as the adaptive resonance theory (ART) and the fuzzy ART network where cluster creation is being controlled by the use of an explicit parameter known as 'vigilance thresholds' (Carpenter et al., 1991) have also been used elsewhere for similar applications. In this study, multiple training/testing processes using the SOM produce neuron numbers. These firing neurons are then plotted in a histogram indicating the five major classes [Fig. 6.5(a) and Fig. 6.5(c)]. Subsequently, the FCM technique is used to segment the data sets [Fig. 6.3(c)] of the firing neurons to obtain the five segmented sets of the original backscatter profile data. The FCM-generated segmented profiles are presented in a color code using the geographic information system (GIS)

software ArcGIS (Fig. 6.2). In this work, a MATLAB-based FCM algorithm was employed for clustering of the profile data.

6.6 Estimation of fine-scale Roughness Parameters

The use of the SOM/FCM techniques along with the spectral estimation to the segmented sections emphasizes the significance of the method employed here. The computations of the PSD of the segmented profiles are employed. The power law equation as given in (Chakraborty et al., 2006) is employed here. The power is expressed in m^2/cycles per kilometer and the wave number as cycles per kilometer. A straight-line fit of power law equation with a PSD provides the "spectral exponent" of the power law curve β (that corresponds to the slope of the straight line) and the intercept a' (meters) of the input profile. Welch method was implemented using the MATLAB toolbox through the "pwelch" function. A Hamming window was introduced to compute the modified periodogram of each segment. The PSD is presented on log_{10}-log_{10} plots of the PSD versus the wave number (Fig. 6.8). Multiple humps in the spectrum in [Fig. 6.8(a) are generally observed within the ~ -1.5 cycles/km to -0.2 cycles/km. If the profile represents appropriate β (slope) and a' (intercept) values, then its periodogram would be well fitted by a straight line (power law) in the log_{10}-log_{10} space. The "humps" are being identified as artifacts and are associated with edge effects, which could partially be improved by the edge tapering (Goff et al., 1999). However, a clear-cut drop in power occurs somewhere between the wave number (beyond in the -0.2 in the log_{10}-log_{10} scale) [Fig. 6.7(a)]. At higher wave numbers (smaller scales), the periodogram does appear to provide appropriate straight-line fitting. The straight-line fitting parameters, β (slope) and a' Parameters such as the correlation coefficient and SSR of the data points within the windows for the PSD (drawn from the segmented data) and the corresponding power law function provide and values of the segmented profiles (Seuront, 2010) [Fig. 6.7(b)].
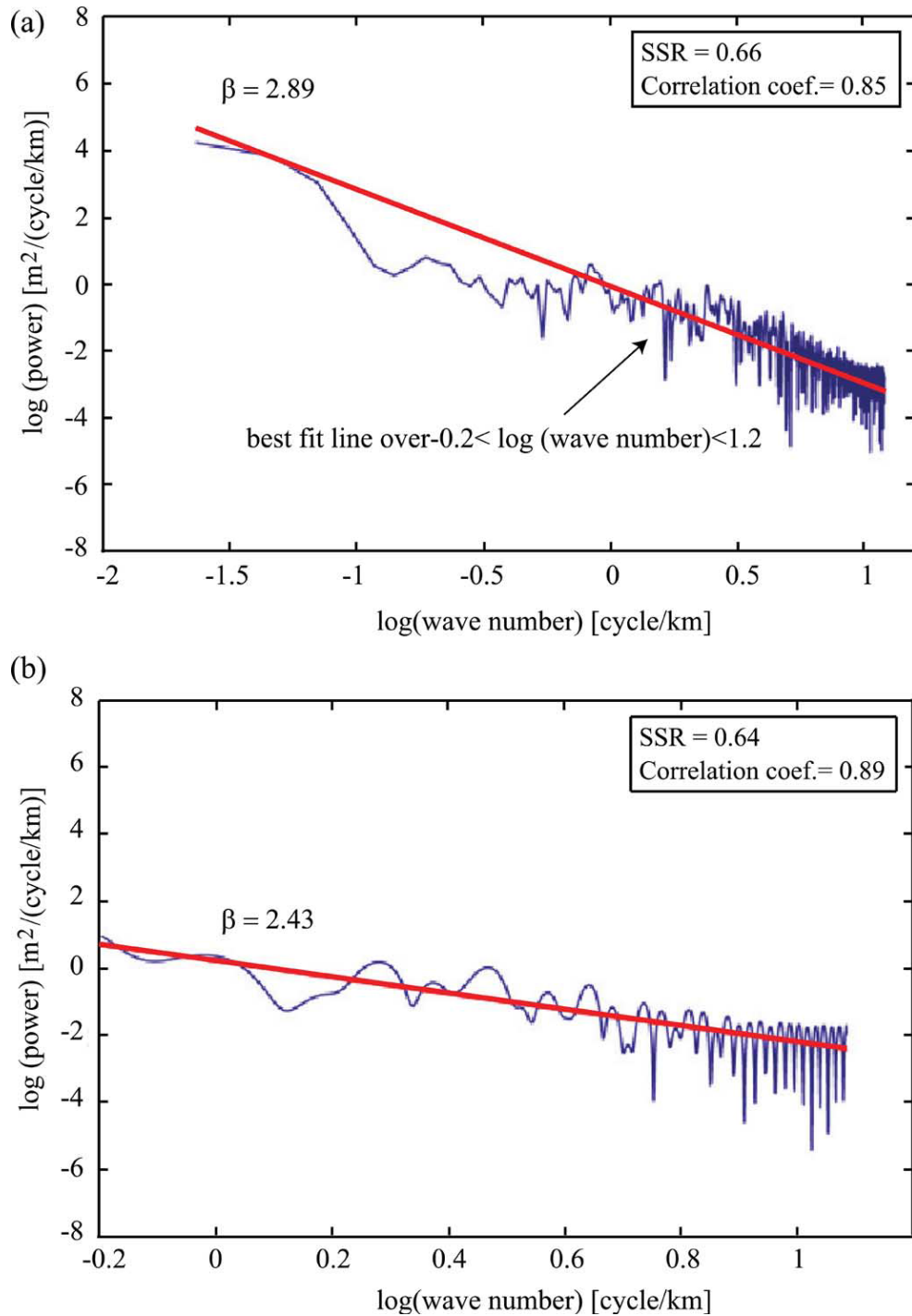
Fig. 6.7 - (a) Plot of the Welch's averaged modified periodogram ("pwelch" function in MATLAB) applied to a representative segment; (b) After selecting the appropriate range of wave numbers for curve fittings of the remaining – plot of the power spectral density versus the wave number belonging to the same segment (the power law parameter fitting SSR and correlation coefficients are given in the inset).

6.7 Results

Using the SOM architecture, the numbers of classes were determined by counting the number of occurrences of prominent neurons [bar diagram, Fig. 6.5(a) and Fig. 6.5 (c)]. For example, during the one-time training/testing process of the entire profile data, most of the neuron firings occurred at the neuron position 28, and the rest were observed at neuron positions 8, 22, 36, and 45, as shown in [Fig. 6.5(a)]. Similar training/testing process is repeated a number of times (~100) for the entire data sets, i.e., the 17 profiles. For each training/testing process, the number of classes is determined from the numbers of occurrences versus the number of classes as plotted in a histogram [Fig. 6.5 (b)]. The number of classes occurring maximum number of times (at the end of a repeated cycle or the entire data) is considered to be the number of classes existing in the data. This process provides the number of classes available in a given data set without any prior information. To examine the consistency of the employed technique and the method of preprocessing the variables such as the sliding window width, etc., the averaging of 30 backscatter data points, i.e., 1 - 30 and so on, was also being tested alternatively. It could be observed that there was no change in the number of class estimations using the SOM technique [Fig. 6.5(c) and Fig. 6.5(d)].

Though the soft-computing techniques (SOM and FCM) are useful for real-time data segmentation purposes, there is a necessity to validate the extent of success employing other diverse techniques such as the multimodel **pdf** curve fitting mentioned above. Five classes (Fig. 6.6) were obtained from the backscatter values of the 17 profiles. The limits of the backscatter strengths of each class and their overlapping areas are also seen. The five classes obtained using multimodel **pdf**s match with the number of classes obtained employing SOM.

The segmentation of the 17 profiles generated 243 segments within the five classes. However, the estimation of the seafloor roughness such as β and a' of the 160 segments was determined. Due to the increased inaccuracies in the estimation parameters of the smaller profile lengths, only 160 segmented profiles having varied profile lengths could be used for β and a' estimation. Using these β values, a map was generated utilizing the kriging method (ESRI, 1999). The "Jenks (1967) natural breaks" (used in the ArcGIS analyst module) algorithm (North, 2009) was used to classify the entire map into five gridded blocks. The raster data maximizes the variance between the different β blocks, and minimizes the variance within similar blocks of β values. A map is presented utilizing the predicted β values (Fig. 6.2). The results of the segmented classes of the backscatter profiles and the five sets of gridded values are superimposed over the backscatter raster map using Arc GIS 8.3. The predicted β values, i.e., map-generated data points, are compared with the estimated β values that are located over the profiles. The histogram of the error values (the difference between the estimated and predicted β values) for 7599 data points from the 17 profiles indicates the accuracy of prediction [Fig. 6.8(a)]. This figure shows the extent of fluctuations in the estimated values. In addition, relationships among the estimated and predicted β values are also indicated by correlation coefficients (0.862) [Fig. 6.8(b)]. This study reveals that the predicted slope β values of the map data are fairly accurate. Overall, the β values match with the background map.

In general, higher values β (2.13 – 2.76) fall within the fault region of the WCMI, whereas lower values (1.26 - 1.93) indicating small-scale or fine-scale sedimentary region exist toward the shallower eastern end of the shelf. A spatially located intermediate region depicts β within (1.93 - 2.12). Moreover, the five classes allocated from the profiles using SOM and FCM techniques are also overlaid on the backscatter
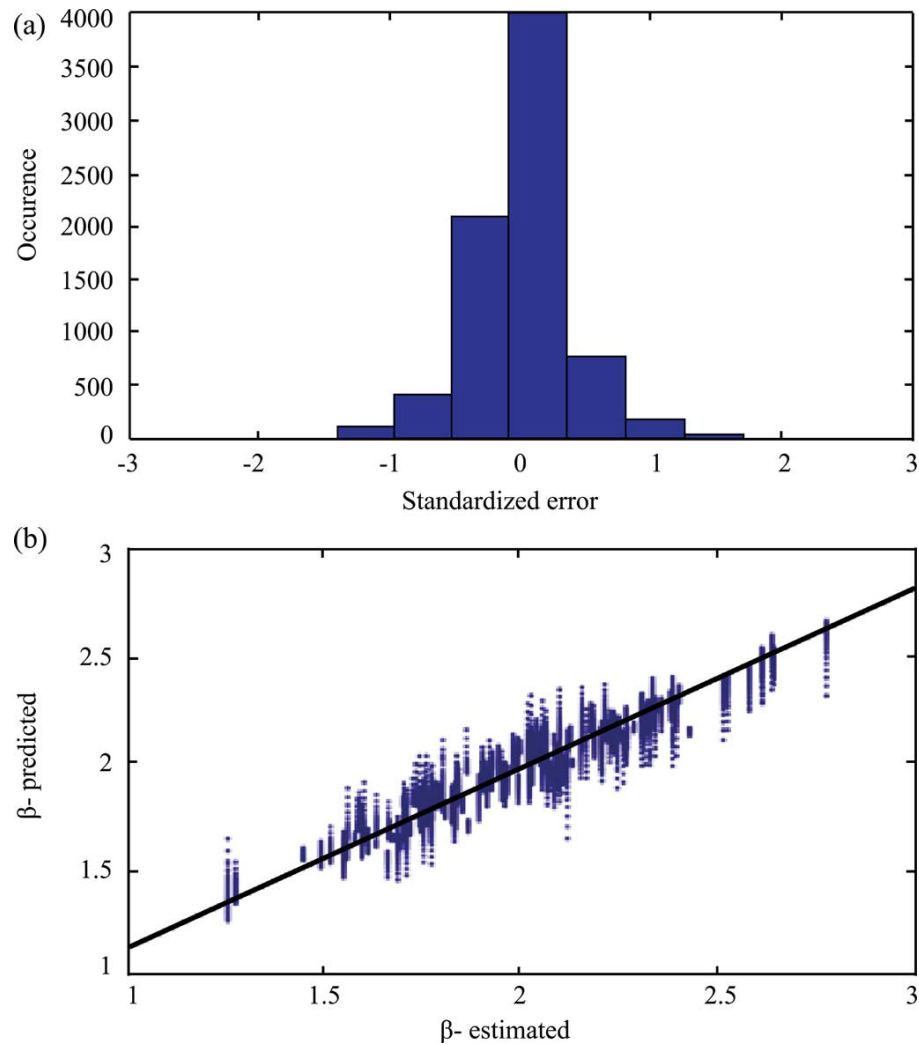
Fig. 6.8 - (a) Histogram of standardized errors between the computed and predicted values (gridded) of the segmented data points (7599 data points) obtained using ArcGIS; (b) Scatter plot between the estimated versus predicted values. The straight-line fitted curve indicates 80% correlations.

map. It can be seen that there are more segments toward the comparatively shallower water sedimentary regions. Here, the fine-scale roughness is higher (lower β values), and the segments are classified as regions I and II. Similarly, near the fault trace site, the fine-scale roughness is comparatively low (higher β), and the segments are classified as regions IV and V. Intermediate β values are classified as region III, i.e., medium roughness that exists between the fault trace and the shallower region toward the continental shelf. The estimated slope β values from the straight-line fitted power law of

the 160 profile data reveal a variation from 1.26 to 2.76 and a corresponding intercept a' values from -0.77 to +0.71.
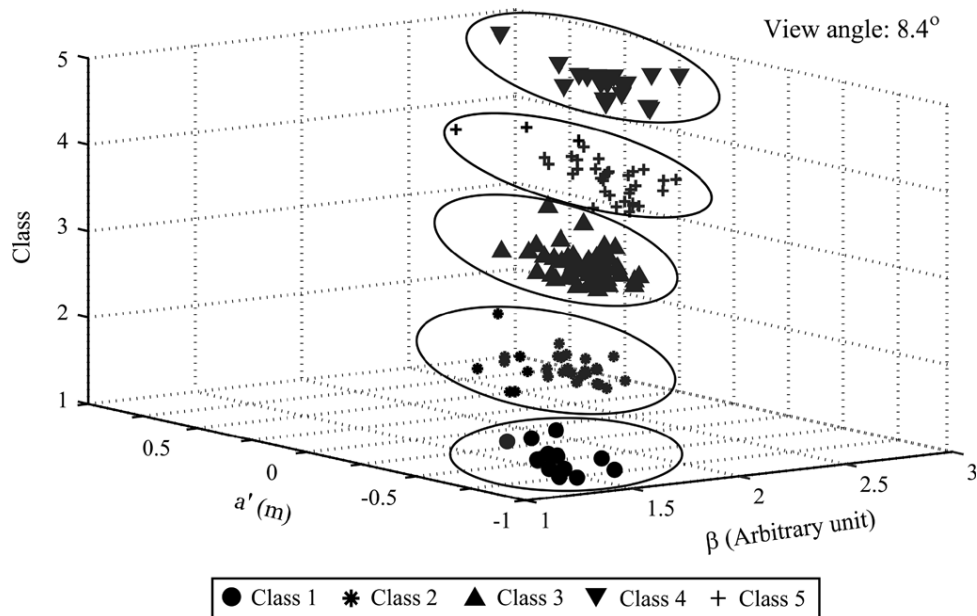
Fig. 6.9 - Scatter plot of power law derived parameters such as (β) and intercept (a') estimated from 160 segments along with the classes determined using SOM and FCM.

The three-axes presentation of the slope (β), intercept (a'), and classes (SOM and FCM output) of the segmented profiles show a distinct clustering when observed at a view angle of 8.40º (Fig. 6.9). The mean, maximum, and minimum values of the estimated slope (β) and intercept (a') for classes I, II, III, IV, and V are: [β=1.67 (max. 2.07, min. 1.45); a' = -0.48 (max. -0.06 , min. -0.75)], [β=1.75 (max. 2.32, min. 1.26); a' = -0.43 (max. 0.42, min.-0.78)], [β=2.05 (max. 2.76, min. 1.73); a' = -0.24 (max. 0.62, min. 0.60)], [β=2.14 (max. 2.60, min. 1.67); a' = -0.24 (max. 0.64, min.-0.80)], and [β=2.30 (max. 2.63, min. 1.98); a' = -0.14 (max. 0.71, min. -0.60)], respectively. In total, 160 segments that are used for PSD-based class determination reveal 23, 29, 45, 36, and 20 segments for classes I, II, III, IV, and V, respectively. The overlapping between the five classes (β and a') is observed, however, the power law plots (*log–log*) of the mean values within the wave numbers (from -0.25 to 1.25 cycles/km) show a dominant small-scale roughness. This affirms the highest fine-scale roughness (lowest β) to be the

class I type [Fig. 6.9(a)]. The fine- or small-scale roughness (PSD) is found to be decreasing with the increase in β values within the wave numbers beginning from class I to class V. The segmented profiles having five classes can be observed overlying the backscatter map (depicted in color) (Fig. 6.2).

The performances of the segmented backscatter profiles using the SOM and the FCM, and Jenks-algorithm-based gridded blocks of the segmented β values ascertain the success of the employed data segmentation techniques. The percentages of roughness data pixels (β values) reveal 100% matching with two classes I and V. However, 92.2%, 97%, and 97% correspondence is observed for classes II, III, and IV, respectively. The comparison made here demonstrates that the proposed data-driven approach can be used as a preprocessor to increase the efficiency of the classifier.

6.8 Discussion

The acoustic backscatter strength of the study area ranges from -26 to -57 dB, which can be attributed to the seafloor slope, sediment type, and relief. In the deeper water (210 m) region [Fig. 6.1(b)], several pockmarks in the proximity of the fault zone show high backscatter (from -27 to -40 dB). Along the fault zone, the strong seafloor backscatter, i.e., increased acoustic impedance is due to the coarse-grained seafloor sediment as well as high calcium carbonate content (60%) (Thamban et al., 1997). Earlier study (Dandapath et al., 2010) had shown that the areas along the faulted region possess maximum pockmarks [Fig. 6.1(b)]. Based on the application of the box-counting technique to the image blocks of the study area, the estimated higher fractal dimension of the backscatter image blocks shows greater roughness (i.e., the rough, fragmented, space-filling seepage distributions) (Dandapath et al., 2012). Structurally, the pockmark shapes are found to be circular, elliptical and composite types with north of northeast–north of northwest (NNE–NNW) orientations, and the seep direction indicates the north of north-
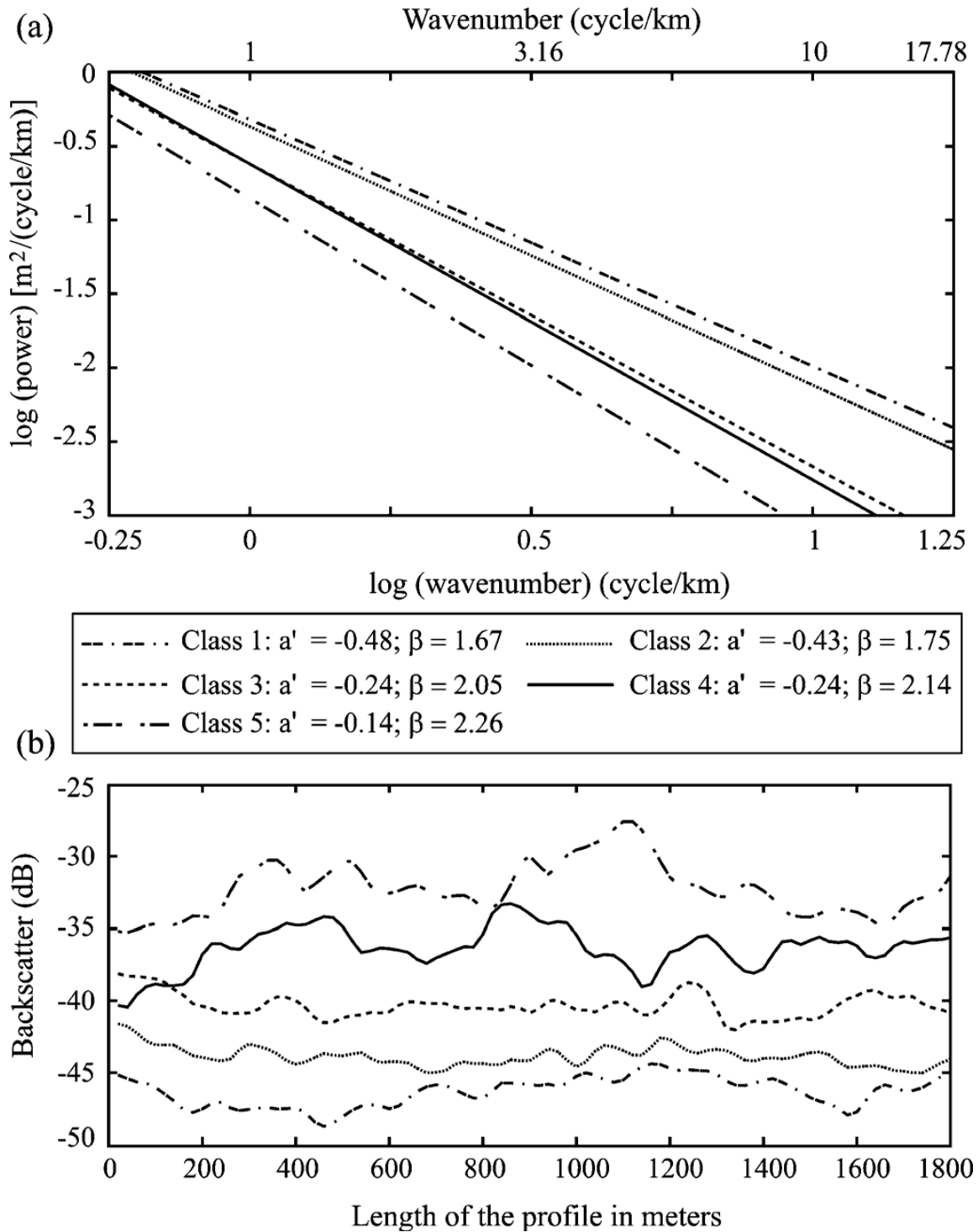
Fig. 6.10 - (a) Mean power law parameters (β and a') estimated from the five seafloor classes revealing the extent of roughness within the given wave-number ranges; (b) Representative profiles of the five classes generated from the rasterized backscatter data indicating the degree of seafloor roughness.

west–south of southeast (NNW–SSE) orientation. Seafloor pockmarks, bottom simulating reflectors (BSRs), acoustic blanking, and gas-charged sediments were detected during geological and geophysical surveys. In addition, more than 90% seeps were found to be

located in the eastern flank of the pockmarks, which is an important aspect of the seepage-dominated fault zone. Interestingly, this study depicts low seafloor roughness, i.e., higher β values (2.13 –2.76) [Fig. 6.10(a) and Fig. 6.10(b)] in the area as revealed by the north–south-oriented segmented backscatter profile data (based on SOM and FCM techniques), which also show dominant IV and V classes. The higher β values are contrary to the previously reported box dimension values where higher seafloor roughness was estimated.

Toward the shallower end (210 m.) where seafloor gradient is gentle, backscatter strengths are generally low (~ -45 dB). As previously reported by Dandapath et al. (2010), the area is covered with soft terrigenous clayey sediment producing average seafloor backscatter strength. However, the sediment data from the seven locations in the study area show dominant coarse-grained sandy sediments along with abundant shell material [Fig. 6.1(b)] (Dandapath et al., 2012). Based on the fractal dimensions using the box-counting method of the image data of this shallower site, a smooth seafloor roughness was indicated. However, present study using power law parameter fittings of the power spectral density function to the north–south-oriented backscatter profiles shows atypical results. The lower β values (1.26 – 1.92) show higher seafloor roughness within the given fine-scale wave-number ranges [Fig. 6.10(a)]. Generally, the coarse-grained sediment along with abundant shell materials reveals high backscatter strength. The existing seafloor relief is quite obvious due to the prevalent monsoonal bottom currents in this area (Shetye, 1990). Regional oceanic circulations, characterized by seasonal reversal of monsoon-driven surface and bottom currents, summer upwelling, and winter downwelling (Naqvi, 2010), create an unstable oceanographic condition over this part of the area. Bottom currents are wide (~40 km) and run opposite to the direction of surface currents. Measured mean current speed and directions during the southwest monsoons are

12.6 cm/s and 94.5º N, respectively. Similarly, during the north–east monsoon, speed and direction measured here are 12.5 cm/s and 296.6º N, respectively (Amol, 2010). Therefore, we presume that the lower backscatter strengths at the fine-scale level strengthen the existence of seafloor relief due to the bottom currents for coarse-grained shelly seafloor sediments.

In this study, the computed β values of backscatter profile data show the highest roughness (low β) toward the shallower region (210 m). Box dimensions using the box-counting computation involve box sizes of 500 x 500 m, which cover backscatter image data due to the different patterns of the seafloor seepage patches. The lower box dimension values reflect lower roughness within the given box sizes (Dandapath et al., 2012). These values are not comparable to those of fractal-dimension-computed values using the estimated β for the north–south-oriented backscatter profile. The anisotropic seafloor (Dandapath et al., 2010) behavior is obvious in this study area due to the north–south-oriented dominant bottom currents (as already explained) in the shallower region than the deeper water fault zone. The dominant bottom currents within the shallower area show low backscatter (higher seafloor roughness) even for compacted coarse-grained sediments. Moreover, the estimated dimension parameters are box-size sensitive. Therefore, the self-affine technique such as the spectral method (Malinverno, 1990) employed in this investigation is more effective than the earlier study using box-counting analyses of the seafloor area image (Dandapath et al., 2012). The box-counting method appears to be inadequate for analyzing the anisotropic seafloor patterns, but it is found to be valid for a statistically self-similar seafloor type.

6.9 Conclusion

In this paper, a novel technique was proposed to characterize the seafloor backscatter data acquired using the MBES system that is also applicable to the SBES system. A successful analysis has been carried out in the WCMI (off northern part of the Goa coast). This technique provides an approach towards the real-time seafloor roughness information using the remote acoustic method, and is helpful for geological applications having limited sampled data. A soft-computational method is adopted to determine the presence of five classes from the 17 backscatter and bathymetric profile data. The presence of the five classes has been further validated employing the multimodal curve fitting to the histograms of the backscatter profile. This indirectly suggests a logical reasoning for the employment of only two features such as the backscatter and the "roughness" parameter of the depth data. A data-driven approach based on the SOM and FCM segmentation is used to estimate the fine-scale roughness parameters using PSD of the backscatter profiles. Application of the present technique proffers that the utilization of calibrated sonar image profiles for real-time classification and characterization is promising, which considerably reduces the survey time.

CHAPTER – 7

THE CORALLINE BANKS

7.1 Introduction

The coralline banks lie off coastal Karnataka in the Konkan basin that forms an integral part of the eastern Arabian Sea and the western part of the peninsular shield of India. The two coralline banks, *viz.* Gaveshani (Nair and Qasim, 1978; Qasim, 1978; Rao et al., 1993) and an unnamed bank (Rao, 1995) located along a buried channel, off Malpe, present a diverse geological setting in the WCMI. Coral structures are important for coastal protection; they act as barriers against waves and storms, thus preventing loss of life and erosion. They are also important as spawning and feeding grounds for many marine species, and harbor diverse ecosystem providing habitats for varied marine organisms (Beger et al., 2002).

The bathymetry and backscatter data for the present study (Gaveshani and the unnamed bank) was acquired in February 2008, using EM1002 MBES (Kongsberg AS) operating at 95 kHz installed on board CRV Sagar Sukti (Cruise No. SaSu-164). The survey lines were oriented parallel to the coast in N-S direction. The bathymetric data was processed using Neptune software (Kongsberg AS) incorporating corrections for propagation, refraction errors, and tide. The backscatter data was processed using PROBASI II (PROcessing BAckscatter SIgnal) algorithm (Fernandes and Chakraborty 2009), for data normalization, and subsequently imported to CFLOOR (Cfloor AS) software for gridding and improved visualization. Gridded rasterized maps (bathymetry and backscatter) of Gaveshani (Menezes et al., 2015) and the unnamed bank were prepared.

7.2 Gridding Resolution

The multibeam data processing of the coralline bank data is similar to that of the seepage seafloor described in Chapter 6. Minor modifications were incorporated to adapt the basic technique discussed in Chapter 2. The bathymetric grid resolution is controlled by two important factors, the size of the footprint and the distance between individual soundings (Kenny et al, 2003).The density of the soundings used to create the grid is the key factor for determining its resolution, i.e. the denser the data, the higher the resolution that can be achieved. Increased concentration of soundings density and individual beams with small footprint produce higher spatial resolution grid. The average footprint size of the bathymetric data over the Gaveshani bank summit could be approximated to 1.34 m. Gridding the Gaveshani bathymetric data with grid size close to 1.34 m resulted in data gaps in the rasterized map, attributable to reduced soundings density due to comparatively decreased acquisition rate caused by the higher ship speed and rejected soundings. When areas with low data density generate data gaps in the rasterized output, data interpolation may be resorted to (Boldes, 2017). Although a higher resolution could be incorporate with a smaller grid size, increasing the grid size facilitated the creation of raster coverage without data gaps. The spatial density of the data covering the banks was the guiding factor for choosing the optimum resolution, where the average distance between the individual sounding is less that 2.2 m and the raster cell size could accommodate as many as three soundings. Accordingly a grid resolution of 2.2 was adopted for Gaveshani bank for creating the rasterized map using kriging method that uses the geostatistical properties of the data when interpolating (Smith et al, 2002). For kriging the multibeam data, Environmental Systems Research Institute (ESRI) ArcGIS 10.0 software Spatial Analyst and Geostatistical Analyst Extensions were utilized (ESRI, 2010). Kriging method is a good interpolator for sparse data. In the case of the unnamed

bank lying in comparatively deeper waters, located 37 km north of the Gaveshani bank, the average foot print size of a single beam could be approximated to 2.7 m. Interestingly the density of soundings was considerably large due slow ship speed resulting in more pings and overlapping swaths. The average distance between the individual soundings could be approximated to 1.6 m. A grid size of 1.6 m could be directly used to create rasterized map with cell size that could accommodate up to four soundings without data gaps in the raster map. The respective grid sizes selected for the two banks, allowed creation of rasterized maps without any gaps. The conditions here are different from the data acquisition environment of seepage seafloor area (Chapter 6) where the chosen grid size of 10 m is appropriate for the average footprint, based on the operational depth of 200 m.

7.3 Pre-processing of Data for ANN based analysis

EM 1002 MBES primarily measures the time average of the backscatter signal envelope in each of its 111 beams. The raw data recorded by the MBES require post processing such as removal of Lambert's law, correction of actual bottom slope, and the insonified area. The signal envelopes are corrected for time variable gain (TVG), predicted beam patterns and the insonified area, and are recorded in a packet format called datagram. All Kongsberg data types are stored in scaled units of dB within the different datagrams. Datagrams are used to communicate echo sounder data to and from the EM 1002 system (Fernandes and Chakraborty 2009). The Kongsberg systems provide value for '*Beam Intensity*', which represents the average signal level over a given beam's footprint that gets recorded in the datagram for every ping as representative of the seafloor's backscatter strength. The intensity level after corrections for transmission loss and insonified area is the physically meaningful BS. The BS value here can be considered as near absolute as it would be corrected for the spherical spreading, absorption loss and

the area insonified by each beam providing relative backscatter strength as a function of incidence angle.

The angular backscatter data strength frequently exhibit higher values at normal incidence compared to the outer beam angles. Such backscatter data produce artifacts along the centre beam path during data acquisition (de Moustier, 1986). Often rectification is required to be carried out to compensate for the outer beams backscatter strength data so as to minimize the effect of angular backscatter intensity. Consequently sonar-related preprocessing of the backscatter data was carried out to diminish the effect of artifacts along the centre beam path and inevitably cleared out by using median filter (Menezes et al., 2015). The quality of the image data is increasingly enhanced utilizing the four stage image processing technique (Blondel, 2009; Haris et al., 2012, 2015).

From the gridded maps the six profiles extracted from the Gaveshani bank data covered a total of 5970 data values with depth ranging from 80 m around the bank to 38 m on the top of the feature. The extent of the area comprising of the coralline bank and contiguous area was nearly 3.5 km^2. While in the case of unnamed bank, a total of 28743 data values of processed MBES backscatter data were utilized from eleven profiles with water depths around the unnamed bank varying from 79 m around the bank to 55 m on the top of it. The backscatter maps show significant variation in backscatter intensity on the summit of the banks (Fig. 7.1).

The data processing technique used here can be effectively employed to classify the survey area using linear data traces (backscatter and bathymetric) with N-S orientation (Fig. 7.2). These traces are referred as 'profiles'. Six such profiles were used in the case of the Gaveshani bank. Each profile extracted from the gridded backscatter map of the Gaveshani bank consists of 995 data points. The average separation between the six

parallel profiles is ~300 m. Similarly eleven profiles were drawn from the gridded backscatter map of the unnamed bank. Each profiles extracted from the unnamed bank area consists of 2613 data points. The average separation between the eleven parallel profiles is ~280 m.
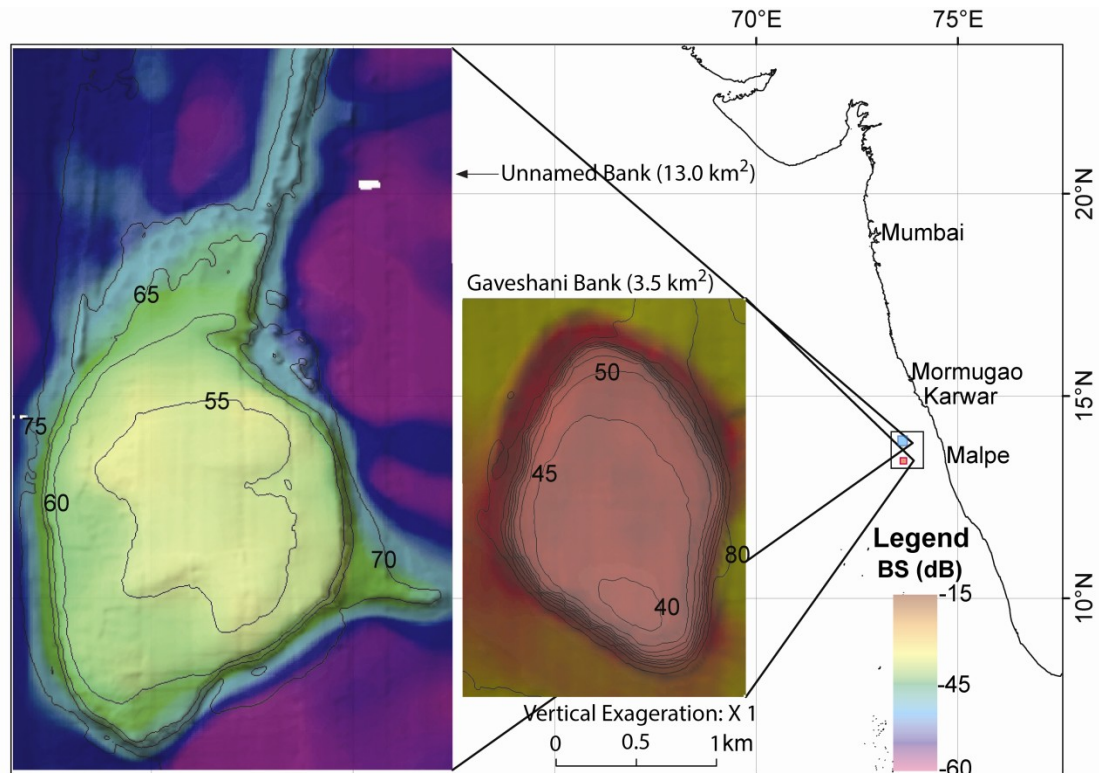
Fig. 7.1 - Location of the coralline banks; Gaveshani and the unnamed bank depicting backscatter and bathymetry.

7.4 ANN-SOM based classification techniques

The soft computing technique making use of SOM and Fuzzy c-means (FCM) has been implemented utilizing the MBES data acquired around the Gaveshani and the unnamed banks. Six profiles each extracted from the bathymetry and backscatter data of the Gaveshani bank and 11 profiles each of bathymetry and backscatter from the unnamed bank were subjected to preprocessing individually as described earlier. Normally to smoothen out short-term fluctuations, a 20-point moving average filter is
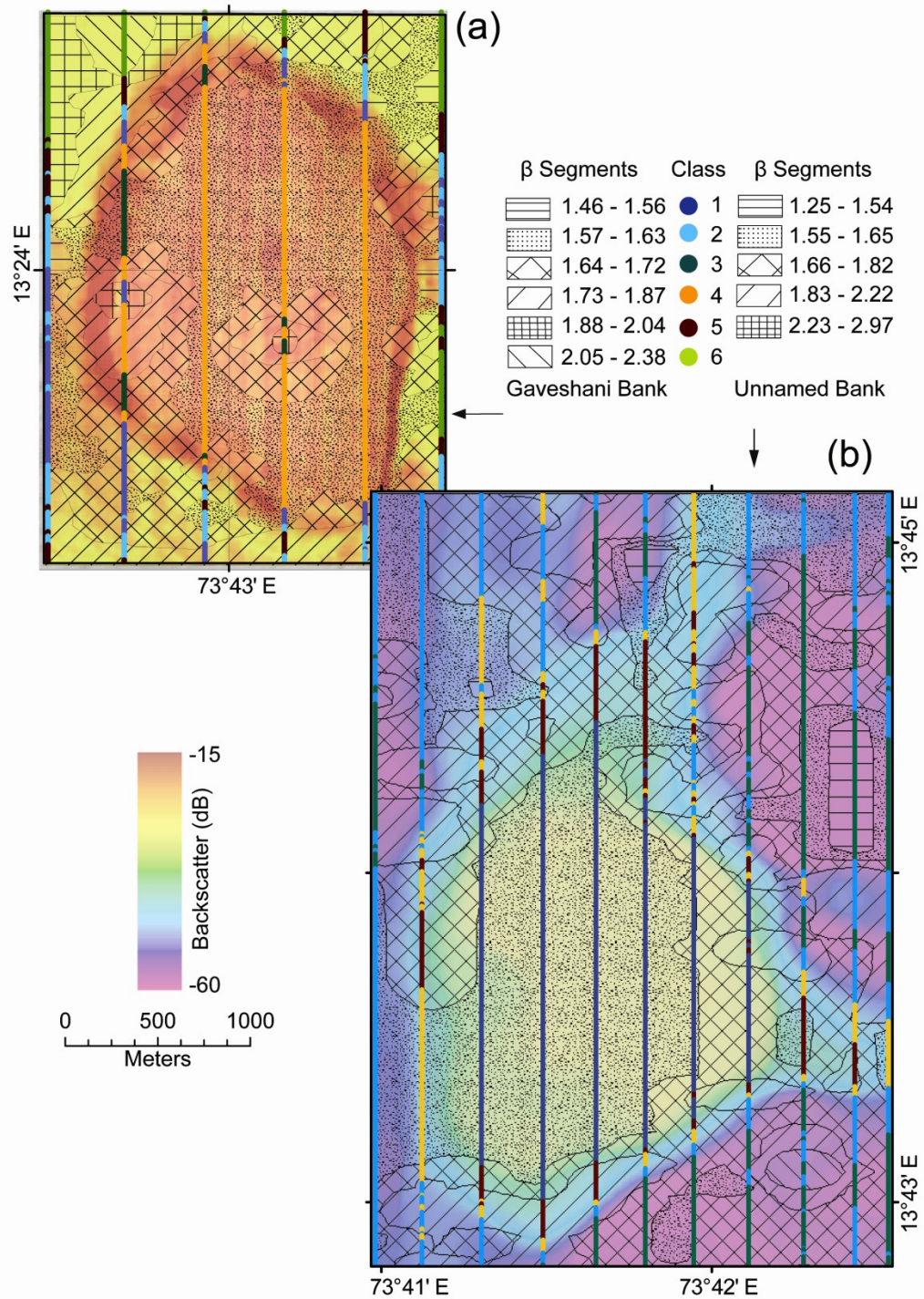
Fig. 7.2 - (a) Six backscatter profiles classified into six different classes (depicted in color) overlaid on the rasterized map of β values, estimated using each segmented data of the bathymetric profiles in the case of Gaveshani bank; (b) Eleven profiles, five classes in the case of the unnamed bank.

generally applied to all the profiles, i.e. the first element from the moving average would be the average of the first 20 points; the next element would be the average of the next 20 points that excludes the first number from the previously selected 20 points and includes the next number that follows the original 20 points by 'shifting forward' by one point. However the data here was found to be already smooth, (after a couple of trial runs), particularly the backscatter data, hence no further filtering was carried out. Thereafter the data is normalized (within +1 and −1) and the two parameters (bathymetry and backscatter) are used as input vectors for the network [Fig. 7.3(a)].
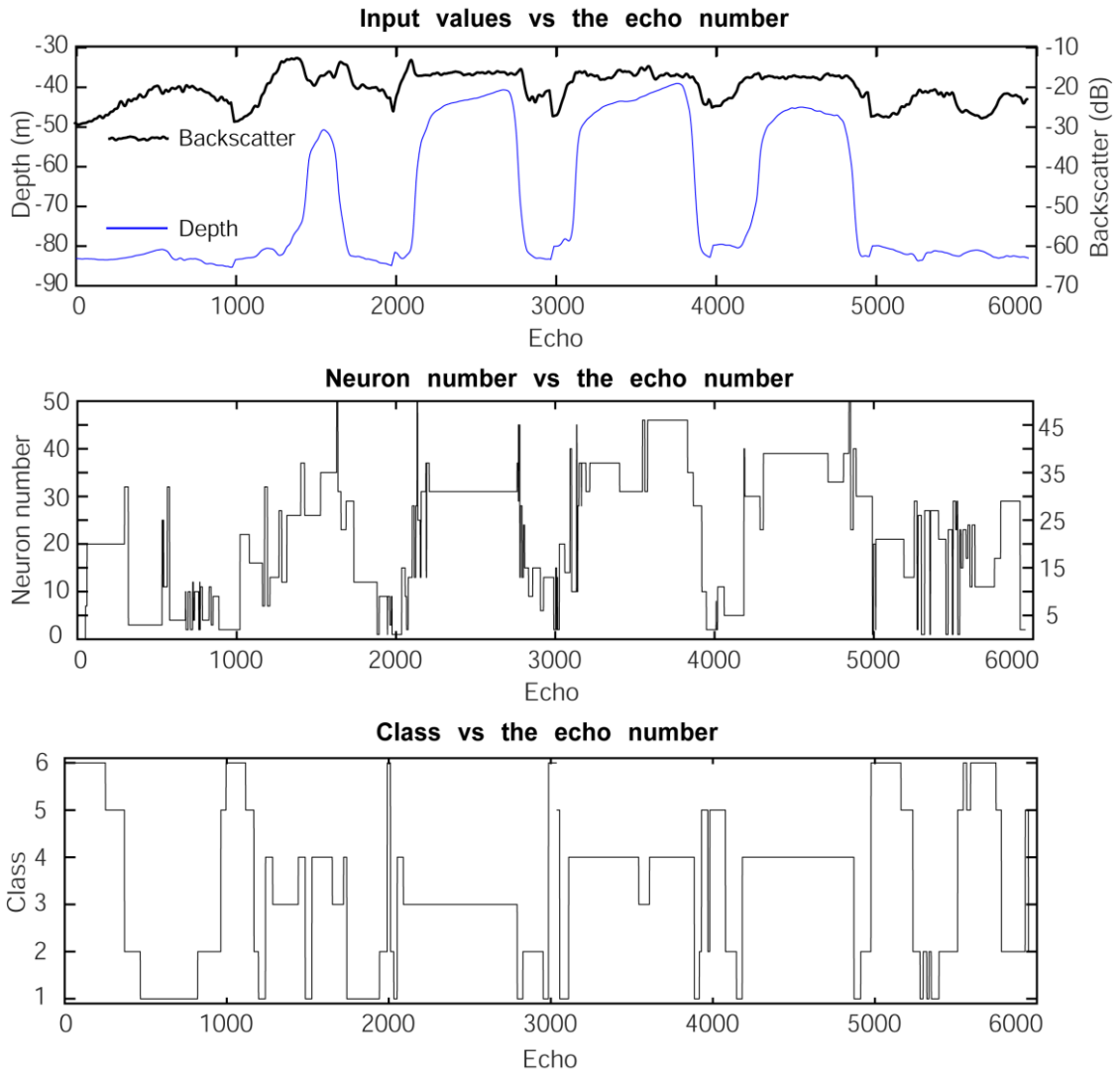
Fig. 7.3 - (a) Plot of the SOM input (bathymetry and backscatter) of Gaveshani bank; (b) Firing neurons corresponding to the SOM output; (c) Classification of the data points using FCM.

The methodology and the algorithm for data segmentation have been adapted from Chakraborty et al., (2015) to estimate the number of data classes. The SOM architecture employed here comprises of one layer two-dimensional flat grid, consisting of 2x50 neurons that accepts the input vectors for determining the number of data classes. An optimum number of 50 training data points is selected after few trial runs. The normalized input data representing the backscatter and bathymetry are segmented in a serial order with an overlap of 50 data points in a moving average sense as 1-50, 2-51 successively till the end of data. When the data is presented to SOM, the neurons in the grid compete among themselves to get activated, and the closest neurons get selected to be the firing neuron or the wining neuron as described in the flowchart (Fig. 7.4). In order
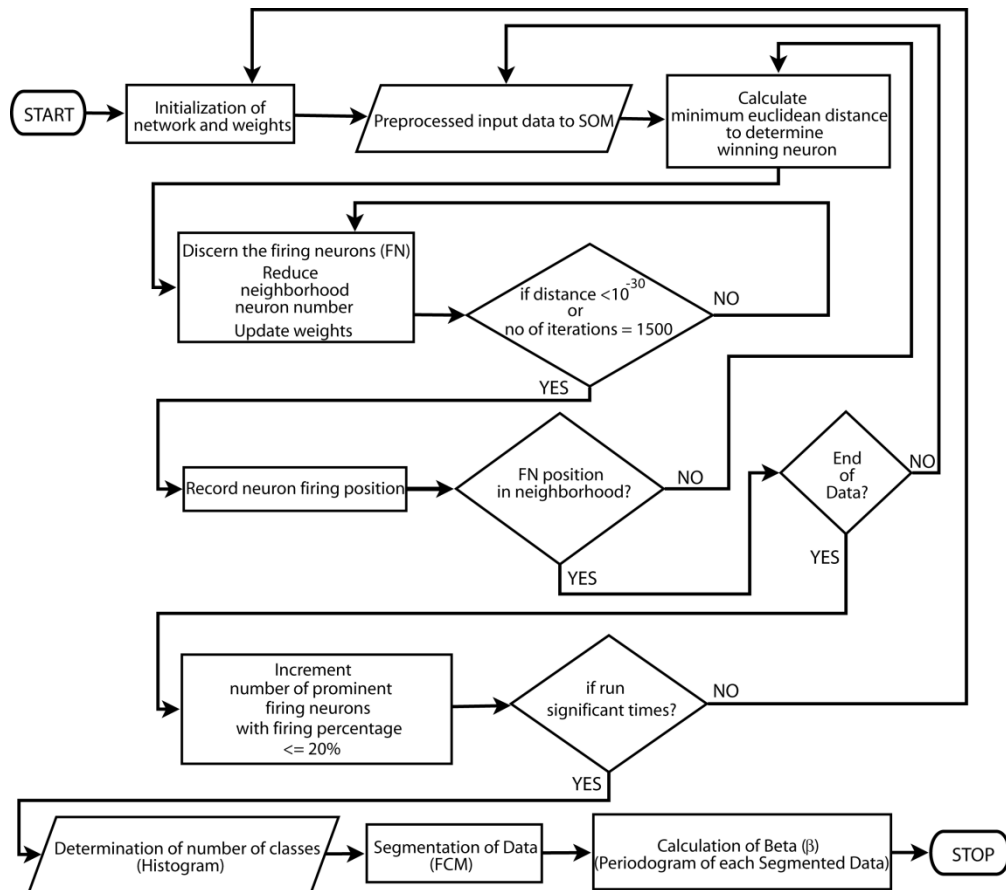
Fig. 7.4 - Flowchart of the methodology followed for determining the number of data classes with SOM (using backscatter and bathymetry data from the profiles), and data clustering utilizing FCM.

to determine the number of data classes using the SOM architecture, a training process is initiated with a training sample of 2x50 input vectors, depth and backscatter values [Fig. 7.3(a)].

The SOM algorithm organizes the nodes in the grid into local neighborhood groups of 5 neurons. Thereafter the weights of the neighborhood neurons, the two neurons each on either side of the winner neuron along with the winner neuron are updated iteratively using the learning function [$h(t)\sim 0.4/t^{0.2}$] (where t is the iteration number), and the neighborhood neuron number is reduced to 1 by neighborhood reduction technique used by SOM architecture (Chakraborty et al., 2015). During this training process the Euclidean distance between the input vector and the weight of the neurons in the grid is computed and the neuron with the smallest distance is designated as the "winner" neuron. The training stops once the error goal (the Euclidean distance between the input vector and the neuron weights) of 10^{-30} is reached or the predefined maximum iteration number 1500 is attained. To compute the shortest Euclidean distance, the weight matrix of the two-dimensional flat grid, consisting of 2x50 neurons is used, in conjunction with the training dataset of 2x50 input vectors representing backscatter and depth.

When the testing result throws up the winning neuron within the group of the trained neuron cluster, then it is assumed that it belongs to the same class, where the data was formerly trained; if not it is considered as belonging to another class. After completion of the initial training process, the SOM network is tested with the remaining data segments. Similar training-testing process is carried out using all the remaining consecutive segments. The excited neurons obtained from each testing process are plotted with respect to the neuron positions in a bar diagram. The SOM output of the one training-testing process carried out with one of the segments of Gaveshani Bank shows that the highest neuron firings (35) occurred at the neuron position 27 and the other prominent

neurons were observed at 3, 15, 23, 34 and 44 [Fig. 7.5(a)]. Similarly, the highest neuron firings (30) in the case of the unnamed bank took place at position 18 the rest at 12, 23, 30 and 47 [Fig. 7.5(b)]. The maximum number of classes is estimated by counting the presence of the number of prominent fired neurons (bars). The neuron positions (bar) with 20% or more of the highest neuron firings are considered as prominent neuron firings. The 20% selection criterion is chosen based on initial trial runs. The representative percentages of the number of times the neurons have been fired for the entire data set are plotted as bar diagram with respect to the number of neurons [Fig. 7.3 (b)]. The maximum numbers of classes that exist are equal to neuron firings that are 20% or more of the highest neuron firing [Fig. 7.5(a) and 7.5(b)].

The SOM network ascertains the number of data classes by tallying the occurrences of the number of prominent neuron firings. The training-testing process performed on the successive different data segments may produce disjointed number of classes. All the occurrences of the varying number of classes are finally plotted in a histogram [Fig. 7.5(c) and 7.5(d)] for Gaveshani and the unnamed bank signifying six and five classes respectively. This process enables to ascertain the maximum number of data classes (cluster centers) available in a given data set without any prior information.

The testing and training process for the entire data set is repeated for a number of epochs depending on the stability of the SOM classification in achieving a stable firing neuron number. (An epoch is considered when the entire dataset has passed through the neural network on one occasion only). One epoch is not enough as it can lead to 'underfitting' results. The neuron numbers produced during the multiple training-testing processes using the SOM [Fig. 7.3(b)] are plotted in a histogram for discerning the major classes [Fig. 7.5(c) and 7.5(d)].
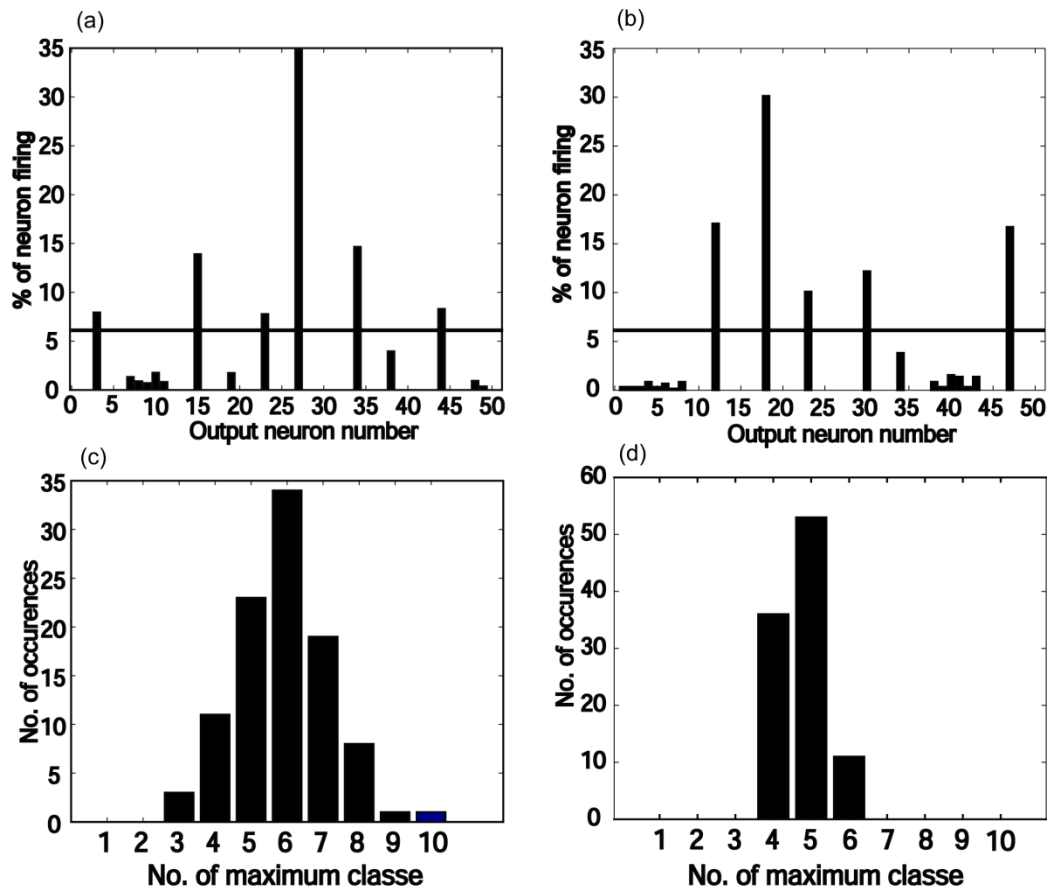
Fig. 7.5 - (a) and (b) shows % of neuron firing versus output neuron number obtained from one training-testing process. The number of bars above the line corresponds to the number classes obtained from one training/testing process. In (a) the six bars above the line indicating six classes in the case of Gaveshani bank and in (b) five classes for the case of the unnamed bank. The horizontal lines represent the line of 20% of the maximum number of neuron firings. For figure (c) and (d) histograms of the number of occurrences of maximum number of classes obtained from the ~100 training-testing process employing SOM analysis i.e., indicating no. of classes available in the datasets of Gaveshani and the unnamed bank respectively.

7.5 Application of Fuzzy c-means for segmentation

Thereafter Fuzzy c-means method is employed, utilizing the number of data classes determined by the SOM, for segmenting the bathymetric data profiles. In this work, MATLAB based FCM algorithm (www.math-works.com) is made use of for clustering the profile data to beget the segments. In situations like the present one, fuzzy clustering is more natural than hard clustering. De and Chakraborty (2009) have elucidated the advantages of the hybrid network SOM and FCM combination. The FCM generated segmented profiles (color coded) overlaid on the backscatter map can be seen in [Fig.

129

7.2(a) and 7.2(b)]. The six classes generated from the training and testing of the firing neurons correspond to the six segmented sets of the bathymetric data from the profiles [Fig. 7.5(c)] of the Gaveshani bank and five segments for the unnamed bank [Fig. 7.5(d)].

7.6 Roughness parameter estimation

This study aims at developing a system for classification of the seafloor (based on SOM and FCM) and subsequent characterization, making use of PSD function of segmented bathymetric profiles. The use of the SOM-FCM techniques along with the spectral estimation of the segmented sections of the profiles underscores the significance of the method employed. A liner fit to the PSD output of the segmented profiles is carried out employing the power law equation as given below (Chakraborty et al., 2006):

$$\log_{10} P_H = (-\beta)\log_{10} k + \log_{10} a' \qquad (1)$$

where P is power [m^2/(cycles/km)] and k is wave number (cycles/km). A straight line fit of this expression with a PSD provides β (that corresponds to the slope of the straight line) and the intercept a' (meters) of the input profile. The estimated β from the above equation is known as the 'spectral exponent' of the power law curve. At higher wave numbers (smaller scales), the periodogram appears to provide an appropriate straight line fit. The straight-line fitting parameters: β (slope) and a' (intercept) values are estimated within the chosen $\log_{10}$ (wave number) window ranges. Parameters such as correlation coefficient and root mean square error (RMSE) of the data points within the windows for the PSD (drawn from the segmented data) and corresponding power law [W(k)] function provide β and a' values of the segmented profiles. Each of the straight-line fitting parameters β and a' depict distinct seafloor classes based on the roughness characteristics of the two coralline banks. Fig. 7.6(a) and Fig. 7.6(b) depict two distinct power law (log-log) plots as representative of the two banks being examined.
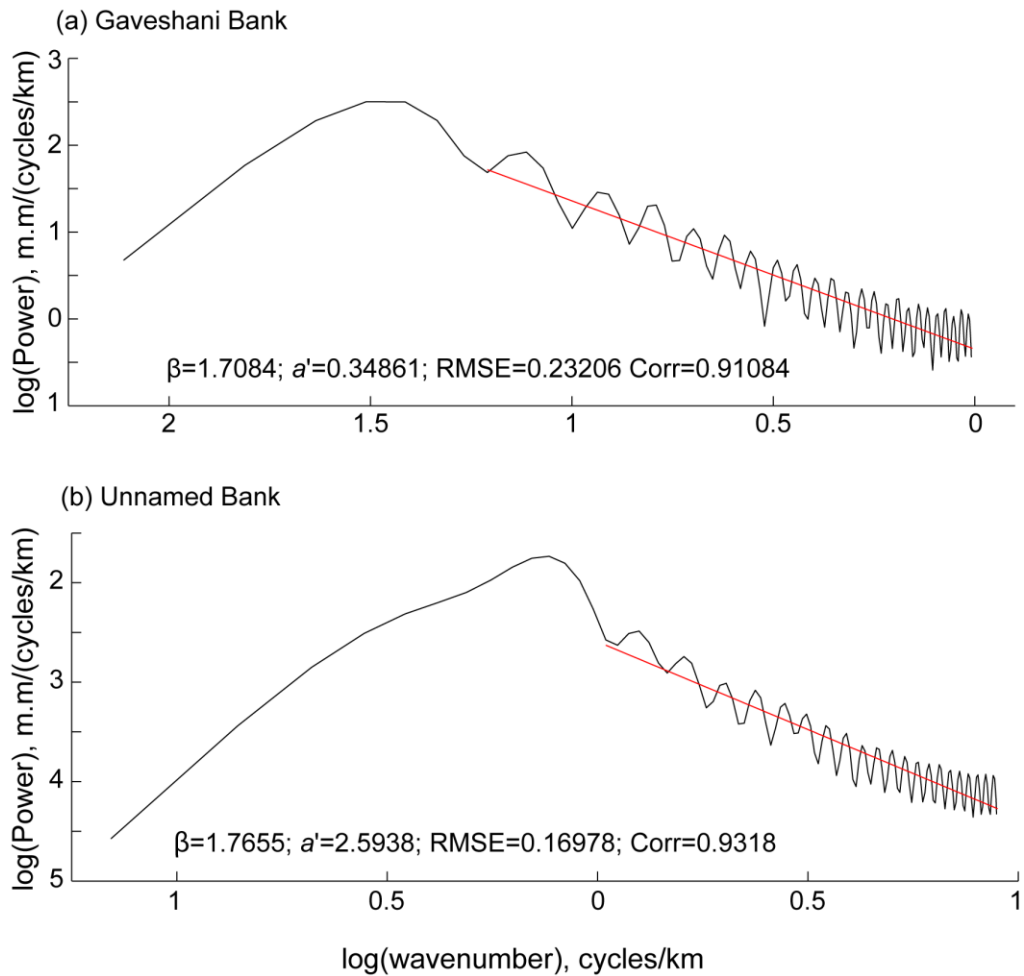
Fig. 7.6 - Representative power-law (log-log) plots of (a) Gaveshani bank and (b) Unnamed Bank.

7.7 Results

The data classes obtained using SOM and FCM could be validated using multimodal statistical technique; the multimodal fitted curves obtained from Probability Density Functions (PDF) of the backscatter mosaic of the respective profiles of the two banks could establish corresponding number of PDF components matching with the data classes obtained with SOM (Menezes et al, 2018).

The validity of the number of classes obtained using SOM and FCM, the histograms of the 6 and 11 backscatter profiles data of the two coralline banks (Gaveshani and the unnamed bank) were fitted using multimodal curves (Fig. 7.7). Using multimodal PDF of the backscatter strengths the estimated amplitude (to scale the height of the curve), mean

and standard deviation of the PDF components were computed (indicated in figures). The parameters were estimated from the curve fitting between the experimental and predictive PDFs involving the estimated correlation coefficients and the sum square of the residuals (SSR criteria). The mixtures of the normal distribution of the six components could be ascertained from the Gaveshani bank profiles [Fig. 7.7(a)] and five components from the unnamed bank [Fig. 7.7(b)]. The highest correlation coefficients and the lowest errors (SSR) have been considered in determining the predictive components and the resultant (mixture) PDFs through the use of the experimental data. The estimates confirm the same number of classes in the data sets as determined by the SOM-based classification system.
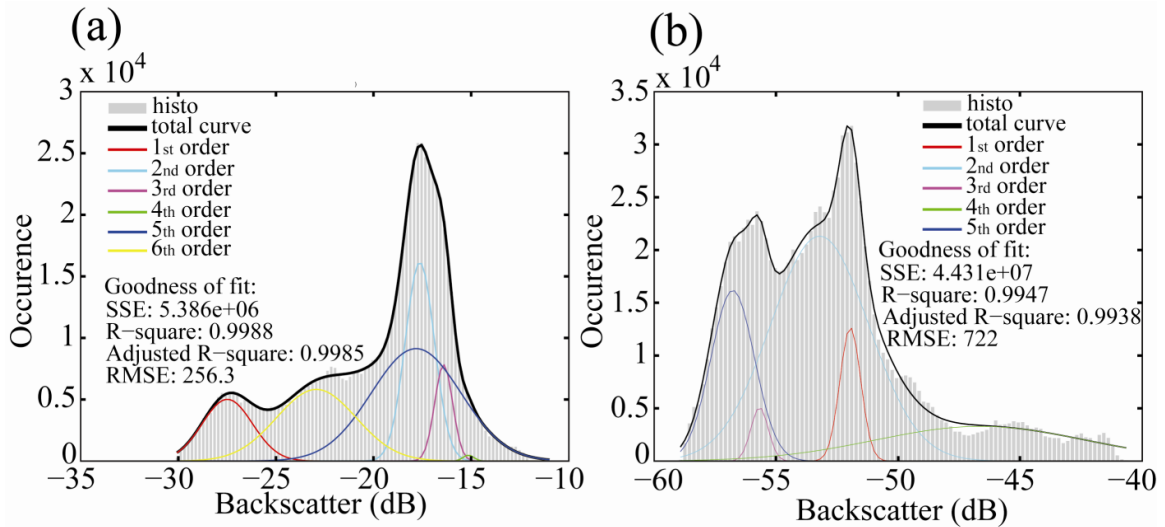
Fig. 7.7 - Occurrences of backscatter strength (dB) with respect to the rasterized backscatter pixels of the two coralline banks and the fitted multi-modal curves of the total, and the six and five PDF components of; (a) Gaveshani bank; (b) The unnamed bank (adapted from Menezes et al., 2018)

Also the number of data classes is found to be similar for estimated β (roughness) using bathymetric data. The segmentation of the six bathymetric profiles by FCM could produce 60 segments within the six classes of the Gaveshani data. Short segments (< 45 m) were ignored for the estimation of β and a', as short segments introduces bias. It could be discerned from the estimates that segments less than 45 m were not consistent, hence marked down. Using the estimated β values from the segmented data of each profile,

predicted β values were generated employing kriging method for better discernment. Kriging is important for the generation of map of the estimated roughness (β) values so that the contours of the predicted β values can be depicted [Fig. 7.2(a) for the Gaveshani and Fig. 7.2(b) for the unnamed bank]. The estimated β values match with the overlaid contour map drawn (Fig. 7.2) using the predicted β. The predicted values, i.e., map-generated data points, were validated for its likely closeness with the estimated values of the profiles. The histogram of the error values (the difference between the estimated and predicted values) for the 7599 data points from the 6 profiles depicts the accuracy of prediction [Fig. 7.8(a)] and the correlation coefficients of the estimated and predicted β values was 0.9590 [Fig. 7.8(c)]. Likewise the histogram of error values of the estimated and predicted β values (28664) of the unnamed bank is indicted in [Fig. 7.8(b)] and the correlation coefficients being 0.8371 [Fig. 7.8(d)]. From the above the predicted β values come out to be reasonably close. By and large the predicted β values compare well with the background map.

The β values of the Gaveshani bank and its surrounds range from 1.46 to 2.38. The intercept values a' range from -4.24 to +0.48. The color coded segmented profiles representing the six classes, determined using the SOM and FCM, overlaid on the backscatter intensity map are found with most of the larger segments stretching over the summit of the bank. The backscatter strength of the Gaveshani bank summit ranges from -20 to -15 dB, i.e. very high backscatter. Overall the backscatter strength over the summit and the edges of the coral bank varies within -30 to -15 dB; the fluctuation effect is due to the uneven edges. Likewise the β values of the Gaveshani coral bank summit vary from 1.57 to 2.04 [Fig. 7.2(a)], which is indicative of the Gaveshani bank summit being rougher compared to its surroundings. However, the extremely small portion of middle part of the summit has a roughness (β =1.73 to 2.04), which covers a negligible portion
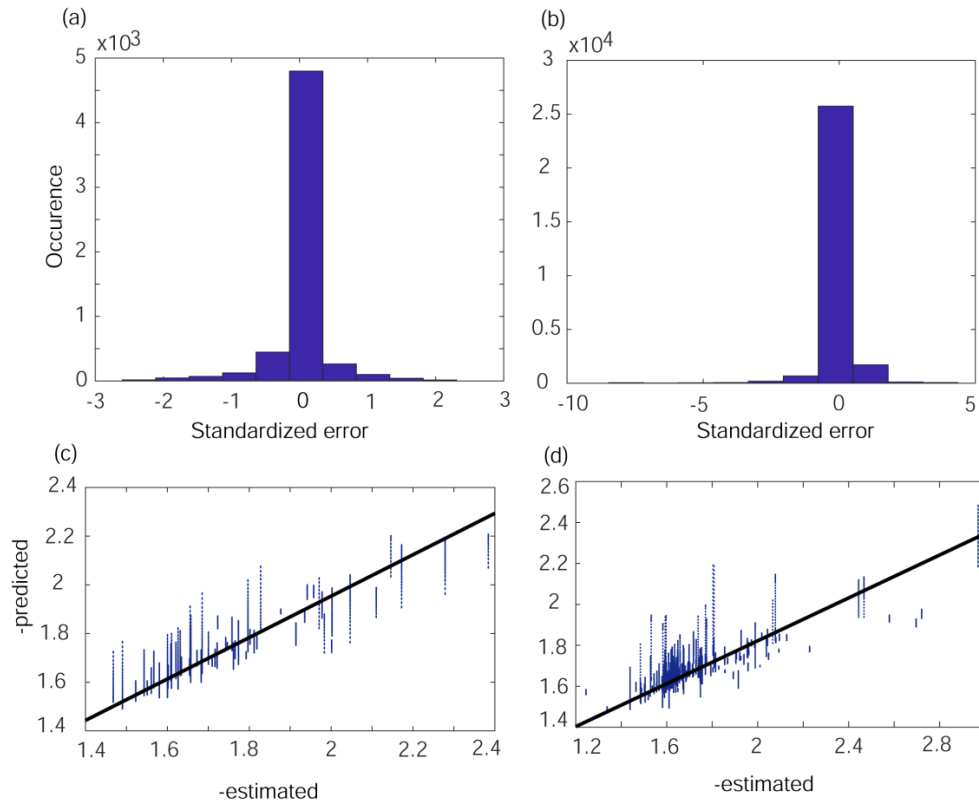
Fig. 7.8 - (a) Histogram of standardizes errors between the estimated and predicted β values of the segmented profiles; (b) Scatter plot of the predicted β and computed β

of the total. This allows us to surmise that the prevailing seafloor roughness parameter (β =1.57 to 1.72) found atop the Gaveshani bank summit is dominant. The estimated slope β and intercept a' values of the straight line fitted power law for the 11 bathymetric profile data of the unnamed bank produce β varying from 1.25 to 2.97, and the corresponding intercept a' values, -7.18 to -0.51. Two hundred and nine data segments could be generated using SOM and FCM. Here again, the short segments (<80 m) are not considered to reduce inaccuracies in the estimated power law parameters The β values atop the unnamed bank are found to be varying from 1.55 to 1.82, indicating that its summit has roughness similar to that of the Gaveshani bank summit. Likewise the backscatter values on the summit of the unnamed bank vary from -49.50 to -31.0 dB, even though the backscatter strength of the entire area has a broad variation (-61.0 to -30.0 dB). Both the banks have more segments corresponding to its periphery as compared to the summit of the banks.

7.8 Discussions

The histograms of the estimated β values for the Gaveshani bank and the unnamed bank seafloor are depicted in [Fig. 7.9(a) and 7.9(c)] respectively. [Fig. 7.9(b) and 7.9(d)] represent the concentration of lower β values (higher roughness) of the summit of the respective Gaveshani and the unnamed banks. The extent of the segmented profiles of the
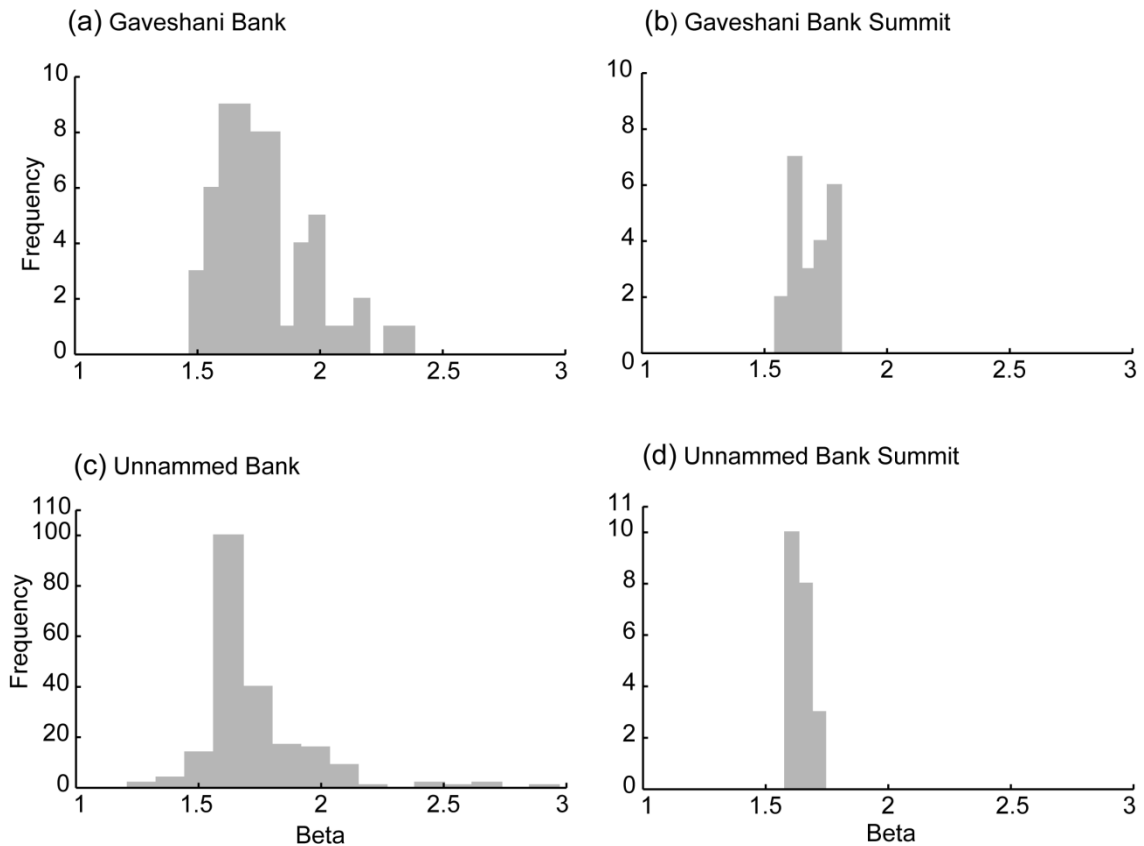
Fig. 7.9 - Histograms of estimated β values of (a) Gaveshani bank; (b) Gaveshani bank summit; (c) Unnamed bank; (d) Unnamed bank summit.

summit are large and few in number. Most of the large data segments atop the banks are confined to a singular class having higher roughness (Fig. 7.2). As mentioned earlier, the roughness of the unnamed coral bank summit is comparable to that of the Gaveshani bank. The estimated ranges of β (~1.56 to 1.82) values show relatively a rough seafloor surface over the summits of both the banks. The regional oceanic circulations, characterized by seasonal reversal of monsoon-driven surface and bottom currents,

summer upwelling and winter down welling, create an unstable oceanographic conditions in the WCMI at ~ 250 m water depth (Amol et al., 2012). The possibility of the bottom current affecting the two coralline banks, located at the 80 m water depth is not probable. Hence the possible reason for the morphological traits of the two coral banks can be further evaluated. The two coralline features are situated on the left bank of a buried channel (Fig. 7.10). The channel could have been originally formed as fluvial drainage. The high backscatter strength and the corresponding β values of the Gaveshani bank summit are indicative of higher roughness. Histogram of the β values depicts a tapering coverage [Fig. 7.9(a)]. With the Gaveshani bank lying on top of a sub-aerial headland, the likelihood of absence of fluvial erosion or deposition effect cannot be precluded. The perspective map generated from the Shuttle Radar Topography Mission (SRTM) data, reveals that the Gaveshani bank is located on what was probably a subaerial headland during the Holocene transgression, and protracted without the effect of any sediment deposition as a submerged headland (Fig. 7.10). On the other hand, the unnamed coral bank lies on a lowland and has less backscatter strength. The estimated β values and the corresponding lower backscatter intensity suggest comparatively lower roughness (except atop its summit and nearby areas) than the Gaveshani bank. It is also observed that the paleo-drainage of the former river-shelf system may possibly be linked to the inland drainage system off the coast of Goa-Karnataka. The widespread distribution of the β values corresponding to lower roughness in comparison to the Gaveshani bank is probable due to heterogeneity of the process involved in the unnamed bank data series. The presence of a series of paleo-channels and a few coral reefs in the present study area has been reported earlier (Karisiddaiah et al., 2002). The drainage pattern along the Goa and Karnataka coast linked to the river courses extend from the continental shelf to the
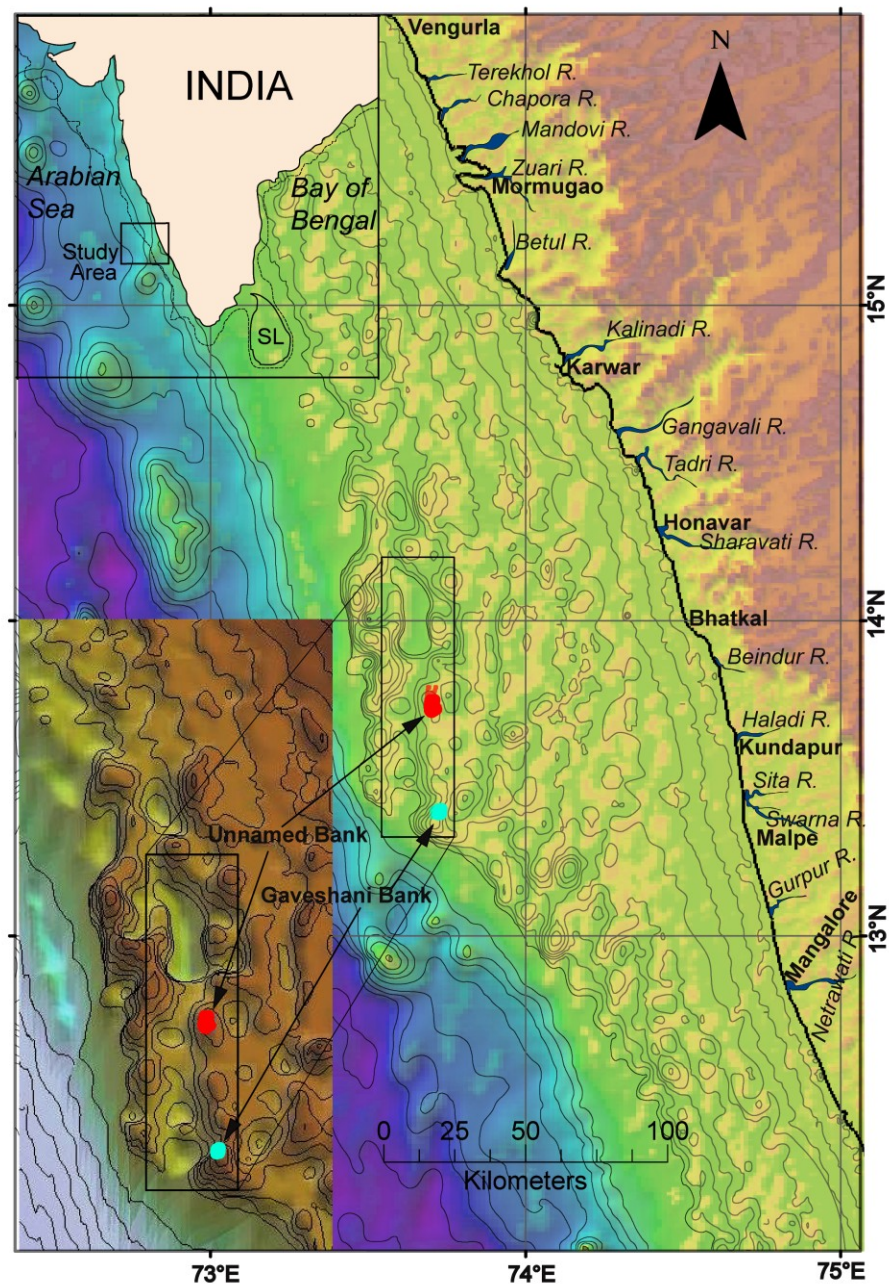
Fig. 7.10 - A broad perspective view of Gaveshani and the unnamed bank with bathymetry from SRTM data. (Adapted from Chakraborty et al. (2016).

shelf edge. Even before the Holocene period, the prevalence of fluvial deposition continued, which has subsequently smoothened the walls of buried channels. During the Holocene transgression period the two coral banks were submerged and the reduction in the flow of sediments could have initiated sediment backfilling along the slope of the channel (Chakraborty et al., 2016). Likewise the waves and currents have also modified

the present morphology of the study area. The distinct difference in the two coral bank morphologies could be discerned by making use of the estimated roughness parameters. The two banks exhibit relatively higher backscatter intensity on its summit, the intensity values of Gaveshani being higher than that of the unnamed bank. The variation in backscatter intensity on the summit of the unnamed bank is indicative of higher sediment accumulation, however along the edge of the banks, the backscatter intensity reduces with decreasing depth. In this research, the seafloor roughness is estimated using depth data. The depth values are assigned using echo-waveform peaks of the seafloor backscatter data. The low backscatter strength of the summit of the unnamed bank indicates a thin layer deposit. However the presence of such layer may not attenuate to the backscatter signal. According to Jackson et al., the acoustic seafloor roughness includes two major roughness types: i) interface and ii) sediment volume roughness (in the presence of soft sediment), and the estimation of the interface roughness varies due to the sediment volume (Jackson and Briggs 1992; Jackson and Richardson 2007). Interestingly in the present case, the scattering signals are not attenuated due to the slim fluvial deposits. Therefore the estimated roughness parameters continue unchanged on the summit of the unnamed bank.

7.9 Conclusions

In the present study, the seafloor classification technique for determining the number of data classes utilizing the backscatter and bathymetric data has been successfully applied to the Gaveshani and the unnamed bank data. The data driven technique making use of SOM for estimating the numbers of data classes, and FCM for segmentation of the bathymetric profiles into homogeneous segments has been extended. The application of the soft-computing method could determine the presence of six classes from backscatter and bathymetric data profiles of the Gaveshani coralline bank. Likewise, five classes

could be ascertained from unnamed coral bank site. Additionally the bathymetric segments have been used to estimate the roughness parameters using PSD. The estimated power law exponent (β) and intercept (a') generated from each of the profile segments employing power spectral density function, provide an assessment of the seafloor roughness. The gridded maps prepared using the roughness estimate (β) of the segmented bathymetric data profiles overlaid on the co-registered backscatter map, offer an improved understanding of the distribution and characteristics of the overlying sediment material of the banks. The two coralline banks lie on a buried channel that was formerly shaped by the fluvial drainage in a paleo-environment earlier than the Holocene. The two coralline banks situated on the left bank of a buried channel with the Gaveshani bank positioned on a submerged headland. The high backscatter strength and the corresponding (β) values of the Gaveshani bank summit can be attributed to the coral growth and absence of fluvial erosion or deposition effect. The unnamed coral bank situated on a low land, having relatively lower backscatter strength and roughness (except atop the summit of the bank), compared to Gaveshani Bank, points to the heterogeneity of the process involved in the unnamed bank data series.

CHAPTER - 8

SUMMARY AND CONCLUSION

8.1 Summary and Conclusion

With the advent of fast processors and automated classification software, seafloor classification has facilitated several applications in connection with the understanding of seafloor processes. Knowledge of the seafloor, combined with ground truth, is of great importance for validating seafloor data classification results. This study was focused on classification and characterization of seafloor data, making use of soft computing techniques, of the central part of the western continental margin of India in the Arabian Sea. The spotlight was on the characterization of the slope morphology, the adjacent seepage area dotted with pock marks and the shallow seafloor with two coralline banks. The methods employed for seafloor characterization and classification are simple, adaptable and effective for the diverse seafloor areas.

In this work (Chapter 4) offers new insights into the characterization of the seafloor specifically, the slope morphological characteristics of the WCMI, revealing that the gullies and ridges have acquired varying slope angles while that of the slump zone from north to south is comparable. The scatter plot linking the average slope gradient, rms relief and mean depth of the thirty-three profiles, depict huddling of the ridge profiles, whereas the gullies and the slump zones show good clustering. These observations have been validated using PCA. The slope area exhibit fault traces and pockmark seepages signifying a structurally weak zone. It has been ascertained that there is presence of gas-charged sediments, gas-escape features in the form of fluid flow systems such as pockmarks, mud volcanoes (MV), enhanced reflectors and pockmarked gullies, based on seismic construal. Such features are normally observed in passive and active continental

margins and are important factors for seabed stability studies. The gullies and ridges in the slope region particularly in the northern part appear to be connected with the Holocene turbidite events while the southern slump zone has rendered itself to erosional processes. The erosional activities may be linked to the poleward bottom currents in the slope region off Goa (during the winter) and weakened equator ward bottom currents (during the summer monsoon). These processes may have caused tapering off the shelf with the varied current patterns and the resultant changes in seafloor topography portend a slow uncertain transformation of the inherent slope morphology.

For the characterization of the pockmarked seepage area (Chapter 6), Kohonen's self-organizing mapping technique was utilized, for estimating the most likely number of cluster centers corresponding to different unknown data classes without any prior information. The ANN-SOM based soft-computational technique could determine the presence of five data classes in the pockmarked seepage area. The presence of the five classes of backscatter strength has been further validated employing the multimodal curve fitting to the histograms of the backscatter profile. The five classes obtained using multimodal **pdf**s match with the number of classes obtained employing SOM. Fine scale roughness parameters (β and a') were computed applying PSD to the backscatter profiles and using power law fitting. The data reveal different segment lengths. The estimated roughness parameters of the segmented profiles provide quantitative information about the area seafloor roughness. A gridded map of the estimated roughness parameter is generated using the "kriging" method. The gridded map and the class of the segmented profiles overlaid on the backscatter map have been presented. The combination of soft-computational (SOM and FCM) and numerical techniques (PSD) have effectively categorized the seafloor processes and the associated sediment-logical dynamics in a

complex geographical environment (with pockmarks and faulted structures) that are subjected to strong bottom currents and seasonal upwelling.

In the study related to the shallow seafloor (Chapter 7), the seafloor classification technique has been successfully applied for characterizing the Gaveshani and the unnamed bank data. The two coralline banks are some of the best studied features in the WCMI. The ANN approach has contributed to new insights into the characterization of the coralline banks. The application of neuro-fuzzy classification (ANN-SOM and FCM) technique for determining the number of data classes utilizing the backscatter and bathymetric data of the Gaveshani coralline bank has revealed the presence of six classes. Likewise, five classes could be ascertained from the unnamed coral bank site. The bathymetric segments of both the banks have been used to estimate the roughness parameters using PSD. The estimated power law exponent (β) and intercept (a') generated from each of the bathymetric profile segments employing power spectral density function, has provided an assessment of the seafloor roughness. The gridded maps prepared using the roughness estimate (β) of the segmented bathymetric data profiles overlaid on the co-registered backscatter map, enhance the comprehension of the distribution and characteristics of the overlying sediment material of the banks. The SRTM data reveal that the two coralline banks lie on the left bank of a buried channel that was formerly formed by the fluvial drainage in a paleo-environment earlier than the Holocene. The Gaveshani bank is located on a submerged headland. The high backscatter strength and the corresponding (β) values of the Gaveshani bank summit can be attributed to the coral growth and absence of fluvial erosion or deposition effect. On the other hand the unnamed coral bank situated on a low land, having relatively lower backscatter strength and roughness (except atop the summit of the bank), compared to Gaveshani Bank, points to the heterogeneity of the processes involved affecting the unnamed bank.

PUBLICATIONS

FROM THESIS WORK:

Menezes A, Mahender, Chakraborty B, Fernandes WA, Vardhan YV, Kurian J (2018) Mapping and analyses of two coralline banks in the western continental margin of India using multibeam echosounder data. **Indian J Mar Sci** 47(07):1345-1352

Chakraborty B, **Menezes A,** Dandapath S, Fernandes W, Karisiddaiah SM, Haris K, Gokul GS (2015) Application of hybrid techniques (self organizing map and fuzzy algorithm) using backscatter data for segmentation and fine-scale roughness characterization of seepage related seafloor along the western wontinental wargins of India. **IEEE J Ocean Eng.** 40(1):3-15

Chakraborty B, Vishnu Vardhan Y, Haris K, **Menezes A,** Karisiddaiah SM, Fernandes WA, John Kurian (2016) Multifractal detrended fluctuation analysis to compare coral bank and seafloor seepage area-related characteriztion along the central western continental margins of India. **IEEE Geosci Remote Sens Lett** 13(10):1542-1546

Chakraborty B, Karisiddaiah AM, **Menezes AAA**, Haris K, Gokul GS, Fernandes W, Kavitha G (2014) Characterizing slope morphology using multifractal technique: a study from the western continental margin of India. **Nat Hazards** 73:547-565

Andrew Menezes, Bishwajit Chakraborty, W. A. Fernandes, S.M Karisiddaiah,, K Haris, John Kurien, Seafloor chracterization of coralline banks: application of soft computing technique (communicated to **Marine Geophisical Research** after revision).

IEEE CONFERENCE PROCEEDINGS RELATED TO THESIS:

Menezes A, Naik M, FernandesW, Haris K, Chakraborty B, Estiberio S, Lohani RB (2015) Fine scale analyses of a coralline bank mapped using multibeam backscatter data. In: IEEE Underwater Technology (UT 2015). Proceedings of a meeting held 23-25 February 2015, Chennai, India, pp 1-4

OTHER THAN THE THESIS WORK:

Chakraborty B, Haris K, Latha G, Maslov N, **Menezes AAA** (2014) Multifractal approach for seafloor characterization. IEEE Geosci Remote Sens Lett 11(1):54-58

Haris K, Chakraborty B, Ingole BS, **Menezes AAA**, Srivastava R (2012) Seabed habitat mapping employing single and multi-beam backscatter data: A case study from the western continental shelf of India. Cont. Shelf Res. 48: 40-49.

Haris K, Chakraborty B, **Menezes AAA**, Fernandes WA, Naik M (2015) Seafloor micro-roughness, benthic macro-fauna, and sediment substrate: A study of their interrelation-ship using high-frequency echo-sounding systems. Indian J Geo-Mar Sci 44: 157-163

Dandapath, S.; Chakraborty, B.; Maslov, N.; Karisiddaiah, S.M.; Ghosh, D.; Fernandes, W.; **Menezes, A.A.A**. (2012) Characterization of seafloor pockmark seepage of hydrocarbons employing fractal: A case study from the western continental margin of India. Mar. Pet. Geol.: 29; 115-128

Dandapath, S.; Chakraborty, B.; Karisiddaiah, S.M.; Menezes, A.A.A.; Ranade, G.; Fernandes, W.A.; Naik, D.K.; PrudhviRaju, K.N (2010) Morphology of pockmarks along the western continental margin of India: Employing multibeam bathymetry and backscatter data. Mar. Pet. Geol.: 27; 2107-2117

Dandapath S, **Andrew Menezes**, Bishwajit Chakraborty, John Kurian, Koppella N Prudhvi Raju (2018) Seafloor Geomorphology and Processes on the Western Continental Margin of India based on Multibeam Acoustic Backscatter Data Analysis. Marine Geodesy 41(2): 177-200

Chauhan, O.S.; Menezes, A.A.A.; Jayakumar, S.; Malik, M.A.; Pradhan, Y.; Rajawat, A.S.; Nayak, S.R.; Bandekar, G.; Almeida, C.; Talaulikar, M.; Ramanamurty, M.V.; Subramanian, B.R (2007) Influence of the macrotidal environment on the source to sink pathways of suspended flux in the Gulf of Kachchh, India: Evidence from the Ocean Colour Monitor (IRS-P4). Int. J. Remote Sens.: 28(15); 3323-3339**.**

Chauhan, O.S.; Jayakumar, S.; Menezes, A.A.A.; Rajawat, A.S.; Nayak, S.R. (2006) Anomalous inland influx of the River Indus, Gulf of Kachchh, India, Mar. Geol.: 229(1); 2006; 91-100.

K. Haris, Bishwajit Chakraborty, **A. Menezes**, R. A. Sreepada, and W. A. Fernandes (2014) Multifractal detrended fluctuation analysis to characterize phase couplings in seahorse (Hippocampus kuda) feeding; J. Acoust. Soc. Am. 136(4)

BIBLIOGRAPHY

Adams EW, Schlager W (2000) Basic types of submarine slope curvature. J Sed Res 70:814-828

Ali MM, Jain S, Ramachandran R (2011) Effect of Temperature and Salinity on Sound Speed in the Central Arabian Sea. The Open Ocean Engineering Journal 4:71-76

Alexandrou D, Pantzartzis D (1993) A methodology for acoustic seafloor classification. IEEE Journal of Oceanic Engineering 18(2): 81-86.

Amol P, Shankar D, Aparna SG, Shenoi SSC, Fernando V, Shetye SR, Mukherjee A, Agarvadekar Y, Khalap S, Satelkar NP (2012) Observational evidence from direct current measurements for propagation of remotely forced waves on the shelf off the west coast of India. J Geophys Res (C: Oceans) 117(C05017):1-15

Anon. (2006) Installation Manual of EM 1002 shallow water multibeam echo-sounder system, Kongsberg Maritime, Norway

Anon. (2012) EM 302 Product Description, Kongsberg Maritime, Kongsberg Maritime, Norway

Arora K, Tiwari VM, Singh B, Mishra DC, Grevemeyer I (2012) Three dimensional lithospheric structure of the western continental margin of India constrained from gravity modelling: implication for tectonic evolution. Geophys J Int 190(1):131-150

Bansal AR, Dimri VP (1999) Gravity evidence for mid-crustal domal structure below Delhi for belt and Bhilwara super group of western India. Geophys Res Lett 26:2793–2795.

Beale R, Jackson T (1990) Neural computing: An introduction. Institute of Physics Publishing Ltd., Bristol and Philadelphia

Beger M, Jones GP, Munday PL (2002) Conservation of coral reef biodiversity: a comparison of reserve selection procedures for corals and fishes. Bio Conserv 111: 53-62

Berkson J, Matthews J (1984) Statistical characterization of seafloor roughness. IEEE J Ocean Eng OE-9(1):48–52.

Beyer A, Chakraborty B, Schenke HW (2007) Seafloor classification of the mound and channel provinces of the Porcupine Seabight: an application of the multibeam angular backscatter data. Int. J. Earth Sci. 96:11-20.

Bhattacharya GC, Chaubey AK (2001) Western Indian Ocean - A glimpse of the tectonic scenario. In:The Indian Ocean: A Perspective, Volume 2, Ed by: SenGupta, R.; Desa, Ehrlich. Vol.2; 691-729p

Biswas SK (1987) Regional tectonic framework, structure and evolution of the western marginal basins of India. Tectonophysics 135: 307-327.

Blondel P (2009) Handbook of Sidescan Sonar. Springer/Praxis Publishing, Chichester, UK, pp.336

Blondel P, Murton BJ (1997) Handbook of seafloor sonar imagery. Chichester, [Eng.]; New York: Wiley published in association with Praxis Pub, pp.314

Boldes JSM (2017) Evaluation of options in producing BASE surfaces used in navigational charting. https://digital.lib.washington.edu/researchworks/handle/1773/39727

Buckley J, Hayashib Y (1994) Fuzzy neural networks: A survey. Fuzzy Sets and Systems 66(1):1-13

Burroughs PA, McDonnell RA, Lloyd CD (1998) Principles of Geographical Information Systems. Oxford University Press, Great Calarendon Street, Oxford, OX2 6DP UK 352pp

Bøe R, Rise L, Ottesen D (1998) Elongate depressions on the southern slope of the Norwegian Trench (Skagerrak): morphology and evolution. Marine Geol 146:191-203

Carpenter GA, Grossberg S, Rossen D (1991) Fuzzy ART: Fast stable learning and categorization of analog patterns by an adaptive resonance system, Neural Netw 4:759-771

Caress DW, Thomas H, kirkwood WJ, McEwen R (2008) High-resolution multibeam, sidescan, and subbottom surveys using the MBARI AUV D. Allan B. Monterey Bay Aquarium Research Institute, DOI: 10.4027/mhmta.2008.04

CARIS (2007) HIPS/ SIPS User's Guide 6.1. Fredericton, Canada

CARIS HIPS and SIPS 7.1 Service Pack 2 User Guide, 2012. Fredericton, NB Canada. 542 pp

Chakraborty B, Haris K (2012) Seafloor roughness estimation employing bathymetric systems: An appraisal of the classification and characterization of high-frequency acoustic data. Advances in Ocean Acoustics. Proc. of the 3rd International Conference on Ocean Acoustics. (3. Intl. Conf. on Ocean Acoustics (OA2012); Beijing; China; 21-25 May 2012). (AIP Conf. Proc.). American Institute of Physics; USA: 1495:283-296.

Chakraborty B, Schenke HW, Kodagali VN, Hagen R (2000) Seabottom characterization using multibeam echosounder angular backscatter: An application of the composite roughness theory. IEEE Trans. Geosci. Remote Sens.: 38(5):2419-2434.

Chakraborty B, Kaustubha R, Hegde A, Pereira A (2001) Acoustic seafloor sediment classification using self organizing feature maps, IEEE Trans. Geosci. Remote Sens 39(12): 2722-2725

Chakraborty B, Lourenco E, Kodagali VN, Baracho J (2003a) Application of artificial neural networks to segmentation and classification of topographic profiles of ridge-flank seafloor. Curr Sci 85(3): 306-312.

Chakraborty B, Kodagali VN, Baracho J (2003b) Sea-floor classification using multibeam echo-sounding angular backscatter data: A real-time approach employing hybrid neural network architecture. IEEE J Ocean Eng 28:121-128

Chakraborty B, Mahale VP, DeSouza C, Das P (2004) Seafloor classification using echo-waveforms: A method employing hybrid neural network architecture. IEEE Geosci. Remote Sens. Lett 1(3):196-200

Chakraborty B, Mukhopadhyay R, Jauhari P, Mahale V, Shashikumar K, Rajesh M (2006) Fine-scale analysis of shelf - slope physiography across the western continental margin of India. Geo-Mar Lett 26(2):114-119

Chakraborty B, Fernandes W (2012) Bathymetric Techniques and Indian Ocean Applications, In: Blondel, P (Ed.), Bathymetry and Its Applications, InTech, Croatia, pp. 3-30

Chakraborty B, Karisiddaiah AM, Menezes AAA, Haris K, Gokul GS, Fernandes W, Kavitha G (2014a) Characterizing slope morphology using multifractal technique: a study from the western continental margin of India. Nat Hazards 73:547-565

Chakraborty B, Haris K, Latha G, Maslov N, Menezes AAA (2014b) Multifractal approach for seafloor characterization. IEEE Geosci Remote Sens Lett 11(1):54-58

Chakraborty B, Menezes A, Dandapath S, Fernandes W, Karisiddaiah SM, Haris K, Gokul GS (2015) Application of hybrid techniques (self organizing map and fuzzy algorithm) using backscatter data for segmentation and fine-scale roughness characterization of seepage related seafloor along the western wontinental wargins of India. IEEE J Ocean Eng 40(1):3-15

Chakraborty B, Vishnu Vardhan Y, Haris K, Menezes A, Karisiddaiah SM, Fernandes WA, John Kurian (2016) Multifractal detrended fluctuation analysis to compare coral bank and

seafloor seepage area-related characteriztion along the central western continental margins of India. IEEE Geosci Remote Sens Lett 13(10):1542-1546

Chaubey AK, Ajay KK (2008) Structure and tectonics of western continental margin of India: Implication for geologic hazards. Proceedings volume of Workshop on Natural Hazards and Coastal Processes of Indian Coast (NHACPIC-2008) 25-33p.

Dandapath S, Chakraborty B, Karisiddaiah SM, Menezes AAA, Ranade G, Fernandes W, Naik DK, PrudhviRaju KN (2010) Morphlogy of pockmarks along the western continental margin of India: Employing multibeam bathymetry and backscatter data. Mar. Petrol. Geology 27(10): 2107-2117

Dandapath S, Chakraborty B, Maslov N, Karisiddaiah SM, Ghosh D, Fernandes W, Andrew Menezes (2012) Characterization of seafloor pockmark seepage of hydrocarbons employing fractal: A case study from the Western Continental Margin of India. 29:115-128

Dandapath S, Andrew Menezes, Bishwajit Chakraborty, John Kurian, Koppella N Prudhvi Raju (2018) Seafloor Geomorphology and Processes on the Western Continental Margin of India based on Multibeam Acoustic Backscatter Data Analysis. Marine Geodesy 41(2):177-200

Davis JC (2002) Statistics and data analysis in geology, 3rd ed. John Wiley and Sons, New York, 638 pp

Davis KS, Slowey NC, Stender IH, Fiedler H, Bryant WR, Fechner G (1996) Acoustic backscatter and sediment textural properties of inner shelf sands, northeastern Gulf of Mexico. Geo-Marine Letters 16(3):273-278

De Boer DH (1992) Hierarchies and spatial scale in process geomorphology: a review. Geomorphology 4:303-318.

De C, Chakraborty B (2011) Model-Based Acoustic Remote Sensing of Seafloor Characteristics IEEE Transactions on Geoscience and Remote Sensing 49(10):3868-3877

De C, Chakraborty B (2010) Estimation of Mean Grain Size of Seafloor Sediments using Neural Network Mar Geophys Res 33:45-53

De C, Chakraborty B (2010) Preference of echo features for classification of seafloor sediments using neural networks. Mar Geophys Res 31:215-221.

De C, Chakraborty B (2009) Acoustic characterization of seafloor sediment employing a hybrid method of neural network architecture and fuzzy algorithm. IEEE Geosci Remote Sens Lett 6(4): 743-747

de Moustier C (1986) Beyond bathymetry: mapping acoustic backscattering from the deep seafloor with Seabeam. J. Acoust. Soc. Am. 79: 316-331

de Moustier C (1988) State of the Art in Swath Bathymetry Survey Systems. IHO, Monaco, 65(2)

de Moustier C, Alexandrou D (1991) Angular dependence of 12-kHz seafloor acoustic backscatter. J. Acoust. Soc. Am. 90(1):522-531

de Moustier C, Kleinrock M C (1986) Bathymetry artifacts in the Sea Beam data: How to recognize them and what causes them. J. Geophys. Res. 91(B3): 3407-3424.

Dewangan P, Ramprasad T (2007) Velocity and AVO analysis for the investigation of gas hydrate along a profile in the western continental margin of India. Mar. Geophys. Res. 28: 201-211

Dillon WP, Lee MW, Fehlhaber K, Coleman DF (1993) Gas hydrates on the Atlantic continental margin of the United States – controls on concentration. In: Howell DG, Wiese K, Fanelli M, Zink LL, Cole F (eds) The future of energy gases. US Geol SurvProf Pap 1570:313-330

Dillon WP, Danforth WW, Hutchinson DR, Drury RM, Taylor MH, Booth JS (1998) Evidence of faulting related to dissociation of gas hydrate and release of methane off the southeastern United States In: Henriet JP, Mienert J (eds) Gas hydrates: relevance to world margin stability and climate change. Geol Soc Lond Spec Publ 137:293-302

Dimri VP (2005) Fractals in geophysics and seismology: an introduction. In: Dimri VP (ed) Fractal behaviour of the earth system. Springer, Berlin, pp 1-22

Dowdeswell JA, Cofaig CO, Noormets R, Larter RD, Hillenbrand CD, Benetti S, Evans J, Pudsey CJ (2008) A major trough-mouth fan on the continental margin of the Bellingshausen Sea. West Antarctica: the Belgica Fan. Marine Geol 252:129-140. doi:10.1016/j.margeo.2008.03.017

Ergün M, Dondurur D, Çifçi Günay (2002) Acoustic evidence for shallow gas accumulations in the sediments of the eastern Black Sea. Terra Nova 14:313-320

ESRI (2010) ArcGIS Desktop. Redlands, CA: Environmental Systems Research Institute

Farr HK (1980)Multibeam bathymetric sonar: Sea beam and hydro chart. Marine Geodesy 4(2):77-93

Faruque BM, Ramachandran KV (2014) Chapter 15 The continental shelf of western India Geological Society, London, Memoirs, 41:213-220 https://doi.org/10.1144/M41.15

Fernandes (2007) An approach towards solving refraction problems in EM1002 multibeam echo sonunder system. National Institute of Oceanography Dona Paula Goa, Technical report no. NIO/TR-03/2007

Fernandes W, Chakraborty B (2009) Multi-beam backscatter image data processing techniques employed to EM 1002 system. In: IEEE OES Proceedings of the International symposium on Ocean Electronics (SYMPOL 2009) Kochi, India, pp 93-99

Field ME, Gardner JV, Prior DB (1999) Geometry and significance of stacked gullies on the northern California slope. Marine Geol 54:271-286

Finkl CW, Makowski C (2016) Seafloor Mapping along Continental Shelves: Research and Techniques for Visualizing Benthic Environments. Springer International Publishing AG Switzerland

Fox C, Hayes D (1985) Quantitative methods for analyzing the roughness of the seafloor. Rev Geophys 23(1):1-48

Garrison T (1993) Oceanography: An invitation to Marine Science. Belmont, California: 31 Wadsworth. 608 pp

Gay A, Lopez M, Berndt C, Se´ranne M (2007) Geological controls on focused fluid flow associated with seafloor seeps in the Lower Congo Basin. Marine Geol 244:68-92

Goff JA, Orange DL, Mayer LA, Clarke JEH (1999) Detailed investigation of continental shelf morphology using a high-resolution swath sonar survey: The Eel margin, northern California," Mar Geol 154(1-4):255-269 Goff JA (2001) Quantitative classification of canyon systems on continental slopes and a possible relationship to slope curvature. Geophys Res Lett 28(23):4359-4362

Good P I, Hardin JW (2009) Common Errors in Statistics (And How to Avoid Them) (3rd ed.). Hoboken, New Jersey: Wiley. 211 pp

Green AN, Goff J, Uken RU (2007) Geomorphological evidence for upslope canyon-forming processes on the northern Kwazulu-Natal shelf, SW Indian Ocean, South Africa. Geo Marine Lett 27:399-409

Guptha MVS, Mohan R, Muralinath AS (2002) Slumping on the western continental margin of India. GeoActa 1:45-48

Hammerstad E (1995, modified in 2000). EM Technical Note: Backscattering and Seabed Image Reflectivity. Kongsberg Technical Documentation

Haris K, Chakraborty B, Ingole BS, Menezes AAA, Srivastava R (2012) Seabed habitat mapping employing single and multi-beam backscatter data: A case study from the western continental shelf of India. Cont. Shelf Res. 48: 40-49

Haris K, Chakraborty B, Menezes AAA, Fernandes WA, Naik M (2015) Seafloor micro-roughness, benthic macro-fauna, and sediment substrate: A study of their interrelation-ship using high-frequency echo-sounding systems. Indian J Geo-Mar Sci 44: 157-163

Haris K, Chakraborty B, De C, Prabhudesai RG, Fernandes (2011) Model-based seafloor characterization employing multibeam angular backscatter data—A comparative study with dual-frequency single beam. J Acoust Soc Amer 130: 3623-3632

Hernandez-Molina FJ, Ercilla D, Van Rooij D (2011) Along-slope oceanographic processes and sedimentary products around the Iberian margin. Geo Mar Lett 31:315-341

Hertz J, Krogh A, Palmer RG (1991) Introduction to the theory of neural computation. Lecture Notes Volume I, Addison-Wesley Publishing Co. The Advance Book Program, USA.

Hewlett JS, Jordan DW (1993) Stratigraphic and combination traps within a seismic sequence framework, Miocene Stevens turbidites, Bakersfi eld Arch, California. In: Weimer P, Posamentier H (eds) Siliciclastic Sequence Stratigraphy: American Association of Petroleum Geologists (AAPG) Memoir 58, pp 135-162

Hovem JM (2013) Ray Trace Modeling of Underwater Sound Propagation. In Modeling and Measurement Methods for Acoustic Waves and for Acoustic Microdevices. Eds. Marco G. Beghi, InTech , pp598 (http://creativecommons. org/ licenses/by/3.0) http://dx.doi.org/10.5772/55935

Hughes Clarke JE, (2003) Dynamic Motion Residuals in Swath Sonar Data: Ironing out the Creases. IHO 4(1):

Hughes Clarke JE (2012) Optimal use of multibeam technology in the study of shelf morpho-dynamics. In: Sediments, Morphology and Sedimentary Processes on Continental Shelves, ser. Advances in Technologies, Research and Applications, IAS Special Publication #44. Chichester, U.K.: Wiley-Blackwell, pp. 1-28

Hughes Clarke JE, Mayer LA, Wells DE (1996) Shallow-water imaging multibeam sonars: A new tool for investigating seafloor processes in the coastal zone and on the continental shelf: Marine Geophysical Research 18:607-629.

Hovland M, Judd AG (1988) Seabed Pockmarks and Seepages Impact on Geology, Biology and the Marine Environment. London, U.K.:Graham &Trotman, 1988, ch. 10.

Hovland M, Gardner JV, Judd AG (2002) The significance of pockmarks to understanding fluid flow processes and geohazards. Geofluids 2:127-136

Hussain N, Guptha MVS (1985) Ooids in a deep sea core from the western continental margin of India. Indian J Mar Sci 14:123-126

Huvenne VAI, Blondel P, Henriet JP (2002) Textural analysis of sidescan sonar imagery from two mound provinces in the Porcupine Seabight. Mar. Geol. 189:323-341

Irvin BJ, Ventura SJ, Slaterc BK (1997) Fuzzy and isodata classification of landform elements from digital terrain data in Pleasant Valley, Wisconsin. Geoderma 77(2-4):137-154

Jackson DR, Winebrenner DP, Ishimaru A (1986) Application of the composite roughness model to high-frequency bottom backscattering. J. Acoust. Soc. Am. 79:1410-1422.

Jackson DR, Briggs KB (1992) High-frequency bottom backscattering: Roughness vs. sediment volume scattering. J Acoust Soc Am 92:962-977

Jackson DR, Richardson MD (2007) High-Frequency Seafloor Acoustics. Springer-Verlag, New York

Jackson DR, Briggs KB, Williams KL, Richardson MD (1996) Test of models for high-frequency seafloor backscatter. IEEE Journal of Oceanic Engineering 21(4):458-470

Jenks GF (1967) The data model concept in statistical mapping. International Yearbook of Cartography 7:186-190

Johnston K, Ver Hoef JM, Krivoruchko K, Lucas N (2004) Using ArcGIS geostatistical analyst. ESRI Press, pp.300

Jolliffe IT (1986) Pincipal component analysis. New York: Springer, pp. 488

Karisiddaiah SM, Veerayya M (1994) Methane-bearing shallow gas-charged sediments in the eastern Arabian Sea: a probable source fo greenhouse gas. Cont Shelf Res 14:1361-1370

Karisiddaiah SM, Veerayya M, Vora KH, Wagle BG (1993) Gas-charged sediments on the inner continental shelf off western India. Mar Geol 110:143-152

Karisiddaiah SM, Veerayya M, Vora KH (2002) Seismic and sequence stratigraphy of the central western continental margin of India: late quaternary evolution. Mar Geol 192(4):335-353

Kenny AJ, Cato I, Desprez M, Fader G, Schüttenhelm RTE, Side J (2003) An overview of seabed-mapping technologies in the context of marine habitat classification. ICES J Mar Sci 60(2): 411- 418; https://doi.org/10.1016/S1054-3139(03)00006-7

Katz MB (1978) Tectonic evolution of the Archean granulite fades belts of Srilanka — South India. J. Geol. Soc. India. 19(5): 185-205.

King H, MacLean B (1970 Pockmarks on the Scotian shelf. Geol Soc Amer Bull 81:3141-3148

Kluesner J, Brothers D, Hart P, Miller N Hatcher G (2018)Practical approaches to maximizing the resolution of sparker seismic reflection data. Marine Geophysical Research; https://doi.org/10.1007/s11001-018-9367-2

Kohonen T (1989) Self-organization and associative memory. 3rd Edition, Springer-Verlag, Berlin.

Kohonen T (1990) Self-organizing map. Proc. IEEE 78(9):1464-1480

Kvenvolden KA (1993) Gas hydrates - Geological Perspective and global change. Reviews of Geophysics 31(2): 173-187

Kumar A, Rao YB, Sivaraman TV, Gopalan K (1996) Sm-Nd ages of Archaean metavolcanics of the Dharwar craton, south India. Precambrian Res 80(3):205-216

Lastras G, Canals M, Urgeles R, Amblas D, Ivanov M, Droz L, Dennielou B, Fabre´s J, Schoolmeester T, Akhmetzhanov A, Orange D, Garcı´a-Garcı´a A (2007) A walk down the Cap de Creus canyon, northwestern Mediterranean Sea: recent processes inferred from morphology and sediment bedforms. Mar Geol 246:176-192

Le Gonidec Y, Conil F, Gibert D (2003) The wavelet response as a multiscale NDT method. Ultrasonics 41:487-49

Leon R, Somoza L, Medialdea T, Maestro A, Dıaz-del-Rıo V, Fernandez-Puga MC (2006) Classification of sea-floor features associated with methane seeps along the Gulf of Cadiz continental margin. Deep Sea Res II 53:1464-1481

Lucieer V, Roche M, Degrendele K, Malik M, Dolan M, Lamarche G (2018) User expectations for multibeam echo sounders backscatter strength data-looking back into the future. Mar Geophys Res 39(1-2):23-40

Lurton X (2002) An Introduction to Underwater Acoustics: Principle and Applications. (PRAXIS, Chichester, Chap. 8, pp. 247-292.

Lurton X, Lamarche G (Eds) (2015) Backscatter measurements by seafloor-mapping sonars: Guidelines and Recommendations. pp 200; http://geohab.org/wp-content/uploads/ 2014/05/ BSWG

Maillet GM, Vella C, Berne S, Friend PL, Amos CL, Fleury TJ, Normand A (2006) Morphological changesand sedimentary processes induced by the December 2003 flood event at the present mouth of theGrand Rhone River (southern France). Mar Geol 234(1-4):159-177. doi:10.1016/j.margeo.2006.09.025

Malinverno A (1989) Segmentation of topographic profiles of the seafloor based on a self-affine model. IEEE J Ocean Eng 14(4):348-358

Mayer LA (2006) Frontiers in Seafloor Mapping and Visualization. Mar Geophys Res 27(1):7-17

McCulloch WS, Pitts W (1943) A logical calculus of ideas immanent in nervous activity. Bulletin of Mathematical Biophysics, 5:115-133.

Menezes A, Naik M, FernandesW, Haris K, Chakraborty B, Estiberio S, Lohani RB (2015) Fine scale analyses of a coralline bank mapped using multibeam backscatter data. In: IEEE Underwater Technology (UT 2015). Proceedings of a meeting held 23-25 February 2015, Chennai, India, pp 1-4

Menezes A, Mahender, Chakraborty B, Fernandes WA, Vardhan YV, Kurian J (2018) Mapping and analyses of two coralline banks in the western continental margin of India using multibeam echosounder data. Indian J Mar Sci 47(07):1345-1352

Michalopoulou ZH, Alexandrou D, de Moustier C (1995) Application of neural and statistical classifiers to the problem of seafloor characterization. IEEE Journal Oceanic Engineering, 20(3): 190-197

Mingoti SA, Lima JO (2006) Comparing SOM Neural Networkwith Fuzzy C-Means, K-Meansand Traditional Hierarchical Clustering Algorithms. European Journal of Operational Research 174:1742-1759

Mills GB, Perry RB (1992) EEZ bathymetric mapping for ocean resource management. Sea Technology 33(6):27-34

Minsky ML Papert SA (1969) Perceptrons. MIT Press, Cambridge, MA.

Mitchell NC (2005) Interpreting long profiles of canyons in the USA Atlantic continental slope. Mar Geol 214:75-99. doi:10.1016/j.margeo.2004.09.005

Mitchell NC (1991) Improving GLORIA images using Sea Beam data. J. Geophys. Res. 96:337-351

Mitchell NC, Somers L (1989) Quantitative backscatter measurements with long range side-scan sonar. IEEE J. Ocean. Eng. 14:368-374

Moss JL, Cartwright J, Moore R (2012) Evidence of fluid migration following pockmark formation: examples from the Nile deep sea fan. Mar Geol 303-306:1-13

Mukhopadhyay R, Rajesh M, De S, Chakraborty B, Jauhari P (2008) Structural highs on western continental slope of India: Implications for regional tectonics. Geomorphology 96(1-2):48-61

Nair RR, Qasim S.Z (1978) Occurrence of a bank with living corals off the south-west coast of India. Indian J Mar Sci 7(1):55-58

Naqvi SWA, Bange HW, Farias L, Monteiro MS, Scranton MI, Zhang J (2010) Marine hypoxia/anoxia as a source of CH4 and N2O. Biogeosciences 7:2159-2190

North MA (2009) A Method for Implementing a Statistically Significant Number of Data Classes in the Jenks Algorithm. Sixth International Conference on Fuzzy Systems and Knowledge Discovery, Tianjin, China, 14-16, DOI: 10.1109/FSKD.2009.319

O'Grady DB, Syvitski JPM, Pratson LF, Sarg JF (2000) Categorizing the morphologic variability of siliciclastic passive continental margins. Geology 28:207-210

Pal S, Pal NR (2003) Connectionist models for approximate solutions of non-linear equations in one variable. Neural, Parallel and Scientific Computation 11:185-206

Pearson JD, Morrell CH, BrantLJ (1992) Mixture models for investigating complex distributions. J Quant Anthropol 3:325-345

Pilcher R, Argent J (2007) Mega-pockmarks and linear pockmark trains on the West African continental margin. Mar Geol 244:15-32

Peyton DR, Beaudoin J, Lamplugh M (2009) Optimizing Sound Speed Profiling for Hydrographic Surveys. IHO 10(11)

Pike, R.J., Evans, I.S., Hengl, T (2008) Geomorphometry: a Brief Guide. In: Hengl, T. and Reuter, H.I. (Eds), Geomorphometry: Geomorphometry: Concepts, Software, Applications. Developments in Soil Science, vol. 33, Elsevier, 1-28 pp

Pratsch JC (1978) Future hydrocarbon exploration on continental margins and plate tectonics. J Petrol Geol 1(2):95-105

Qasim SZ (1978) Further observations on Gaveshani Bank, Indian J Mar Sci 8(4):261-262

Rao ChM, Murty PSN (1990) Geochemistry of the continental margin sediments of the central west coast of India. Journal Geological Society Of India 35: 19-37

Rao BR, Veerayya M (2000) Influence of marginal highs on the accumulation of organic carbon along the continental slope off western India. Deep-Sea Research (II: Topical Studies in Oceanography) 47:303-327

Rao DG, Paropkari AL, Krishna KS, Chaubey AK, Ajay KK, Kodagali VN (2010) Bathymetric Highs in the mid-slope region of the Western Continental Margin of India - Structure and mode of origin. Mar Geol 276(1-4):58-70

Rao KL (1972) India's Water Wealth. Orient Longmans, New Delhi, pp. 286

Rao PS (1995) Physiography and depositional environment on the central western continental margin of India. Ph.D Thesis, Indian School of Mines, Dhanbad, India

Rao PS, Kodagali VN, Ramprasad T, Nair RR (1993) Morphology of a coral bank, western continental shelf of India: A multibeam study, J Geol Soc India 41(1):33-37

Rao VP (2003) Four Decades of Marine Geosciences in India - A Retrospect. Journal of the Geological Society of India 61(1):118-120

Rao YH, Subrahmanyam C, Rastogi A, Deka B (2002) Slope failures along the western continental margin of India: a consequence of gas-hydrate dissociation, rapid sedimentation rate, and seismic activity? Geo-Mar Lett 22: 162-169; DOI 10.1007/s00367-002-0107-9

Rao YH, Subrahmanyam C, Rastogi A, Deka B (2001) Anomalous features related to gas/gas hydrate occurrences along the western continental margins of India. Geo Mar Lett 21:1-8

Rao, V.P. and Rao, B.R. (1995) Provenance and distribution of clay minerals in the sediments of the western continental shelf and slope of India. Continental Shelf Research, 15:1757-1771

Rao PS, Rao CHM, Reddy NPC (1988) Pyritized ooids from the Arabian Sea Basin. Deep Sea Res 35:1215-1221

Rao VP, Wagle BG (1997) Geomorphology and surficial geology of the western continental shelf and slope of India: A review. Curr Sci 73(4):330-350

Rastogi A, Deka B, Bhattacharya GC, Ramprasad T, KameshRaju KA, Srinivas K, Murty GPS, Chaubey AK, Ramana MV, Subrahmanyam V, Sarma KVLNS, Desa M, Paropkari AL, Menezes AAA, Murty VSN, Antony MK, SubbaRaju LV, Desa E, Veerayya M (1999) Gas hydrates stability zone thickness map of Indian deep offshore areas - A GIS based approach. PETROTECH-99. Papers of the Third International Petroleum Conference and Exhibition, 9-12 January 1999, Vigyan Bhavan, New Delhi. Vol. 4: Hydrocarbon exploration. ed. by: Bhatnagar, A.K. (3. Int. Petroleum Conf. and Exhibition; Vigyan Bhavan, New Delhi; India; 9-12 Jan 1999). Indian Oil Corporation; New Delhi; India.

Reineck HE, Singh IB (1980) Depositional Sedimentary Environments, second ed. Springer-Verlag, Berlin. 549pp

Rosenblatt F (1962) Principles of neurodynamics. Spartan Books, Wasington DC

Satyanarayana Y, Naithani S, Anu R (2007) Seafloor sediment classification from single beam echo sounder data using LVQ network. Mar Geophys Res 28(2):95-99

Satyavani N, Thakur NK, Aravind Kumar N, Reddi SI (2005) Migration of methane at the diapiric structure of the western continental margin of India insights from seismic data. Mar. Geol. 219: 19-25

Seuront L (2010) Fractals and Multifractals in Ecology and Aquatic Science. New York NY USA: CRC Press ch. 7

Shanmugam G (2012) New Perspectives on Deep-water Sandstones: Origin, Recognition, Initiation, and Reservoir Quality: (Handbook of Petroleum Exploration and Production eds. John Cubitt) Elsevier; 1 edition vol. 9

Shenoi SSC, Antony MK (1991) Current measurements over the western continental shelf of India. Continent. Shelf Res 11: 81-93.

Shetty MGAP (1972) A description of sediment cores from the Arabian Sea. Proceed Int Geol Cong 8:109-119

Shetye SR, Gouveia AD, Shenoi SSC, Sundar D, Michael GS, Almeida AM, Santanam K (1990) Hydrography and circulation off the west coast of India during the southwest monsoon 1987. J Mar Res 48(2):359-378

Siddiquie HN, Hashimi NH, Vora KH, Pathak MC (1987) Exploration of the continental margins of India 64(1): 91-110.

Simons DG, Snellen M (2009) A Bayesian approach to seafloor classification using multi-beam echo-sounder backscatter data. Appl Acoust 70(10):1258-1268

Sivanandam SN, Deepa SN (2011) Principles of Soft Computine. 2nd Ed. New Delhi, India: Wiley India.

Sivanandam S N, Sumathi S, Deepa SN (2006) Introduction to neural networks using MATLAB 6.0. Tata McGraw-Hill Publishing Co. Ltd., New Delhi.

Smith SMLT, Alexander L, Armstrong AA (2002) The navigation surface: A new database approach to creating multiple products from high-density surveys. International Hydrographic Review 976 https://scholars.unh.edu/ccom/976

Spinelli GA, Field ME (2001) Evolution of continental slope gullies on the northern California margin.J Sediment Res 71(2):237-245

Stackelberg UV (1972) Faziesverteilung in sedimenten des Indisch-Pakistanishen Kontinentalrandes 'Meteor'' Forschungsergebneisse 9:1-73

Stow DAV, Hernandez-Molina FJ, Llave E, Sayago M, Diaz del Rio V, Branson A (2009) Bedform-velocity matrix: the estimation of bottom current velocity from bedform observations. Geology 37(4):327-330

Subrahmanyam C, Chand S (2006) Evolution of the passive continental margin of India- a geophysical appraisal. Gondwana Research 10(1-2):167-178

Syvitski JP, Alexander CR, Field ME, Gardner JV, Orange DL, Yun JW (1996) Continental slope sedimentation:the view from northern California: oceanography (Washington, DC), 9:163-167

Sun Q, Wu S, Cartwright J, Dong D (2012) Shallow gas and focused fluid flow systems in the Pearl RiverMouth Basin, northern South China Sea. Mar Geol 315-318:1-14

Thamban M, Rao VP, Raju SV (1997) Controls on organic carbon distribution in sediments from the eastern Arabian sea margin. Geo-Mar Lett17:220-227

Thompson TL (1976) Plate tectonics in oil and gas exploration of continental margins. AAPG Bulletin 60(9):1463-1501

Vail PR, Hardenbol J, Todd RG (1984) Jurassic unconformities, chrono-starigraphy, and sea level changes from seismic stratigraphy and biostratigraphy. In: Schlee JS (ed) Interregional unconformities and hydrocarbon accumulation. AAPG Mem 36:129-144

Weatherall P, Marks KM, Jakobsson M, Schmitt T, Tani S, Arndt JE, Rovere M, Chayes D, Ferrini V, Wigley R (2015) A new digital bathymetric model of the world's oceans. Earth and Space Science 2(8):331-345; https://doi.org/10.1002/2015EA000107

Weaver PPE, Wynn RB, Kenyon NH, Evans J (2000) Continental margin sedimentation, with special reference to the north-east Atlantic margin. Sedimentology 47:239-256

Wilson MFJ, O'Connell B, Brown C, Guinan JC, Grehan AJ (2007) Multiscale Terrain Analysis of Multibeam Bathymetry Data for Habitat Mapping on the Continental Slope. Marine Geodesy 30:3-35

Yegnanarayana B, (2001) Artificial neural networks. Prentice-Hall of IndiaPrivate Limited, New Delhi

Zhou X, Chen Y (2005) Seafloor classification of multi beam sonar data using neural network approach. Marine Geodesy, 28(2): 201-206.